Experimental Investigations of Thermodynamic Properties of the LiF−CsF Binary System and FLiNaK

by

Ksenia Lipkina

A thesis submitted to the
School of Graduate and Postdoctoral Studies in partial
fulfillment of the requirements for the degree of

Master of Applied Science in Nuclear Engineering

Faculty of Energy Systems and Nuclear Sciences
University of Ontario Institute of Technology (Ontario Tech University)
Oshawa, Ontario, Canada
July, 2020

©Ksenia Lipkina, 2020

Thesis Examination Information

Submitted by: **Ksenia Lipkina**

Master of Applied Science in Nuclear Engineering

Thesis title: Experimental Investigations of Thermodynamic Properties of the LiF – CsF Binary System and FLiNaK

An oral defense of this thesis took place on June 26, 2020 in front of the following examining committee:

Examining Committee

Chair of Examining Committee	Prof. Hossam Gaber
Research Supervisor	Prof. Markus H.A. Piro
Examining Committee Member	Prof. Matthew Kaye
Thesis Examiner	Dr. Joanna Mcfarlane, Oak Ridge National Laboratory

The above committee determined that the thesis is acceptable in form and content and that a satisfactory knowledge of the field covered by the thesis was demonstrated by the candidate during an oral examination. A signed copy of the Certificate of Approval is available from the School of Graduate and Postdoctoral Studies.

Abstract

Generation IV nuclear power technologies, including various molten salt reactor designs are considered to accommodate growing energy needs with minimal impact on the environment. The development of the molten salt reactor class highly depends on understanding molten fluoride salt physicochemical properties, which are studied and verified by reviewing existing data coupled with modern experimental techniques.

Experimental investigations of thermodynamic properties of several fluorides were performed to fill knowledge gaps identified in the thermodynamics of fluoride salts. A custom crucible design, selection of suitable calibrants, sample preparation refinement, benchmarking, qualification, and new experimental measurements have been performed. Crucibles worked well for phase transition measurements, benchmarking results gave confidence in developed procedures, capabilities and limitations of the proposed approach were also identified. New measurements of the LiF – CsF system filled some knowledge gaps on the melting behaviour and revealed an additional phase that was not previously reported in the open literature.

Keywords: molten salt reactor; fluoride salts; thermodynamics; fission products; DSC

Author's Declaration

I hereby declare that this thesis consists of original work of which I have authored. This is a true copy of the thesis, including any required final revisions, as accepted by my examiners.

I authorize Ontario Tech University to lend this thesis to other institutions or individuals for the purpose of scholarly research. I further authorize Ontario Tech University to reproduce this thesis by photocopying or by other means, in total or in part, at the request of other institutions or individuals for the purpose of scholarly research. I understand that my thesis will be made electronically available to the public.

Ksenia Lipkina

Statement of Contributions

I hereby certify that I am the sole author of this thesis and that no part of this thesis has been published or submitted for publication. I have used standard referencing practices to acknowledge ideas, research techniques, or other materials that belong to others. Furthermore, I hereby certify that I am the sole source of the creative works and/or inventive knowledge described in this thesis.

Preface

The primary objective of this thesis was to develop processes and procedures to perform new thermodynamic measurements of various fluoride systems, including the LiF – CsF system. Unfortunately, the final course of the experimental campaign came to a premature end due to the university closing in response to the COVID-19 pandemic. As a result, the experimental investigation of the LiF – CsF system was stopped partway through and a few mixtures could not be measured.

Acknowledgements

First and foremost, I would like to express my gratitude to my supervisor Markus Piro at Ontario Tech University, who guided me throughout this interesting project. Prof. Piro's persistent help and positive outlook encouraged me to move forward and be professional even when the journey got tough.

I would like to offer my special thanks to postdocs Dr. Ernesto Geiger and Dr. Bernie Fitzpatrick, as well as Dan Hallatt for helping me with the experimental work and endless fruitful brainstorming discussions. My deepest thanks are given to the entire Nuclear Fuels and Materials Group for providing constructive comments and feedback.

The FESNS administrative staff and security officers at Ontario Tech University are greatly acknowledged. I would like to recognize Prof. Matthew Kaye for his support and allowing me to use equipment in his laboratory. The lab technicians Robert Ulrich and Callan Brown deserve to be acknowledged for their help and assistance.

Thanks should be made to Dr. Ondřej Beneš at the Joint Research Centre, Dr. Elisa Capelli at the Frascati Research Centre, Prof. Anna L. Smith and Jaén Ocádiz-Florez at the Delft University of Technology for sharing their molten salts expertise and knowledge. Prof. Theodore M. Besmann and postdoc Dr. Kaitlin Johnson at the University of South Carolina are also acknowledged for extensive collaborative efforts in developing experimental procedures. Also, I would like to thank Dr. Stephen S. Raiman at the Oak Ridge National Laboratory for donating FLiNaK samples.

Finally, I owe more than thanks to my parents and my husband for making me strong and believing in me when I doubted myself.

This research was undertaken, in part, thanks to funding from the Canada Research Chairs

(950-231328) program and from the Discovery Grant program of the Natural Sciences and Engineering Research Council of Canada. Funding for equipment from the Canadian Foundation for Innovation, the Ontario Ministry of Economic Development, Job Creation Trade, and Ontario Power Generation through the Ontario Tech University Research Infrastructure Fund are greatly acknowledged.

Abbreviations

ARE Aircraft Reactor Experiment

BN Boron Nitride

CALPHAD CALculation of PHAse Diagram

CNL Canadian Nuclear Laboratories

DSC Differential Scanning Calorimetry

FP Fission Product

GEN Generation

GIF Generation IV International Forum

ICTAC International Confederation for Thermal Analysis and Calorimetry

IUPAC International Union of Pure and Applied Chemistry

JRC Joint Research Centre

LWR Light Water Reactor

MSBR Molten Salt Breeder Reactor

MSFR Molten Salt Fast Reactor

MSR Molten Salt Reactor

MSRE Molten Salt Reactor Experiment

Ni Nickel

ORNL Oak Ridge National Laboratory

OTS Oxygen Trap System

R&D Research and Development

RM Reference Material

SMR Small Modular Reactor

SS Stainless Steel

STA Simultaneous Thermal Analysis

TEI Terrestrial Energy Incorporated

TGA Thermogravimetric Analysis

TU Delft Delft University of Technology

U.S. United States

VHTR Very-High-Temperature Reactor

XRD X-ray Diffraction

Contents

Abstract v

Author's Declaration vii

Statement of Contributions ix

Preface xi

Acknowledgements xiv

Abbreviations xvi

List of Figures xxv

List of Tables xxvii

1. Introduction 1

1.1. Current nuclear power reactor technologies 1

1.2. The Molten Salt Reactor Design 4

1.2.1. Key Aspects of the Molten Salt Reactor Class 4

1.3. Chemistry of Fluoride Salts 6

1.3.1. Fluoride Salts Properties 6

1.3.2. Differential Scanning Calorimetry 7

1.4. Summary of Fluoride Salts 9

2. Goals of Research **13**

3. Literature Review **15**

3.1. A Brief Historical Background on MSRs 15

3.2. Thermodynamic Investigations of Fluoride Salts 17

3.3. Fluoride Salts Measurements 28

3.3.1. Experimental Techniques 28

3.3.2. DSC Temperature & Sensitivity Calibration 32

3.3.3. Sample Preparation 35

4. Methodology **39**

4.1. Crucible Design 39

4.2. DSC Calibration Procedures 43

4.2.1. Suitable Calibrants 43

4.2.2. Calibration Measurements 46

4.2.3. Calibration Profiles 48

4.3. Sample Preparation 54

4.3.1. Laboratory Equipment 54

4.3.2. Non-Actinoid Fluorides 56

4.3.3. Actinoid Fluorides 57

4.4. Sample Encapsulation in a DSC crucible 63

4.4.1. Single-Component Samples 63

4.4.2. Multi-Component Samples 64

4.5. DSC Measurements 66

4.5.1. Phase Transition Measurements 67

4.5.2. Specific Heat Capacity 67

4.5.3. DSC of Multi-Component Mixtures 69

5. Results **73**

5.1. Benchmarking 73

5.1.1. Measurements of FLiNaK 73

5.1.2. Measurements of ThF_4 . . . 75
5.2. The LiF–CsF system . . . 81
5.3. Error Analysis . . . 84

6. Discussion **91**
6.1. Crucible Design & Qualification . . . 91
6.2. DSC Calibration Campaign . . . 93
6.3. Sample Preparation Refinement . . . 96
6.4. Benchmarking . . . 97
6.4.1. Measurements of FLiNaK . . . 97
6.4.2. Measurements of ThF_4 . . . 98
6.5. The LiF–CsF system . . . 101

7. Conclusions **105**

8. Recommendations **107**
8.1. Temperature Calibration . . . 107
8.2. DSC Measurements . . . 108
8.3. ThF_4 Purification . . . 109

References **111**

List of Figures

1.1. Generations of nuclear reactors over time. 2

1.2. A generic design of an MSR. 5

1.3. A general schematic diagram of the DSC configuration. 9

1.4. Investigated fluoride binary systems reported in the open literature. 11

3.1. A schematic of the 1940's MSR. 16

3.2. An optimized $LiF-ZrF_4$ binary system with experimental measurements superimposed. 18

3.3. The $LiF-ThF_4-UF_4$ system. Copied from Grimes et al. 19

3.4. Assessed $LiF-BeF_2$ binary system from Beneš et al. with superimposed experimental data from Thoma et al. 20

3.5. Isothermal plot of the $LiF-BeF_2-ThF_4$ phase diagram at T=839 K. Copied from Beneš et al. 21

3.6. The optimized phase diagram of the $LiF-ThF_4$ binary system. • - Experimental data obtained by Capelli et al., ○ - Experimental data obtained by Thoma et al. Copied from Capelli et al. 22

3.7. The liquidus projection of the $LiF-CeF_3-ThF_4$ phase diagram assessed in this study. Primary crystallization phase: (1) CeF_3; (2) $ThCeF_7$; (3) $CeTh_2F_{11}$; (4) ThF_4; (5), $LiTh_4F_{17}$; (6) $LiTh_2F_9$; (7) $LiThF_5$; (8) Li_3ThF_7; (9) LiF. Copied from Beneš et al. 23

3.8. A phase diagram of the CaF_2-ThF_4 binary system with experimental data (●). Copied from Capelli et al. 25

3.9. A phase diagram of the $CsF-ThF_4$ binary system with experimentally obtained equilibrium data in this work (■) and reported in literature (○). Copied from Vozárová et al. 25

3.10. The pseudo-binary phase diagram of the LiF – CsI. Copied from Capelli et al. . . 26

3.11. Phase diagram of the LiF – CsF binary system modelled by Capelli et al. with (■, •) superimposed experimental data obtained by Thoma et al. 27

3.12. The liquidus projection of the calculated $LiF-ThF_4-CsF$ system. Primary crystallization fields: (A) LiF; (B) Li_3ThF_7; (C) $LiThF_5$; (D) $LiTh_2F_9$; (E) $CsTh_3F_{13}$; (F) $Cs_2Th_3F_{14}$; (G) α-$CsThF_5$; (H) $LiCsF_2$; (I) ThF_4; (J) $CsTh_6F_{25}$; (K) $CsTh_2F_9$; (L) β-$CsThF_5$; (M) Cs_2ThF_6; (N) Cs_3ThF_7; (O) CsF. Copied from Capelli et al. 27

3.13. Superimposed XRD patterns of the $CaThF_6$ compound obtained experimentally (in red) and calculated (in black). Copied from Capelli et al. 29

3.14. A typical melting sequence measured by DSC. U is the heat flow signal. Copied from Beilmann et al. 30

3.15. JRC DSC Crucible design. Copied from Beneš et al. 31

3.16. An engineering drawing of a non-lined Ni crucible design for DSC measurements of fluoride salts. Copied from Hallatt. 32

3.17. A prototype of Ni crucible design developed for the Netzsch DSC. Copied from Hallatt. 32

3.18. Determination of the onset temperature for the temperature calibration and the peak area for the enthalpy calibration. Modified from the Netzsch Proteus software. 33

3.19. Stacked Ni reaction vessels for purification of actinoid fluorides designed by Hallatt. 37

4.1. Netzsch Jupiter 449 F1 STA used in this work. 40

4.2. A punch set and a hydraulic press setup to fabricate Ni gaskets. 41

4.3. An engineering drawing of a Ni-201 liner developed for DSC measurements of fluoride salts. All units are in mm. 42

4.4. A DSC crucible set for use in a Netzsch Jupiter 449 F1 STA. From left to right: Netzsch SS crucible body, Netzsch SS crucible lid, custom designed Ni-201 gasket, and custom Ni-201 liner. 43
4.5. A full DSC crucible set after the DSC Zn calibration run. The test was stopped after two heating cycles. 44
4.6. An illustration of the temperature range for DSC calibration. 45
4.7. DSC sequences of the Sn calibration run at 2, 5, and 10 K/min heating rates. . . 47
4.8. Evidence of the chemical interaction between a DSC crucible and K_2SO_4 after a calibration run. The sample crept up the walls. 48
4.9. Temperature calibration data at different heating rates. 49
4.10. Linear regression analysis of experimentally obtained temperature calibration values. 50
4.11. Linear regression analysis of experimentally obtained sensitivity calibration values. 52
4.12. The MBRAUN glovebox used for fluoride salts investigations. 55
4.13. A set-up of the dehydration/purification procedures of the fluoride samples, including a Thermo Scientific Cimarec hotplate with a beaker on top and a retort stand with the thermocouple inserted next to the hotplate. 56
4.14. A CsF sample before and after dehydration. 58
4.15. Reaction vessel for the ThF_4 purification procedure used at TU Delft. Photographs provided by Ocádiz-Flores. 59
4.16. JRC DSC crucibles used as sealed reaction vessels for ThF_4 purification using Method B. 60
4.17. Fluoride salt samples are decanted into the DSC crucible then weighed with a high-precision mass balance within the glovebox. 63
4.18. The Netzsch sealing press used to tighten the DSC crucibles. 64
4.19. A pair of crucibles sits on top of inert Al_2O_3 discs (not visible) within the high sensitivity TGA-DSC-C_p sample holder. The Netzsch OTS is shown on the bottom, which is a Zr metal ring. 66
4.20. A DSC sequence of FLiNaK for the phase transition measurements: the 2nd melting shows the onset temperature for melting point determination, while the 3rd shows the peak area for the enthalpy determination. 68

4.21. A DSC sequence of the second heating cycle of the 15 mol% LiF – 85 mol% CsF composition for the phase transition measurements: onset temperature - solidus, offset temperature - liquidus. 71

5.1. A DSC sequence of the FLiNaK melting point determination and enthalpy measurements. 74

5.2. A DSC sequence of FLiNaK specific heat capacity measurements. 75

5.3. Results of specific heat capacity measurements of solid FLiNaK studied in this work and reported values summarized by Romatoski et al. 76

5.4. Results of specific heat capacity measurements of liquid FLiNaK studied in this work and reported values summarized by Romatoski et al. 76

5.5. A DSC sequence of ThF_4 purified with Method A. 77

5.6. A ThF_4 sample prepared with Method A after a DSC measurement. The sample came out as a puck with no observed wall-salt interaction. 78

5.7. A DSC sequence of an as-received sample of ThF_4. 78

5.8. A DSC sequence of the ThF_4 sample purified with Method B. 79

5.9. Mass measurements of the ThF_4 sample by TGA signal during the programmed heating cycles. 80

5.10. A comparison of an as-received sample of ThF_4 before and after the purification procedures with Method B. 80

5.11. DSC melting point determination of pure LiF. 81

5.12. DSC melting point determination of pure CsF. 82

5.13. An entire DSC sequence of the 15 mol% LiF – 85 mol% CsF composition. 83

5.14. Analysis of DSC mixing measurements of the 15 mol% LiF – 85 mol% CsF composition. 85

5.15. Analysis of DSC mixing measurements of the 55 mol% LiF – 45 mol% CsF composition. 86

5.16. A comparison of crucibles before and after DSC measurements, which shows the degree of oxidation. 87

5.17. Open crucible with the solidified 15 mol% LiF – 85 mol% CsF sample and Ni gasket after a DSC measurement, which shows no chemical interaction between the salt and the Ni surfaces. 87

5.18. A modelled LiF – CsF phase diagram (black solid lines) from Capelli et al. with superimposed experimental data (•, ■ - previously obtained experimental data; ⋆ - this work). 88

6.1. Netzsch SS crucibles with inserted BN liners received from the CeraQuest Innovative Solutions, Les Clayes-sous-Bois, France. 92

6.2. Cracked BN liners received from CeraQuest Innovative Solutions, Les Clayes-sous-Bois, France. 93

6.3. The DSC sample carrier behaviour throughout the calibration procedures. 95

6.4. XRD diffraction patterns of (a) an as-received ThF_4 sample, and (b) a purified ThF_4 sample. Copied from Hallatt. 99

6.5. 4740 High Pressure/High Temperature Pressure Vessel 75 mL procured for purification procedures of actinoid fluorides. Image provided by Parr Instrument. 101

6.6. A proposed LiF – CsF diagram based on experimental points obtained by DSC measurements in this work (•) and superimposed experimental data obtained by Thoma et al. (■, •). Dashed lines represent phase transitions that require further investigation. 104

List of Tables

1.1. Various applications of molten salts. Copied from Beneš et al. 8

3.1. Recommended values of temperatures and enthalpies of fusion of pure metals. . . 34
3.2. Compatibilities of calibrants with crucible materials. 35
3.3. Inorganic calibrants (their solid-state transition temperatures and enthalpy of solid-state transitions) compatible with platinum crucible. 35

4.1. DSC temperature calibration matrix developed in this work for the custom crucible design. 45
4.2. Temperature calibration matrix. 51
4.3. Sensitivity calibration matrix. 53
4.4. Summarized purification matrix applied to each ratio of ThF_4 and NH_4HF_2. . . . 62
4.5. Planned experimental DSC test matrix of the LiF – CsF system. 65

5.1. Results of DSC measurements of FLiNaK, including melting point and enthalpy of fusion. 74
5.2. Equilibrium data of the LiF – CsF system obtained by DSC measurements. 84
5.3. Measured mass of compositions for DSC measurements of the LiF – CsF system. . 89

Chapter 1

Introduction

The growing need for electricity is a primary factor in maintaining a high standard lifestyle. Aside from meeting the escalating electricity demand, the world faces the challenge of climate change. As a result, low-carbon emitting electricity generation is a high priority in the energy sector.

For over six decades, nuclear power technologies have proven to be a reliable source of clean (i.e., very low carbon emission) and affordable electricity. As a step forward to leading innovations, there is great interest in enhancing conventional nuclear power reactors that were commercialized several decades. Developing advanced nuclear power technologies requires the following considerations: safety, sustainability, reliability, economic competitiveness, and proliferation resistance. A leading approach to innovation is to acknowledge and leverage existing nuclear power technologies coupled with innovative design concepts.

Currently operating nuclear power reactors and emerging technologies are briefly mentioned in §1.1, an introduction to Molten Salt Reactors (MSRs) is given in §1.2, MSRs peculiarities and properties are discussed in §1.3 and §1.4, respectively.

1.1 Current nuclear power reactor technologies

Nuclear power systems were initially derived from designs developed for military naval use in the late 1940s and 1950s [1]. Figure 1.1 shows the evolution of nuclear power reactor technologies. Generation (GEN) I reactors were essentially "proof-of-concept" [1]. GEN II reactors were designed to be economical and reliable with an anticipated lifetime of about 40 years [1]. GEN II reactors include Pressurized Water Reactors, Boiling Water Reactors, CANDU reactors, Advanced

Gas-Cooled Reactors, and Vodo-Vodyanoi Energetichesky Reactors [1]. GEN III reactors are essentially GEN II reactors with advanced features and about a 60 year lifetime, whereas GEN III+ are modest evolutionary designs of GEN III with additional safety improvements [1]. Commercial power reactors with advanced features and safety improvements are currently operating worldwide [2].

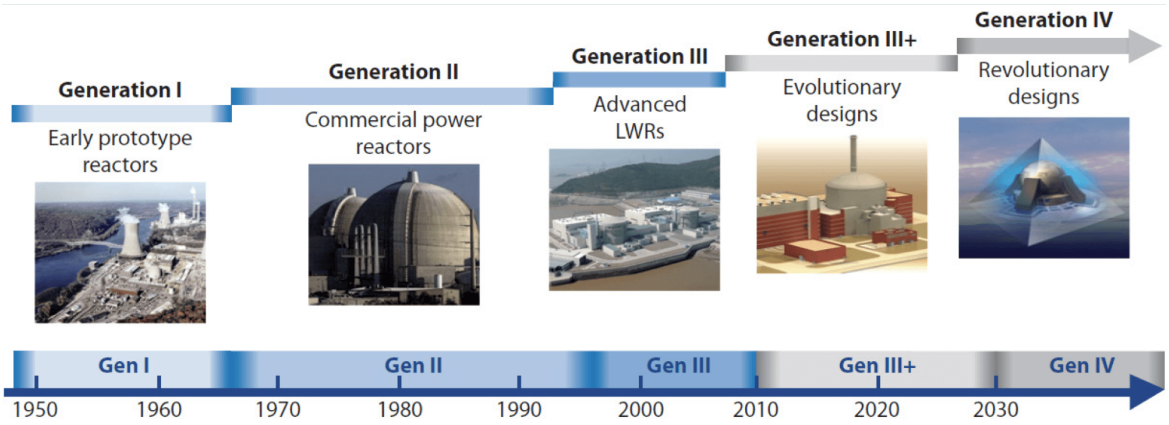

Figure 1.1: *Generations of nuclear reactors over time [2].*

The Generation IV International Forum (GIF) was established in 2001 and currently has eleven contributing nation states [2]. Its primary focus is the development of GEN IV nuclear energy systems [2]. GEN IV designs are intended to use fuel more efficiently than GEN II and GEN III designs, reduce waste production, be economically competitive, and meet stringent standards of safety and proliferation resistance [3]. One of the important components for achieving the sustainability goal is closing the nuclear fuel cycle. This is mainly based on the reprocessing and recycling of spent nuclear fuel [2]. The premise of this approach is that fissile material can be recovered from spent fuel and recycled to make new fuel ready for use in a power reactor [2]. According to the Roadmap Update for GEN IV, almost 95% of used fuel produced from Light Water Reactors (LWRs) can be reused in the form of reprocessed uranium and Mixed Oxide fuel [2]. The economic feasibility of such an activity is still not certain [4].

After an extensive evaluation of over 130 reactor concepts, six systems were selected by the GIF, which are [3]:

- Gas-Cooled Fast Reactor;
- Lead-Cooled Fast Reactor;

- MSR;
- Sodium-Cooled Fast Reactor;
- Supercritical-Water-Cooled Reactor;
- Very-High-Temperature Reactor (VHTR).

A type of reactor with about 300 MW(e) equivalent or less is categorized as a Small Modular Reactor (SMR) [5], which has been gaining worldwide interest as another scale for power generation. Moreover, emphasis is placed on SMR designs based on GEN III or GEN IV technologies (i.e., fast neutron reactors, graphite-moderated high-temperature reactors, LWRs, and MSRs) [2, 5].

Canada recognizes the importance of developing GEN IV systems and SMRs to accommodate growing energy needs with minimal impact on the environment. Furthermore, the government of Canada supports and is open to innovations in this sector of the economy. The full set of detailed recommendations in relation to federal government funding, waste managements risk-sharing, nuclear security, regulatory efficiency, and expected results have been documented in the Roadmap for SMRs, published by the SMR Roadmap Steering Committee [6]. In addition, the potential of SMR deployment in Canada has been recognized with regards to three major applications [7]:

- On-grid power generation replacement coal plants;
- Combination of on-grid and off-grid heat and electrical power for heavy industries;
- Off-grid power and heat for remote communities highly dependent on diesel fuel, especially the Northwest Territories of Canada.

The Canadian Nuclear Laboratories (CNL) has offered its site and expertise to build, at a minimum, one SMR unit by 2026 [7]. Four companies (i.e., Kairos Power, Moltex Energy Canada, Terrestrial Energy Incorporated (TEI), and Ultra Safe Nuclear Corporation) supported by CNL Research and Development (R&D) expertise proposed various SMR designs to deploy at Chalk River [8]. Two privately funded Canadian companies, TEI and StarCore Nuclear located in Ontario and Quebec, respectively, have combined R&D forces with CNL in order to deploy SMRs

on CNL site [9]. Both companies have successfully moved to the Due Diligence stage, where the proposed designs will be fully assessed and the necessary business requirements will be established [10].

The design proposed by StarCore Nuclear is a 14 MW(e) high-temperature gas reactor, which may potentially be built at the Whiteshell or Chalk River CNL sites in Manitoba or Ontario [10]. A different approach in an SMR design was taken by TEI and Moltex Energy. The proposed design from TEI is a 195 MW(e) integral MSR [10]. The integral MSR concept has a liquid fluoride salt fuel and primary reactor components in a sealed and replaceable core unit [11]. A stable salt reactor concept proposed by Moltex Energy is a molten salt fuel assembled in vented tubes similar to a conventional fuel assembly approach [12]. Moreover, having hazardous fission products in the form of stable compounds as opposed to gases, Moltex Energy aims to enhance safety aspects of the reactor operation [12]. While there are multiple reactor concepts currently being considered for deployment in Canada, this thesis will focus on the MSR concept.

1.2 The Molten Salt Reactor Design

1.2.1. Key Aspects of the Molten Salt Reactor Class

The MSR class of designs has gained considerable interest in recent years as a potential large-scale GEN IV plant (e.g., ∼1000–1600 MW(e)) or an SMR design (e.g., ∼100–300 MW(e)). The main distinguishing design feature of the MSR lies in its core in which the fuel can be either a) in a solid state, as in conventional reactors, but with a molten salt coolant, or b) dissolved in a fluoride or chloride salt mixture, which also serves as a coolant. A generic design of an MSR, where molten salt could serve as both the reactor fuel and the primary coolant, is illustrated in Figure 1.2. Heat is generated in the reactor core and transported by the fuel salt to heat exchangers before returning to the reactor core with a lower temperature. In response to an accident, emergency dump tanks that are included in some designs allow the molten salt to drain from the core. It is a passive safety system that is gravity driven and the evacuation of fuel from the core leaves it subcritical [13]. As outlined by Serp et al., MSR coolant operates at much higher temperatures (up to 700–750 °C) than LWRs (e.g., 280–320 °C) but at nearly atmospheric hydrostatic pressure [14]. The latter is indicated as an important safety advantage whereby passive decay heat is removed and there is a

greatly reduced potential for an explosion in case of a leak.

The molten salt used to dissolve a fuel material (i.e., fertile or fissile) is often referred as a fuel solvent. The properties of the fuel solvent must meet the following requirements: low neutron capture cross-section, low melting temperature, and high solubility of actinoid fluorides (e.g., PuF_3, ThF_4, UF_4) and fission products [15].

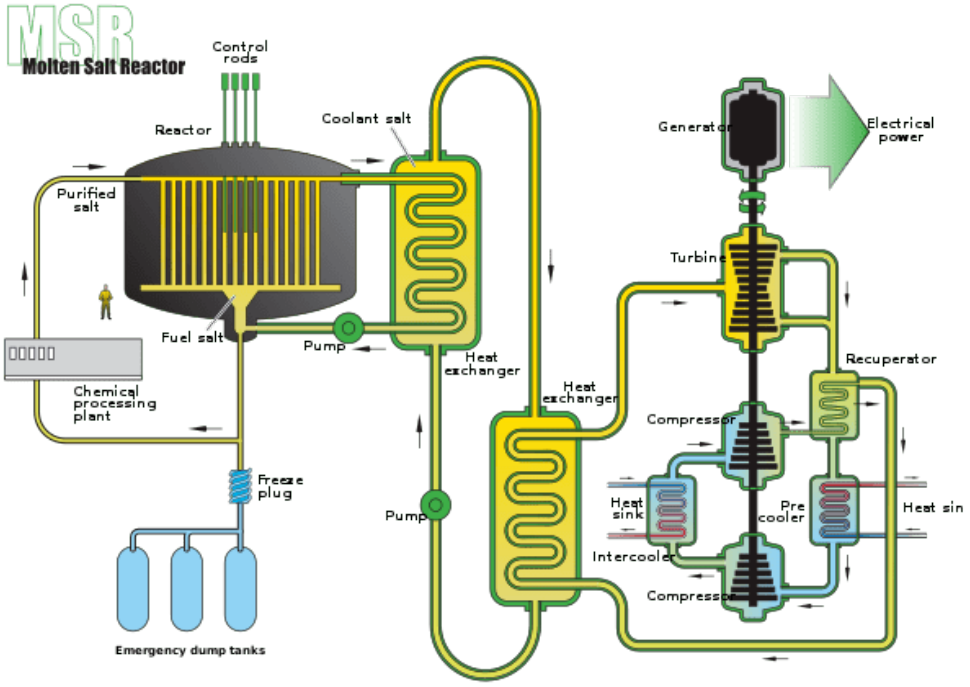

Figure 1.2: *A generic design of an MSR [16].*

Molten fluoride salt studies were first initiated mainly because fluorine has only one stable isotope (i.e., ^{19}F), as opposed to chloride salts, which have several (i.e., ^{35}Cl, ^{36}Cl, and ^{37}Cl) [14]. There are a number of advantages of fluoride salts in comparison to chloride salts, such as: a) a wide range of solubility of the fissionable elements U, Pu, and Th; b) thermodynamic stability and ability to not undergo radiolytic decomposition; and c) very low vapour pressure at typical operating temperatures [17, 18]. Despite the advantages mentioned above, molten fluoride salts can be quite corrosive, even more than chloride salts. The formation of protective oxide layers of the elements added to an alloy-base (e.g., Cr, Al, or Si) is quite chemically unstable in fluoride salts [19].

Structural materials considered for MSR application include the following: INOR 8, Hastelloy-

B, Hastelloy-N, other Nickel(Ni)-based alloys, niobium-titanium alloys, and graphite [20]. A 2 wt% titanium addition to those alloys is proposed in order to prevent irradiation embrittlement. [20]. Challenges of using graphite as an in-core structural material as well as a moderator are the following: dimensional changes and salt penetration due to radiation damage, and xenon absorption leading to an increase of fission product poisoning [20].

Ni-based alloys have proven to be suitable for MSR structural materials for their excellent corrosion resistance to fluorides. For example, compatibility of INOR-8 with graphite is considered acceptable at elevated temperatures (i.e., with sodium-free salts up to 815 °C and with sodium salts up to 700 °C) [2, 20]. Consequently, long-term testing is still required for a modified Hastelloy-N for use with fluorides at temperatures up to 800 °C [2, 20]. After identifying the foregoing challenges in MSR designs, it is essential to outline fundamental principles of fluoride salts where the chemistry of these salts is of great interest.

1.3 Chemistry of Fluoride Salts

Various molten salt compositions outlined by Beneš et al. [21] are under consideration for different MSR designs and applications (see Table 1.1). Several knowledge gaps regarding the chemical behaviour of proposed fuel salt mixtures with Fission Products (FPs) have been identified as an important consideration with respect to reactor performance and safety [22].

Understanding molten fluoride salt physical and chemical properties is a great challenge in the context of performance and safety. Considering previous MSR studies and available data, one needs to verify that collected information complies with constantly evolving safety requirements established by regulatory institutions. Hence, a review of the existing data by employing modern techniques can be valuable for the development of reliable MSRs.

1.3.1. Fluoride Salts Properties

MSR fuel is a multi-component system that has a wide range of physical and chemical properties (i.e., melting point, heat capacity, enthalpy of fusion, thermal conductivity, viscosity, vapour pressure, surface tension, and gas and FP solubility) [23]. Furthermore, understanding such properties is essential to develop reliable and safe MSR technologies. A phase diagram is a fundamental

tool for understanding the chemical behaviour of salt mixtures, which could potentially serve either as a fuel salt or coolant. A number of complex phase transitions can occur in molten salts; for instance, throughout the freezing process, both the melt and frozen solid may vary in composition [23]. In order to provide a comprehensive understanding of the phase behaviour, important material properties, such as heat capacity, melting point, FP solubility, and enthalpy of fusion require an extensive investigation [23]. A slight modification in the composition of a salt may greatly change those properties [23].

The melting point of a salt mixture is one of its key material properties, which varies greatly with composition. Melting points can be predicted and described by thermodynamic modelling utilizing the CALculation of PHAse Diagram (CALPHAD) method [24] coupled with thermodynamic software (e.g., FactSage [25]). To support modelling predictions, melting points can be determined experimentally by using a Differential Scanning Calorimetry (DSC) technique. With regards to safety assessments of the fuel, heat capacity is considered one of the pivotal properties [26]. As a safety aspect, it is important to determine the amount of heat that can be absorbed by the fuel before it attains its critical temperature [26]. Employing the DSC technique allows one to determine the heat capacity of the various salt compositions.

1.3.2. Differential Scanning Calorimetry

DSC is a widely used thermochemical experimental technique that allows one to measure the melting temperature, heat capacity, enthalpy of fusion, and enthalpy of mixing of a material sample. The principle of DSC is based on measuring the heat flow of two crucibles (i.e., the reference crucible and the sample crucible) throughout heating and cooling cycles under well-controlled conditions [27]. A generic schematic diagram of a DSC is presented in Figure 1.3. The reference crucible always stays empty, whereas the sample crucible is filled with the material sample (i.e., to differentiate heat flow between the reference and the sample in the temperature range of interest). A furnace is used to heat the system, which is controlled by the software that takes temperature measured by a thermocouple as input. A detailed description of the DSC technique used in fluoride salts studies is discussed in §3.3.

Table 1.1: *Various applications of molten salts. Copied from Beneš et al. [21].*

Reactor type	Neutron spectrum	Application	Molten salt choice including alternatives
MSR Breeder	Thermal	Fuel	^{7}LiF-BeF_2-AnF_4
	Fast	Fuel	^{7}LiF-AnF_4 (Alternative ^{7}LiF-CaF_2-AnF_4, NaCl-UCl_3-$PuCl_3$)
	Secondary coolant	NaF-$NaBF_4$	
MSR Burner	Fast	Fuel	^{7}LiF-NaF-BeF_2-AnF_3 (Alternative LiF-NaF-KF-AnF_3, LiF-NaF-RbF-AnF_3)
AHTR[a]	Thermal	Primary coolant	^{7}LiF-BeF_2
VHTR[b]	Thermal	Heat transfer[e]	LiF-NaF-KF (Alternative LiCl-KCl-$MgCl_2$)
MSFR[c]	Fast	Primary coolant	LiCl-KCl-$MgCl_2$
SFR[d]	Fast	Intermidiate coolant[f]	$NaNO_3$-KNO_3

[a] Advanced High-Temperature Reactor, graphite - moderated, thermal reactor.
[b] Very High-Temperature Reactor, graphite - moderated, gas cooled reactor.
[c] Molten Salt cooled Fast Reactor, the solid fuel fast reactor with MS as a coolant.
[d] Sodium cooled Fast Reactor.
[e] Heat transfer salt is a medium that will be used to deliver heat from the reactor to the hydrogen production plant.
[f] To separate sodium and the steam circuits.

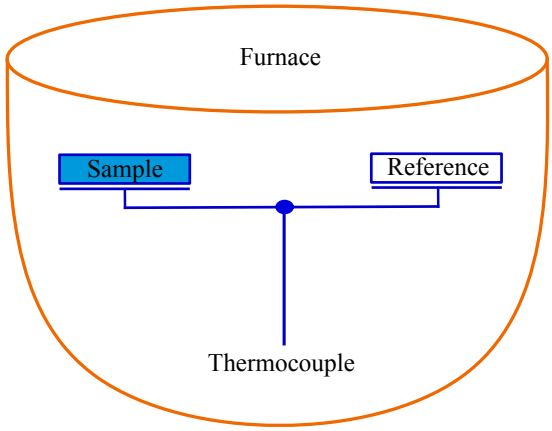

Figure 1.3: *A general schematic diagram of the DSC configuration.*

1.4 Summary of Fluoride Salts

A summary of on-going investigations of fluoride salt chemistry is depicted in Figure 1.4, which allows one to identify knowledge gaps of specific binary systems. There are many systems available worth studying as well as benchmarking. For instance, systems with predominant FPs, such as zirconium, rubidium, molybdenum, iodine, or cesium, are important to examine as they will be produced in appreciable quantities in-reactor. Systems with cesium or iodine are especially of interest to the nuclear community due to the following reasons [23, 26]:

- In case of an accident, the release of radioactive cesium and iodine is a health and environmental concern, which were of a particular issue in the Chernobyl and Fukushima severe accidents. For example, inhaling iodine leads to absorption in one's thyroid, which can be carcinogenic; and cesium's half-life of about 30 years with high energy gamma radiation is known to be a long term complication, which can damage cells and cause cancer.

- In an MSR design, the fuel and coolant are the same salt; hence, FPs are intermixed with the coolant and other core materials, potentially raising corrosion issues of structural materials. The latter may result in raising safety concerns of overall reactor operation.

Preparation as well as handling of high quality fluoride salt mixtures are important aspects to consider for potential experimental work in a university laboratory. The fabrication process of

salts is important to ensure the purity of the sample. Specifically, fluorides are very hygroscopic and must be handled within an inert atmosphere glovebox to prevent contamination coupled with a dehydration process to remove any impurity oxides. While performing DSC measurements of fluoride salts, one must ensure that the DSC crucible does not chemically interact with the sample, which would compromise the accuracy of the measurement.

Overall, in order to execute a comprehensive study of a selected system, one is required to:

- Establish a number of salt fabrication procedures coupled with safety standards;
- Identify and test essential equipment; and
- Perform accurate experimental measurements.

The objectives of this thesis are described in §2, a review of relevant literature is given in §3, the methodology used in this experimental work is described in §4, experimental results are presented in §5, and they are discussed in §6.

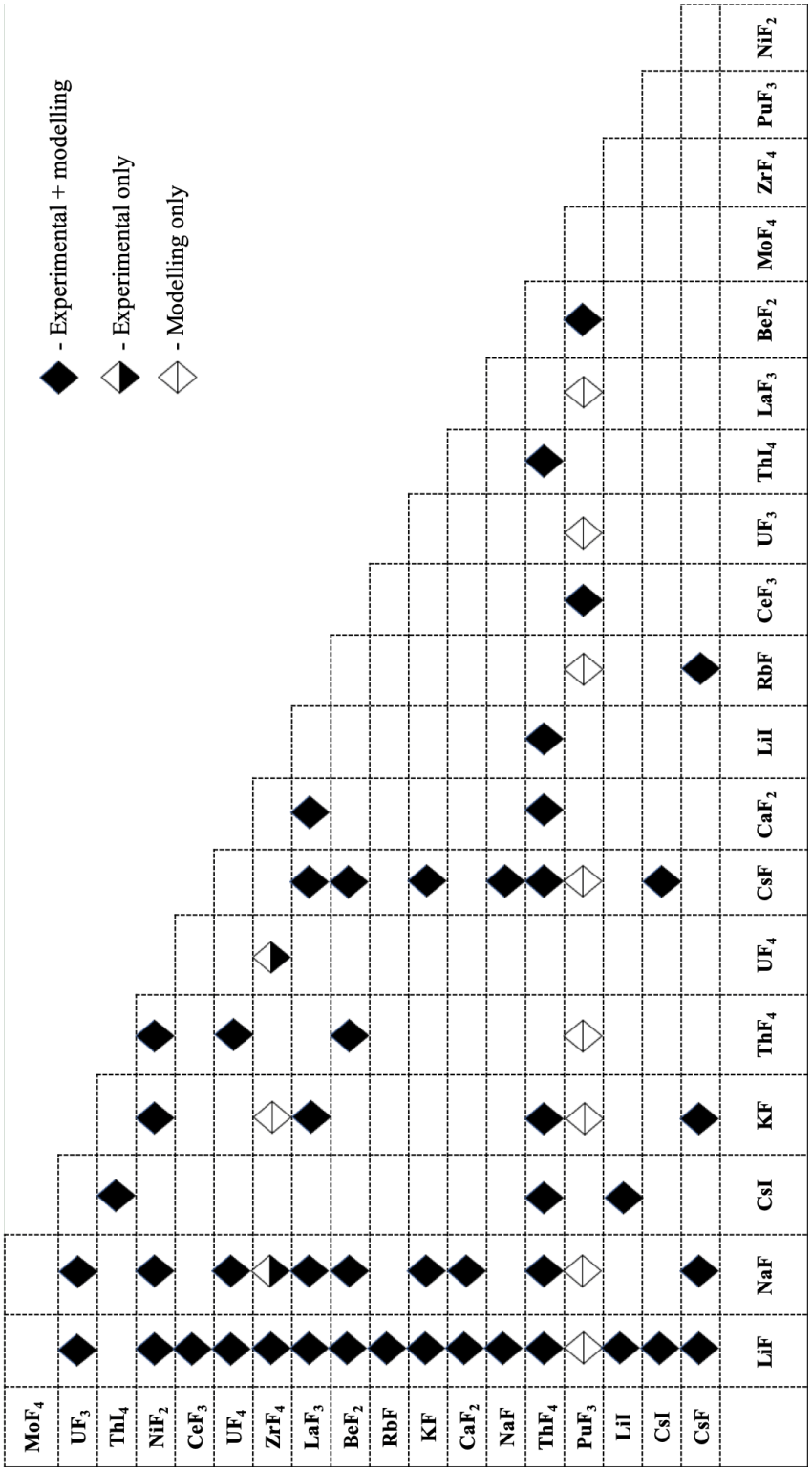

Figure 1.4: *Investigated fluoride binary systems reported in the open literature.*

Chapter 2

Goals of Research

A campaign on thermodynamic investigations of fluoride salts was initiated within the Nuclear Fuels and Materials Group at Ontario Tech University. The overall objective of this campaign is to fill knowledge gaps in fluoride salts to support performance and safety assessments of MSRs in Canada. In support of this campaign, this thesis is dedicated to qualifying a number of procedures and to experimentally measure several fluoride salts. The objectives of this thesis are:

1. Design and qualify a custom crucible compatible with fluoride salts up to 1200 °C in a Netzsch Simultaneous Thermal Analysis (STA);
2. Development of calibration standards for the custom crucible design;
3. Refinement of fluoride salt sample preparation procedures;
4. Phase transition measurements and heat capacity of FLiNaK;
5. Melting point determination of ThF_4; and
6. New phase transition temperature measurements of the LiF – CsF mixtures.

Solubility of cesium in the LiF – CsF binary system was investigated by performing DSC measurements of salt mixtures. Having completed an extensive literature review, several knowledge gaps were identified. For example, the most recent experimental data published in the open literature on the LiF – CsF were obtained by a thermal-gradient quenching testing and differential thermal analysis (i.e., cooling-curve analysis) in 1975 [28]. Re-visiting the LiF – CsF system by employing modern experimental techniques is of great value for the development of molten salt database and can serve a verification procedure for its previously assessed properties.

The LiF – CsF system was relevant to study, considering the importance of cesium solubility as a predominant FP with regards to reactor safety[26]. By applying various well-designed experiments, using modern and well-established techniques, the work described in this thesis gives confidence in the overall experimental approach. Prior to establishing experimental procedures within the laboratory, a comprehensive literature review was performed and is documented in §3.

Chapter 3

Literature Review

This chapter gives a high-level state-of-the-art review on MSR R&D efforts in chemical thermodynamics reported in the open literature to fulfill the objectives of this thesis. This review includes a historical background on MSRs in §3.1, thermodynamic descriptions on previously studied fluoride salt systems (i.e., experimental and modelling activities) in §3.2, and experiences in executing DSC measurements of fluoride salts in §3.3.

3.1 A Brief Historical Background on MSRs

The original idea of MSRs came from the United States' (U.S.) Aircraft Nuclear Propulsion program in the late 1940s [29]. The idea of using molten fluoride salts was proposed by Bettis et al. in the U.S. Aircraft Reactor Experiment (ARE) at the Oak Ridge National Laboratory (ORNL) in Oak Ridge, TN [30].

A schematic of the reactor with the surrounding gas plenum chamber and thermal insulation is illustrated in Figure 3.1 [30]. While the ARE reactor was shut down in 1954, it did manage to successfully operate for 9 days at steady-state with outlet salt temperatures of up to 860 °C and powers up to ~ 0.8 MW(e) [29, 30]. A mixture of NaF, ZrF_4, and UF_4 (53-41-6 mol%, respectively) was used as the ARE fuel salt and beryllium oxide (BeO) was applied as the moderator [30]. Structural materials and piping of the design were made of Inconel 600, which is a Ni-based alloy [29, 30].

MSRs for civilian nuclear use were under consideration as a separate activity from the ARE project. In 1956, a substantial research program initiated by MacPherson et al. showed that for the thermal reactor moderated by graphite, a thorium fuel cycle with ^{233}U recycle would be

the ideal molten salt system [17, 29]. Various MSR concepts explored by MacPherson's group converged on two types of graphite-moderated core designs. A single-fluid design would contain Th and U in the same salt, and a two-fluid design would have Th in a fertile salt, which would be separated from the fissile U containing salt [29]. With growing interest in MSR technology, a two-fluid system was investigated as a thermal breeder reactor producing more fissile ^{233}U from fertile ^{232}Th [17].

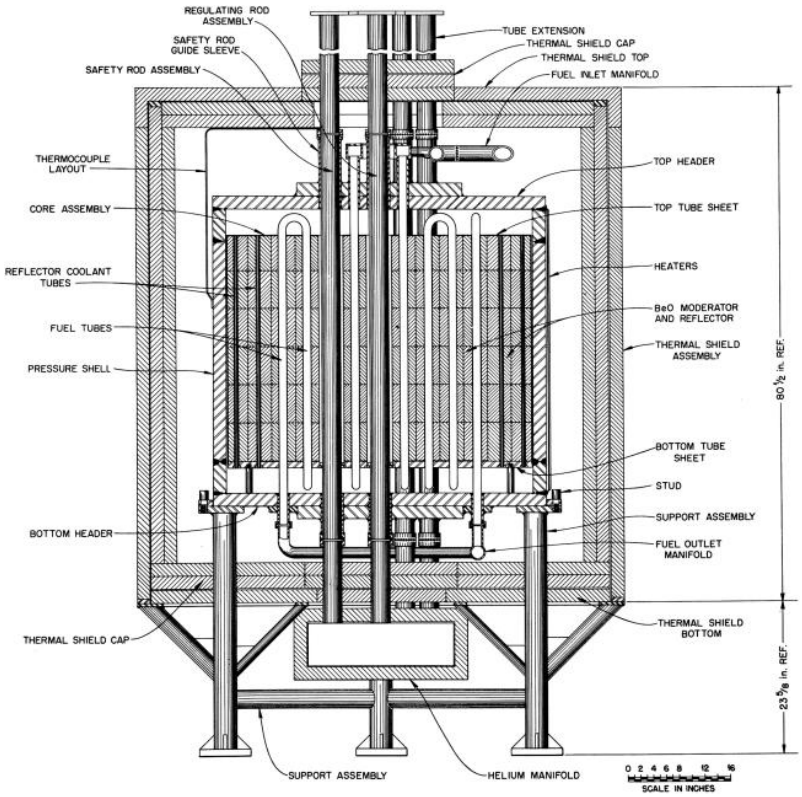

Figure 3.1: *A schematic of the 1940's MSR is shown by Bettis et al. [30]*

In the late 1960, ORNL commenced designing the Molten Salt Reactor Experiment (MSRE) with a focus on its breeding aspect [29]. With both ^{7}Li and Be having very low neutron capture cross-sections, $^{7}LiF-BeF_2$ (commonly referred to as "FLiBe") with 5% ZrF_4 as an oxygen getter was selected as a fuel carrier for the MSRE design [21]. Natural lithium cannot be used as a component in the salt since it contains about 7.6% ^{6}Li, which has a very high parasitic neutron capture cross-section (i.e., $\sigma_{th} = 940$ barn) [21]. Therefore, lithium has to be enriched in ^{7}Li prior to being used as a component in a fuel salt [21].

It was discovered that if FLiBe was chosen as a primary coolant, the undesirable production of

tritium from lithium could occur [31]. Moreover, the formation of tritium fluoride in the molten FLiBe leads to a potential corrosion issue [31]. Structural materials are susceptible to tritium that can diffuse through metal [31].

The MSRE went critical on June 1, 1965 after adding 69 kg of highly enriched ^{235}U in the form of a $LiF-UF_4$ mixture through the drain tanks [32]. The $\sim$ 3.2 MW(e) test reactor operated successfully for 4.5 years until it was shut down in 1969 [32]. The fissile isotopes ^{233}U and ^{235}U were chosen for the MSRE fuel form [32]; Th was not used in the fuel salt mixture as it was intended to simulate only the fuel stream of a two-fluid breeder reactor [32]. As comprehensively reported by Haubenreigh et al. [32] and Engel et al. [33], the MSRE project successfully established key MSR technologies (i.e., molten salt fuel and compatible structural materials).

Following the success of MSRE in the early 1970s, a prototype Molten Salt Breeder Reactor (MSBR) was designed by ORNL to convert ^{232}Th into ^{233}U in a single-fluid design [34]. The design also required a chemical processing facility to clean the fuel salt from fission products and to recover the bred ^{233}U [34]. However, a sudden termination of funding by the US Department of Energy ended the MSBR R&D program [35].

3.2 Thermodynamic Investigations of Fluoride Salts

ORNL proposed a fluoride salt mixture of NaF, ZrF_4, and UF_4 as a fuel and primary heat exchanger fluid [36]. In 1957, an experimental campaign was performed at ORNL to study phase equilibria of two pseudo-binary systems (i.e., $NaF-ZrF_4$ and UF_4-ZrF_4) and one pseudo-ternary system (i.e., $NaF-ZrF_4-UF_4$) [36]. A detailed investigation of the $NaF-ZrF_4$ binary system showed two stoichiometric compounds, Na_3ZrF_7 and $Na_7Zr_6F_{31}$, melt congruently and $Na_5Zr_2F_{12}$, Na_2ZrF_6, and $Na_3Zr_4F_7$ melt non-congruently [36]. In relation to the UF_4-ZrF_4 system, there was a series of solid solutions with a minimum melting temperature of 765 K with 77 mol% ZrF_4 [36].

Subsequently, Thoma et al. studied phase equilibria in the condensed $LiF-NaF-ZrF_4$ ternary system, since the system was chosen as a potential nuclear fuel carrier salt [37]. Experimental studies by Thoma et al. using X-ray Diffraction (XRD) and microscopic techniques revealed nine complex compounds, which presumably formed due to the interchangeability of Li^- and

Na^+ ions in a number of the crystalline phases [37]. Thermal-gradient quenching tests were also employed to investigate phase transition temperatures of the LiF-ZrF_4 binary system [37]. Based on experimental data obtained by Thoma et al. [37] in 1965, a thermodynamic treatment of the LiF – ZrF_4 binary system (liquid solution only) was developed by Beneš [38]. An optimized phase diagram of the LiF – ZrF_4 system is presented in Figure 3.2.

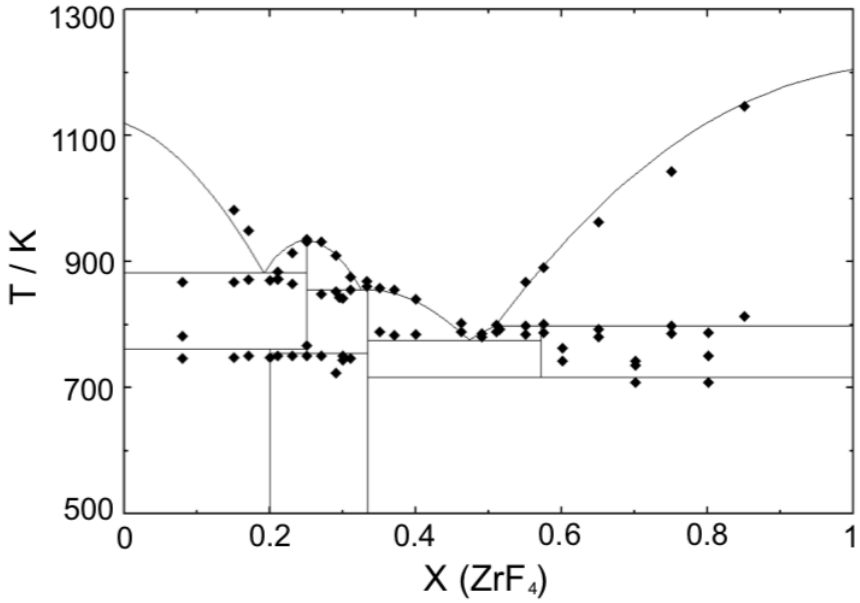

Figure 3.2: *An optimized LiF – ZrF_4 binary system from Beneš [38] with superimposed experimental measurements from Thoma et al. [37].*

In 1970, a detailed summary of R&D activities in support of the MSRE completed by Grimes highlighted studies of the thermodynamic behaviour of various fluorides, including LiF – BeF_2, BeF_2 – UF_4, BeF_2 – ThF_4, LiF – UF_4, and LiF – ThF_4 binary systems [39]. For example, solid phases of the LiF – UF_4 and the LiF – ThF_4 systems studied by Barton et al. [40] and Thoma et al. [41] were obtained by optical measurements and XRD. A thermal analysis and quenching technique revealed non-congruent melt of three compounds and a single eutectic melting at 763 K with 27 mol% UF_4 was present in the system of LiF – UF_4 [39]. The LiF – ThF_4 binary system consisted of four binary compounds with only Li_3ThF_7 melting congruently with two eutectics: 1) at 843 K and 22 mol% ThF_4, 2) at 833 K and 29 mol% ThF_4 [39]. The LiF – ThF_4 – UF_4 system, presented in Figure 3.3, contained no ternary compounds and there was one eutectic freezing at 761 K with 1.5 mol% ThF_4 and 26.5 mol% UF_4 recounted by Grimes and Weaver [39, 42]. A phase

diagram is mainly occupied by phases of solid solutions UF_4-ThF_4, $LiF{\cdot}4UF_4$–$LiF{\cdot}4ThF_4$, and $LiF{\cdot}UF_4$–$LiF{\cdot}ThF_4$, whereas liquidus temperatures decline to the $LiF-UF_4$ region of the diagram [39].

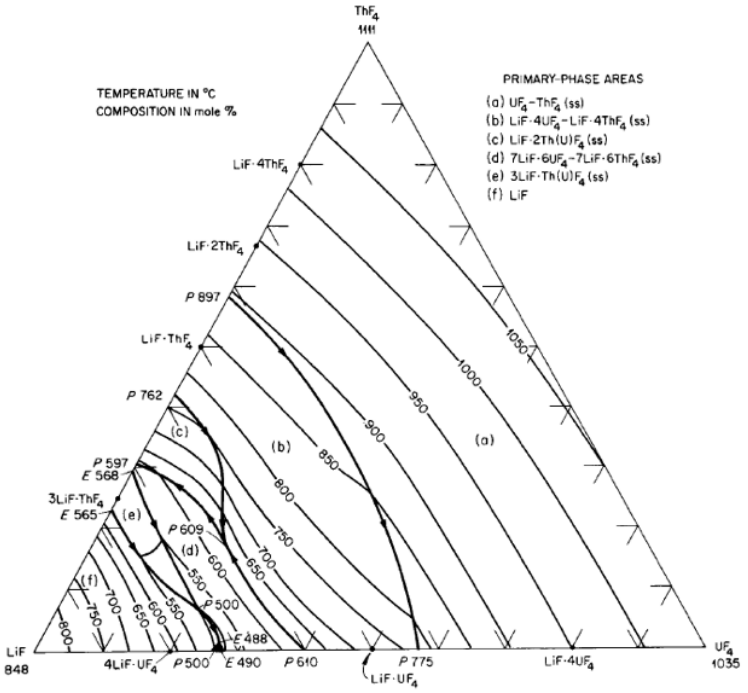

Figure 3.3: *The $LiF-ThF_4-UF_4$ system. Copied from Grimes et al. [39].*

A phase diagram of $LiF-BeF_2$ was characterized by a single eutectic (52 mol% BeF_2, melting at 633 K) between BeF_2 and Li_2BeF_4; the compound Li_2BeF_4 melts non-congruently to solid LiF and liquid at 731 K [39]. Subsequently, van der Meer and Beneš investigated the $LiF-BeF_2$ and the $LiF-BeF_2-ThF_4$ systems by performing a thermodynamic assessment of the pseudo-binary phase diagrams of $LiF-BeF_2$, $LiF-ThF_4$, and BeF_2-ThF_4 systems and the ternary phase diagram of $LiF-BeF_2-ThF_4$ [21, 43]. The difference between the experimental and the calculated phase diagrams appeared to be a miscibility gap in the BeF_2 rich side of the $LiF-BeF_2$ system with the critical temperature of T_c= 812 K and 0.826 BeF_2 [43]. Notably, a miscibility gap was also predicted by Thoma et al. in 1959 [43, 44]. Figure 3.4 represents a calculated phase diagram of the $LiF-BeF_2$ system with experimental data collected by performing various measuring techniques [21]. With the above discussed systems one can see the need for re-evaluation of the previously studied systems in order to support MSR development.

Continuous work on fluoride salts (i.e., the $LiF-ThF_4$ and the $LiF-BeF_2-ThF_4$ systems)

for breeder reactors was performed by van der Meer et al. [45] and Beneš at al. [46] with an emphasis on thermodynamic properties and actinoid solubility. The solubility of actinoids was primarily explained by performing calculations on the solubility of ThF_4 in the $LiF-BeF_2$ salt for the inlet temperature of MSBR (i.e., ∼839 K) [46]. The results are shown in Figure 3.5 [46]. As summarized by Beneš et al., the straight vivid line represents the ratio of 0.818 LiF and 0.182 BeF_2 within the entire region of the phase diagram, and the mole fraction of ThF_4 varies from 0 to 1 when following point "C" towards point "D". The solubility of ThF_4 in the $LiF-BeF_2$ salt is bounded by 9.2 and 20.8 mol% and represented by the interval between points "A" and "B"[46]. The solubility of actinoids is the major issue for transmutation as well as burner fuels [46] and, unfortunately, not many studies were performed on the solubility of PuF_3 as well as on the NpF_4, AmF_4, or CmF_3 solubility [46].

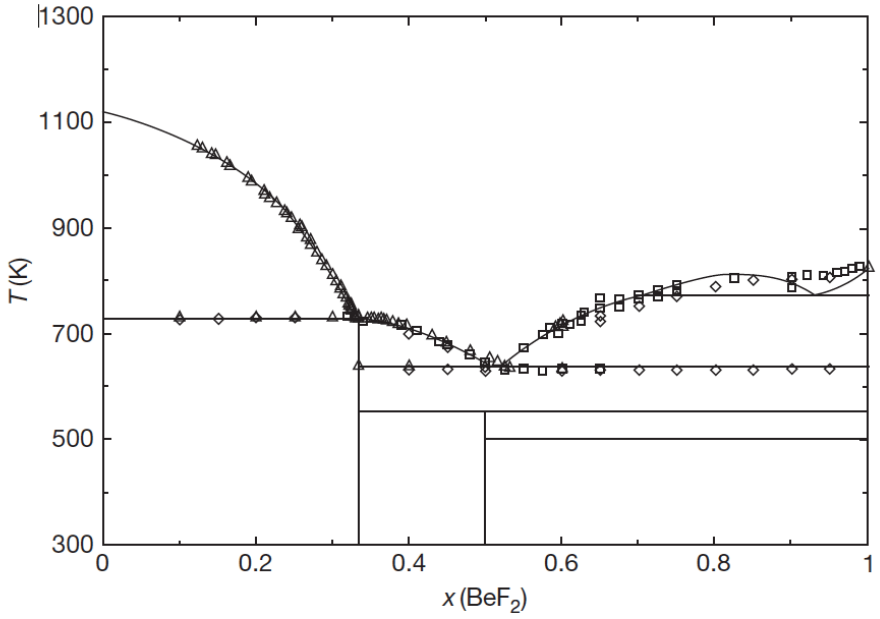

Figure 3.4: *Assessed $LiF-BeF_2$ binary system from Beneš et al. [21] with superimposed experimental data from Thoma et al. [44].*

Subsequently, Capelli et al. proposed a new thermodynamic investigation of the $LiF-ThF_4$ binary system in order to obtain better experimental data [47]. Experiments performed by Thoma et al. showed one congruently melting compound ($LiThF_7$) and three non-congruently melting compounds ($Li_7Th_6F_{31}$, $LiTh_2F_9$, and $LiTh_4F_{17}$) [41]. It should be noted that recent studies by Capelli et al. suggested that $LiThF_5$ was as an intermediate compound as opposed to $Li_7Th_6F_{31}$

[47]. By employing a new technique of mixing enthalpy determination, Capelli et al. re-optimized the $LiF-ThF_4$ binary system (see Figure 3.6) [47]. The complication of the $LiF-ThF_4$ binary system was that mixing would not sometimes occur and the DSC measurements would show some unreacted ThF_4 [47]. Due to complications of the experiments, a limited number of points were taken into account, and two sets of data were obtained: melting temperatures of LiF at 1121 K and ThF_4 at 1383 K [47]. Systematic experimental measurements of systems with actinoids (e.g., ThF_4) performed by various research institutions with benchmarking promote building confidence in obtained results.

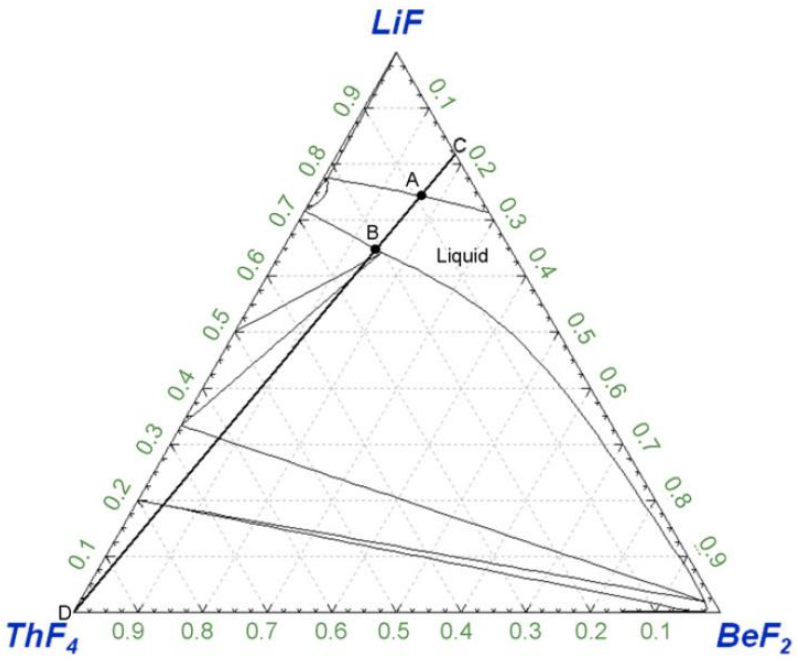

Figure 3.5: *Isothermal plot of the $LiF-BeF_2-ThF_4$ phase diagram at T=839* K. *Copied from Beneš et al. [46].*

To predict the concentration of PuF_3 in a molten salt fuel, Beneš et al. performed the thermodynamic assessment of the full $LiF-CeF_3-ThF_4$ system, using CeF_3 as a surrogate of PuF_3 [48]. Cerium was chosen to eliminate safety concerns with the use of plutonium, assuming that they have similar properties [48]. Another reason to study the $LiF-CeF_3-ThF_4$ ternary system was to obtain the data in order to optimize it for the MSFR concept [48]. Figure 3.7 shows the assessed system. In this study, the calculated lowest ternary melting point of 818 K was confirmed by the experiments [48]. Based on the data obtained by Beneš et al., the melting temperature

of the MSFR fuel containing only PuF_3 as a fissile material is 899 K [48]. If PuF_3 was partially substituted by fissile UF_4, the MSFR fuel melting temperature could be lowered and uranium enrichment should be taken into account in that case [48]. Nonetheless, the experimental approach in studying solubility of PuF_3 can be a valuable contribution to support existing data. It should be noted that not only the concentration of individual components but also the substitution of components may considerably affect the properties of the entire system.

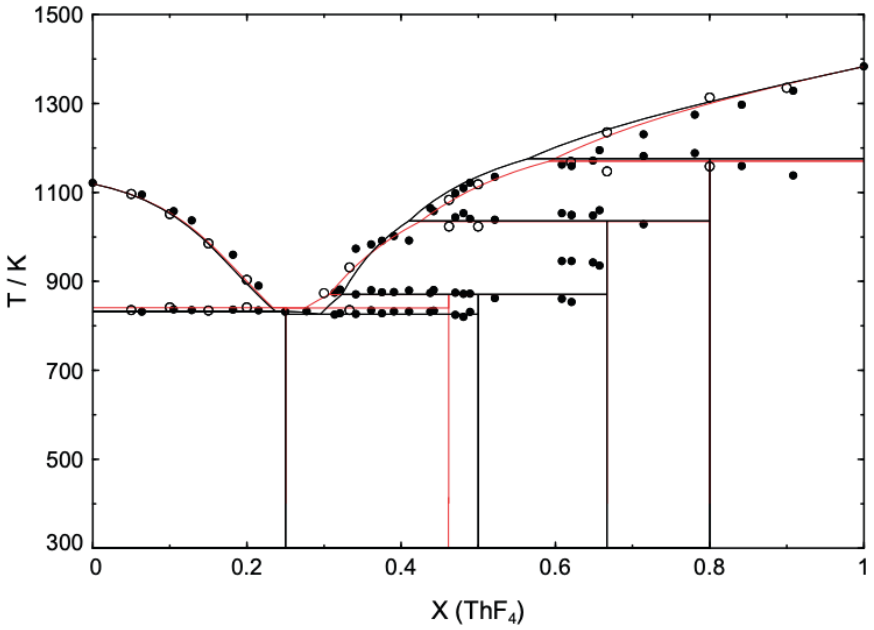

Figure 3.6: *The optimized phase diagram of the $LiF-ThF_4$ binary system. • - Experimental data obtained by Capelli et al., ○ - Experimental data obtained by Thoma et al. Copied from Capelli et al. [47].*

Based on experimental data obtained in the late 60s and 70s, Beneš et al. developed a thermodynamic assessment of the $LiF-NaF-ThF_4-UF_4$ system using the FactSage software [49]. The objective of that work [49] was to optimize the MSFR fuel composition [50]. Furthermore, three compositions potentially suitable as a MSFR fuel were proposed [49]:

1. A composition of 76.4 mol% LiF, 21.05 mol% ThF_4, and 2.55 mol% UF_4 with melting temperature of 835 K;

2. A composition of 47.4 mol% LiF, 30.10 mol% NaF, 19.95 mol% ThF_4, and 2.55 mol% UF_4 with melting temperature of 796 K;

3. A composition of 52.154 mol% LiF, 23.180 mol% NaF, 22.12 mol% ThF_4, and 2.55 mol% UF_4

with melting temperature of 775 K.

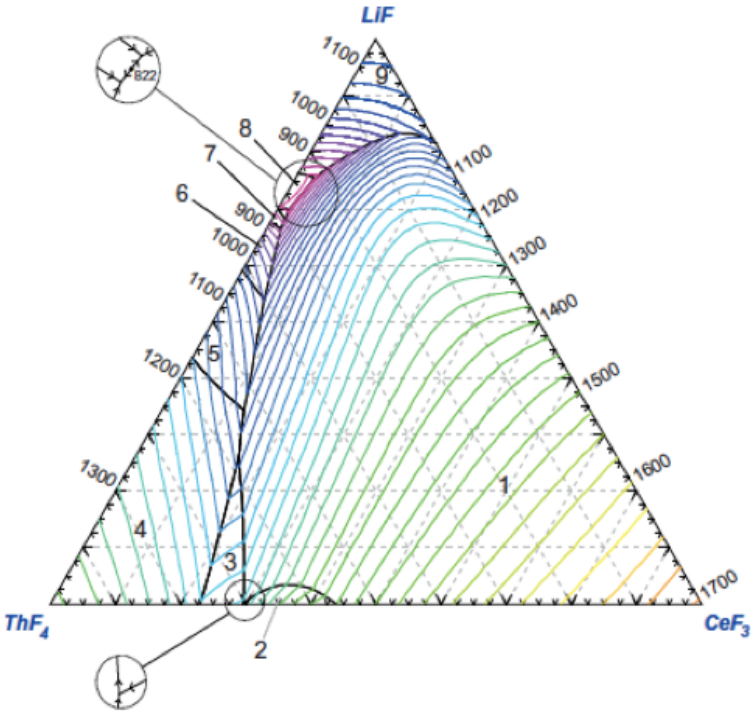

Figure 3.7: *The liquidus projection of the $LiF-CeF_3-ThF_4$ phase diagram assessed in this study. Primary crystallization phase: (1) CeF_3; (2) $ThCeF_7$; (3) $CeTh_2F_{11}$; (4) ThF_4; (5), $LiTh_4F_{17}$; (6) $LiTh_2F_9$; (7) $LiThF_5$; (8) Li_3ThF_7; (9) LiF. Copied from Beneš et al. [48].*

As an extension to the studies by Beneš et al. [49], Capelli et al. completed a thermodynamic assessment of BeF_2-ThF_4 and BeF_2-UF_4 binary systems [51]. Based on the thermodynamic modelling performed in these studies, the final melting temperature could be lowered with the presence of BeF_2 in the molten salt fuel [51].

Capelli et al. also performed a thermodynamic assessment of the $LiF-ThF_4-PuF_3-UF_4$ quaternary system, which is considered as a salt mixture for the MSFR concept with PuF_3 [52]. An experimental part was performed using ThF_4 and CeF_3 as surrogates to UF_4 and PuF_3, respectively [52]. As noted by Capelli et al., the binary systems ThF_4-PuF_3 and UF_4-PuF_3 were assessed for the first time and without any experimental data to support the modelling assessment only referencing to the surrogate systems involving CeF_3 [52]. Experimental data are still needed for accurate assessments of the fluoride salt systems (i.e., ThF_4-PuF_3 and UF_4-PuF_3).

All binary and ternary sub-systems of the $LiF-NaF-CaF_2-LaF_3$ quaternary system have been evaluated by Beilmann et al. with DSC measurements as well as thermodynamic modelling

of the liquid phase [53]. A low concentration of LaF_3 was used in order to simulate amounts of PuF_3 [53]. DSC measurements of several compositions of the ternary ($LiF+CaF_2+LaF_3$), ($NaF+CaF_2+LaF_3$), and the quaternary ($LiF+NaF+CaF_2+LaF_3$) systems resulted in good agreement with the same systems assessed using the classical polynomial and the quasi-chemical models [53].

Potential fuel salts for the MSFR concept have been continuously studied at the Joint Research Centre (JRC) proposing new additives (i.e., NaF, BeF_2, CaF_2) to the reference fuel solvent of the $LiF-ThF_4$ system [54]. A comprehensive thermodynamic investigation of the CaF_2-ThF_4 binary and the $LiF-CaF_2-ThF_4$ ternary systems was performed by Capelli et al. to estimate the feasibility of the above salt composition [54]. The studies included the following: DSC measurements of several intermediate compounds of the binary system mentioned above and XRD analyses to determine the phases in equilibrium as well as the structure of the $CaThF_6$ compound [54].

As explained by Capelli et al., there were no published data on the CaF_2-ThF_4 system; hence, an assessment of several intermediate compositions measured by DSC to determine the temperatures of equilibrium was employed [54]. Figure 3.8 shows a phase diagram of the CaF_2-ThF_4 assessed by Capelli et al. [54]. As one can see in Figure 3.8, phase transition measurements on the CaF_2 rich side (i.e., melting point is 1691 K) could not be experimentally determined due to the temperature limitation of the crucible ($\sim$ 1523 K) [54].

An inclination towards fast spectrum reactor concepts with the $LiF-ThF_4-UF_4-PuF_3$ quaternary system as a fuel salt established a general concern about major fission products being released from the salt, where ^{137}Cs is known to be one of them. An extensive thermodynamic investigation of the $CsF-ThF_4$ binary system was performed by Vozárová for the first time using DSC, XRD, and Knudsen Effusion Mass Spectrometry [55]. A phase diagram was assessed with FactSage employing the CALPHAD method [55]. The obtained experimental data were used as a starting point to model a phase diagram [55]. On the optimized phase diagram presented in Figure 3.9, one could see three eutetic points (i.e., 894.7 K, 1136 K, and 1072.9 K), four peritectic points (i.e., 1113.9 K, 1141.8 K, 1167.6 K, and 1315.7 K), two congruently melting compounds of Cs_3ThF_7 and Cs_2ThF_6 at 1251.8 K and 1155.9 K, respectively [55]. The lowest melting temperature of 894.7 K was identified at the eutectic point of 9.6 mol% ThF_4 [55]. As referring to Figure 3.9, one can notice inconsistency in experimental data obtained by Vozárová et al. [55] and

reported in the open literature. As a result, further experimental investigations of such a system can be recommended.

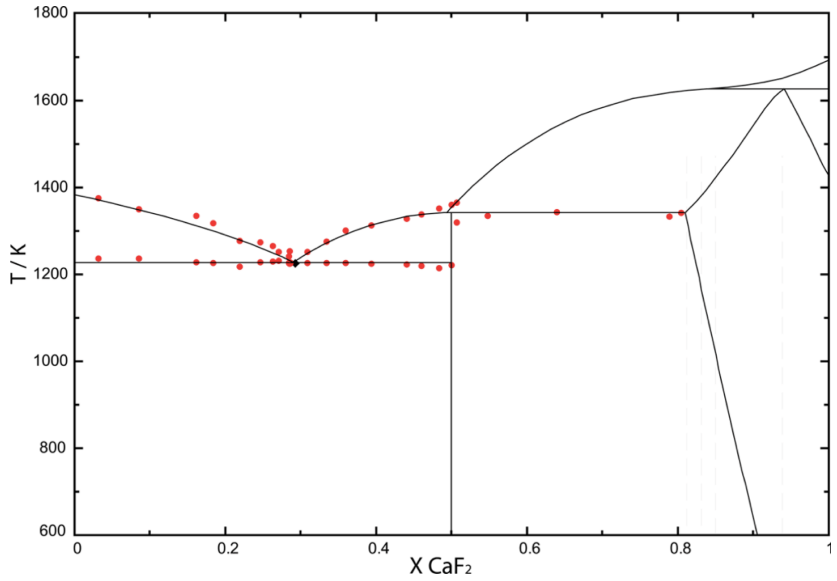

Figure 3.8: *A phase diagram of the $CaF_2 - ThF_4$ binary system with experimental data (•). Copied from Capelli et al. [54].*

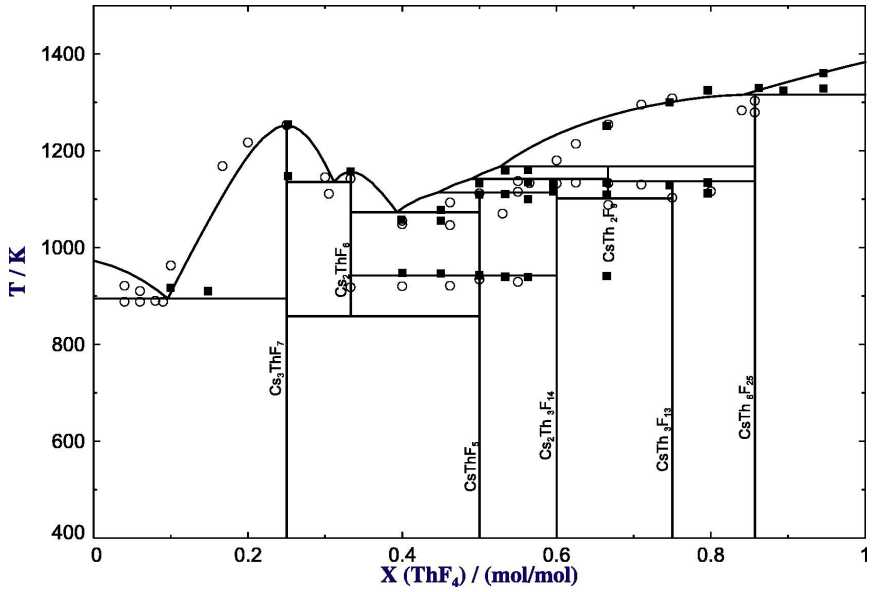

Figure 3.9: *A phase diagram of the $CsF - ThF_4$ binary system with experimentally obtained equilibrium data in this work (■) and reported in the literature (○). Copied from Vozárová et al. [55].*

Capelli et al. continued a thorough thermodynamic assessment of the common-ion binary systems and ternary sub-systems of $LiF - ThF_4 - CsF - LiI - ThI_4 - CsI$ employing the DSC technique

[56]. The CALPHAD method was applied for the thermodynamic modelling of the aforementioned system using FactSage [56]. As outlined by Capelli et al., Cs and I accumulate in the fuel, typically in the form of CsF and CsI [56]. An experimental investigation of LiF-CsI was of interest in this work and experimental results revealed the range of stability of the liquid-liquid miscibility gap, as shown in Figure 3.10 [56]. The LiF – CsF binary system shown in Figure 3.11 was assessed by Capelli et al. based on the melting point of pure CsF ($T_{melting}$=972.7 K) experimentally obtained by Beneš et al. [57] and equilibrium data of mixtures obtained by Thoma et al. [56]. The modelled LiF – CsF system is described by one peritectic point at 765.7 K and eutectic point at 758.1 K with compositions of 0.52 mol% LiF - 0.48 mol% CsF and 0.41 mol% LiF - 0.59 mol% CsF, respectively [56].

The optimized ternary phase diagram (i.e., calculated liquidus) of the LiF – CsF – ThF_4 system was in good agreement with experimental studies [56]. A eutectic temperature of the 36.6 mol% LiF, 61.2 mol% CsF, and 2.2 mol% ThF_4 composition obtained experimentally was 750.2 K, whereas the calculated temperature of the 35.3 mol% LiF, 61.4 mol% CsF, and 3.3 mol% ThF_4 composition was 748.3 K [56]. Figure 3.12 represents a phase diagram of the LiF – CsF – ThF_4 ternary system [56]. As noted by Capelli et al., the volatility of Cs and I may relate to a composition shift during experimental measurements [56].

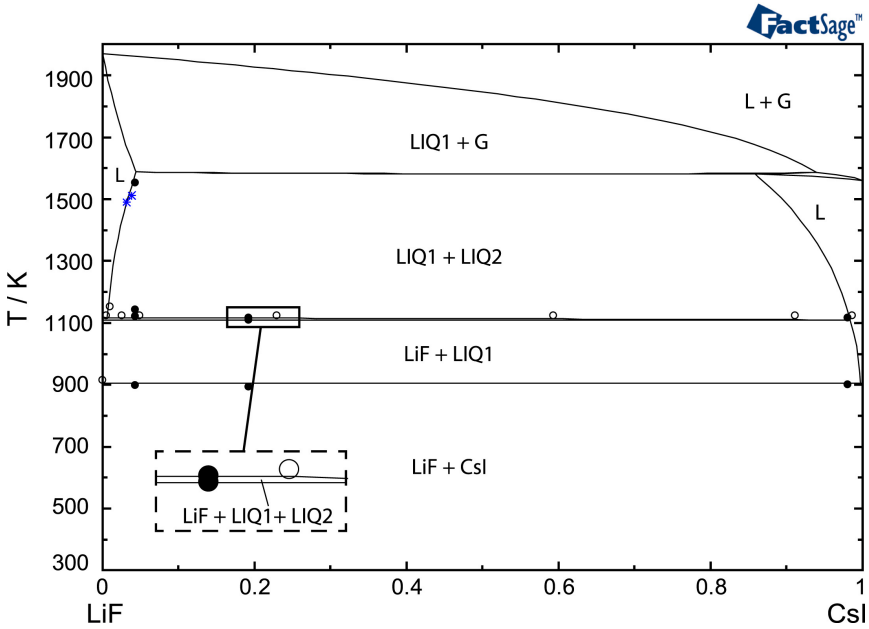

Figure 3.10: *The pseudo-binary phase diagram of the LiF – CsI. Copied from Capelli et al. [56].*

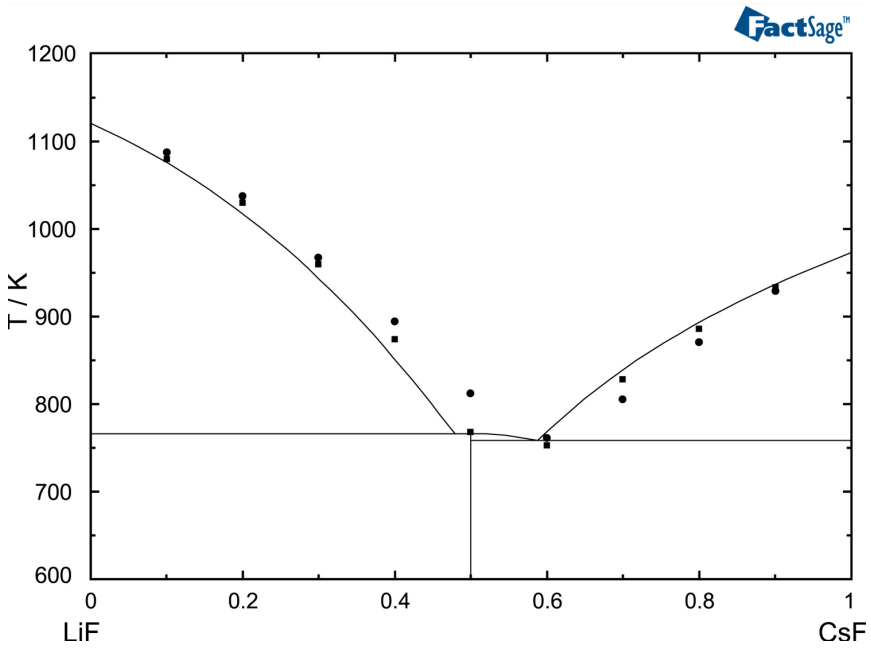

Figure 3.11: *Phase diagram of the LiF – CsF binary system modelled by Capelli et al. [56] with (■, ●) superimposed experimental data obtained by Thoma et al. [28].*

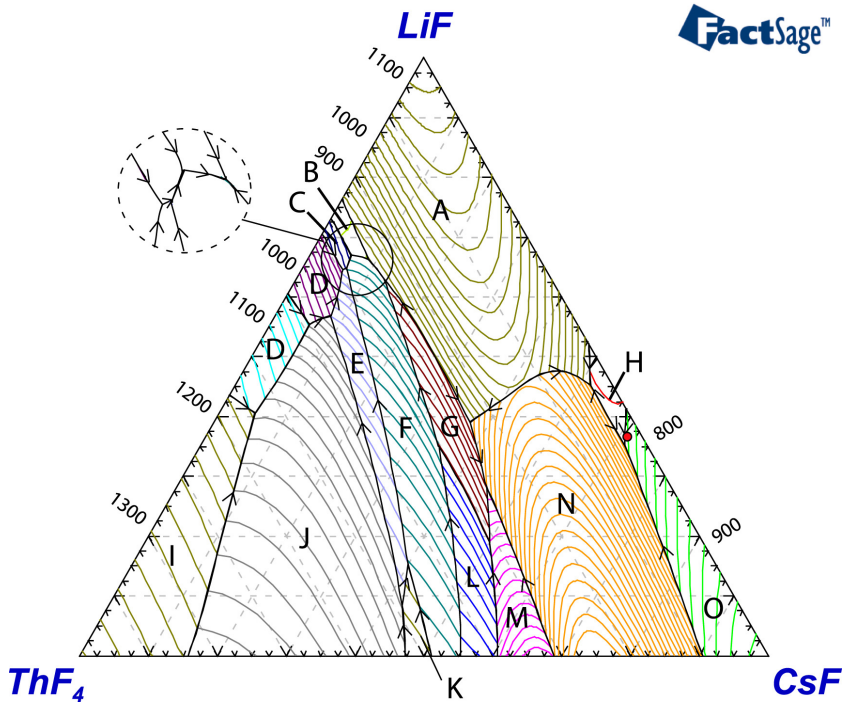

Figure 3.12: *The liquidus projection of the calculated LiF – ThF_4 – CsF system. Primary crystallization fields: (A) LiF; (B) Li_3ThF_7; (C) $LiThF_5$; (D) $LiTh_2F_9$; (E) $CsTh_3F_{13}$; (F) $Cs_2Th_3F_{14}$; (G) α-$CsThF_5$; (H) $LiCsF_2$; (I) ThF_4; (J) $CsTh_6F_{25}$; (K) $CsTh_2F_9$; (L) β-$CsThF_5$; (M) Cs_2ThF_6; (N) Cs_3ThF_7; (O) CsF. Copied from Capelli et al. [56].*

Despite the fact that the systems mentioned above were assessed with modern techniques, several knowledge gaps can be identified. Firstly, experimental determination of melting points of pure components (e.g., LiF, CsF, ThF_4) can validate the reported values in the open literature. Secondly, discrepancies in experimental measurements between multiple sources serves as motivation to repeat the measurements independently to reduce experimental uncertainties. Thirdly, modelled solidus as well as liquidus lines of phase diagrams can be confirmed by experimental studies of various concentrations (i.e., mixing) within the LiF – CsF system.

3.3 Fluoride Salts Measurements

3.3.1. Experimental Techniques

Thermal analysis and gradient quenching techniques were employed by Thoma et al. in the study of several fluoride salt systems [58]. XRD is also applicable to fluoride salts investigations. Capabilities of XRD with regards to fluoride salts studies are the following: determination of crystal structure of phases that are crystalline, salt composition determination, and sample lattice parameters identification. By comparing an experimentally obtained XRD diffraction pattern with a reference database, a sample can be analyzed. XRD patterns of the $CaThF_6$ compound reported by Capelli et al. is shown in Figure 3.13 [54].

Despite the fact that XRD is commonly used in studying fluorides, the results may be inconclusive on their own due to a number of aspects, such as [54, 55]:

- An XRD instrument is not usually equipped with an inert atmosphere, hence a sample can be potential exposed to air. Knowing the hygroscopic nature of fluorides, introducing air to a sample may comprise its purity.
- XRD measurements are commonly performed at ambient temperature, which is not an ideal condition to examine fluoride compounds (i.e., they may become unstable). An alternative technique such as high temperature XRD can be also employed.

XRD can be used to qualitatively assess the sample purity; however, DSC remains a more accurate and robust technique to verify sample purity, albeit in an indirect way. DSC can accurately determine melting points (i.e., ±4 K depending on a instrument uncertainty), enthalpies of

mixing, phase equilibrium data, and heat capacity. It should be noted that if the melting point of a sample is well-understood (e.g., consistent values reported by various institutions), DSC can be employed with confidence as a method to verify sample purity.

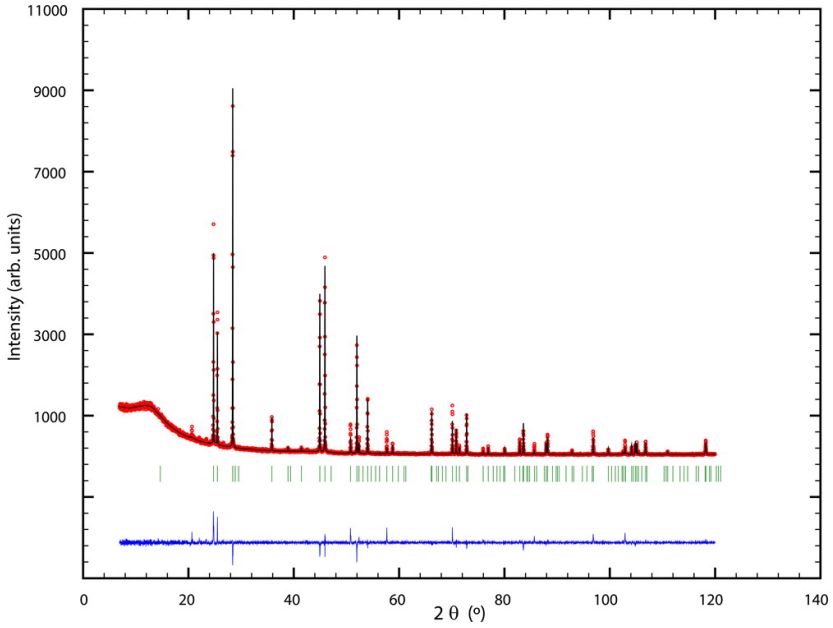

Figure 3.13: *Superimposed XRD patterns of the $CaThF_6$ compound obtained experimentally (in red) and calculated (in black). Copied from Capelli et al. [54].*

Analyses of a DSC signal involves interpretation of melting and cooling peaks (i.e., onset temperature, peak temperature, and offset temperature) created by DSC heat flow at constant heating rate throughout a temperature range of interest [59, 60]. As an example, Beilmann et al. established the eutectic or pertectic temperatures of the $LiF-CaF_2-LaF_3$ mixture by determining the onset temperature (i.e., 989 K) of the first melting peak, whereas the liquidus temperature of that composition was identified by the offset (i.e., 1042 K) of the second peak [53]. A common procedure to determine phase transition temperatures of a sample is to evaluate where a tangent on the baseline intercepts with a tangent on the inflection point [53, 59]. Figure 3.14 represents an analysis of the obtained DSC signal for the composition of 80.9 mol% LiF, 4.9 mol% CaF_2, and 14.2 mol% LaF_3 [53]. It is worth mentioning that a typical DSC instrument is usually equipped with software that allows one to analyze obtained DSC sequences.

There are many challenges to accurately perform DSC measurements of fluoride salts. First, there is a risk to potentially damage the equipment because alkali halide fluorides corrode many materials at elevated temperatures [61]. For instance, platinum is a common material used in

thermocouples of calorimeter detectors, which was observed by Beneš et al. to be corroded by fluorides resulting in equipment damage [61]. Second, one must ensure that the crucible does not chemically interact with the sample, which would compromise the quality of the measurement. Hence, a robust crucible design is a key factor in the experimental framework of fluoride salt investigations to prevent off-gassing, equipment damage, and ensuring that the composition of the sample is not compromised.

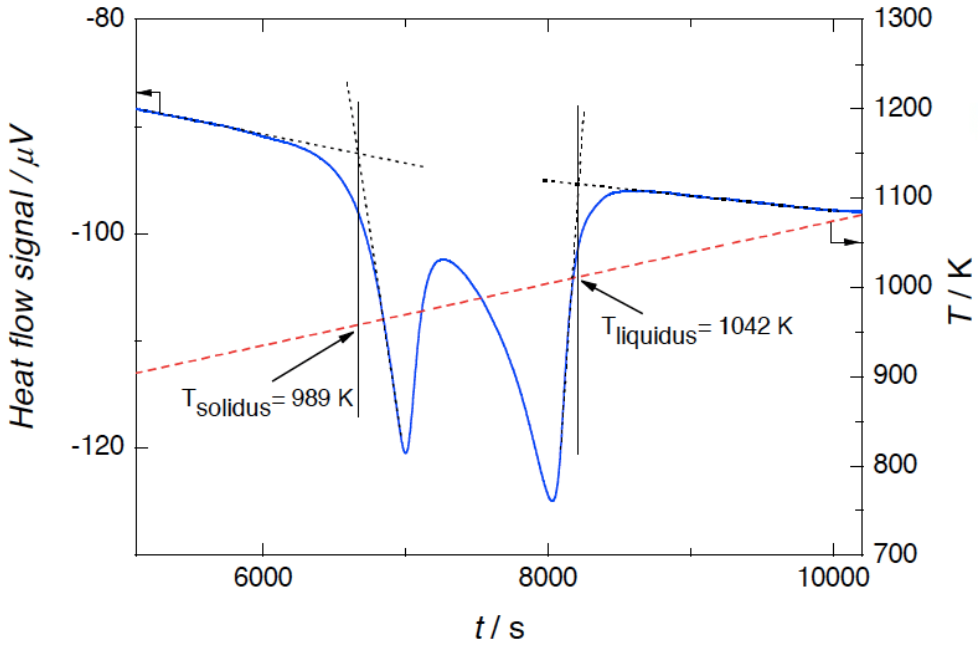

Figure 3.14: *A typical melting sequence measured by DSC. U is the heat flow signal. Copied from Beilmann et al. [53].*

In order to perform DSC measurements of various fluoride salts, Beneš et al. developed a custom crucible design for a SETARAM MDHTC96 calorimeter that is used at JRC [61]. Figure 3.15 shows (a) a detailed engineering drawing including components, and (b) a photograph of the custom made crucible [61]. The JRC DSC crucible meets the requirements mentioned above by using a Boron Nitride (BN) insert; thereby, the risk of potential chemical interaction between a fluoride salt and the crucible is eliminated. Moreover, a leak tight seal is achieved by a Ni gasket and Stainless Steel (SS) stopper. A large number of fluoride salt systems published in the open literature were studied by using this JRC DSC encapsulation technique, as reported by Beneš (JRC) [38], Beilmann (Heidelberg University) [62], Capelli (Delft University of Technology (TU Delft)) [63], and Ocádiz-Flores et al. (TU Delft) [64, 65].

Numerous vendors offer DSC instruments that may vary from one calorimeter design to another. Frequently, commercially available crucibles for those instruments are not suitable for fluoride salt studies. There are no commercially available crucibles from Netzsch, the vendor of the DSC used in this work, that met the discussed requirements. While Netzsch does offer some crucibles that are chemically compatible (e.g., BN, graphite), they are unable to provide a hermetic seal.

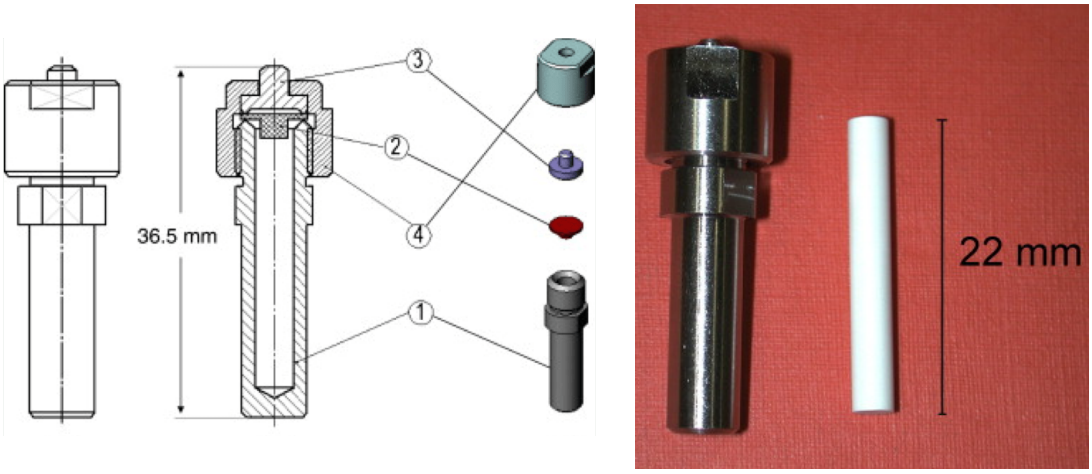

(a) *Engineering drawings of a crucible design and various parts of a crucible: 1, SS crucible body, 2, Ni sealing, 3, SS stopper, and 4, SS closing bolt.*

(b) *A photograph of the JRC DSC custom made crucible with a BN insert.*

Figure 3.15: *JRC DSC crucible design. Copied from Beneš et al. [61].*

A custom crucible made entirely of Ni-201 was explored by Hallatt at Ontario Tech University [66]. Detailed design calculations and engineering drawings (see Figure 3.16) performed by Hallatt resulted in a prototype made by a local machine shop in Cobourg, Ontario [66]. This prototype included three components: a Ni-201 lid, a Ni-201 gasket, and a Ni-201 body (see Figure 3.17) [66]. Unfortunately, this prototype failed to fulfill all design requirements (i.e., crucible mass and wall thickness) [66]. As reported by the local machine shop, the Ni-201 material is incredibly challenging to machine, and they declined requests to make additional units. There are no other cases of crucibles compatible with fluorides while providing hermetic seal for use in a Netzsch DSC that have been reported in the open literature.

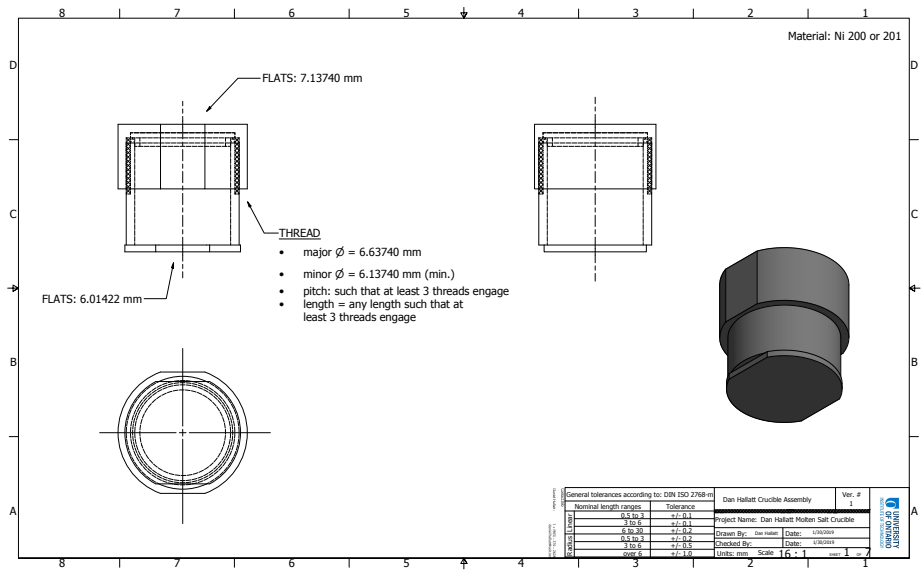

Figure 3.16: *An engineering drawing of a non-lined Ni crucible design for DSC measurements of fluoride salts. Copied from Hallatt [66].*

(a) *A final prototype of Ni crucible design.* **(b)** *Three parts of the prototype, from left to right: Ni lid, Ni gasket, and Ni body.*

Figure 3.17: *A prototype of Ni crucible design developed for the Netzsch DSC. Copied from Hallatt [66].*

3.3.2. DSC Temperature & Sensitivity Calibration

Accurate DSC measurements not only depend on a suitable crucible design but also on the calibration of the system [67]. As DSC is a relative measurement technique, its temperature characteristics are dynamic and measurements are not in the thermal equilibrium [68]. In order to

convert the relative data obtained by DSC to absolute values, a calibration procedure must be employed [68]. Calibration requires the use of Reference Materials (RMs) with well established phase transition temperatures and uncertainties [67, 68]. It is common to perform temperature and enthalpy calibration simultaneously as RMs typically have well-defined phase transition temperatures [68]. It should be noted that the number of RMs chosen for calibration should cover the entire temperature range of interest. Calibration kits with specific RMs for particular applications are often commercially available by the DSC vendor.

Typically, each RM is independently subjected to at least three heating cycles at a chosen heating rate [68, 69]. Calibration analyses are performed by extrapolating the onset temperature of the last two peaks for the temperature calibration and the peak area for the enthalpy calibration (the first peak is commonly discarded as during the first heating cycle machine builds up a thermal history) [68]. Figure 3.18 shows the determination of the onset temperature and the peak area at different heating rates for the temperature calibration and the enthalpy calibration, respectively. The analysis presented in Figure 3.18 was performed by the Netzsch Proteus software [69]. As noted by the Netzsch user manual, a slight shift in the extrapolated onset temperature may be observed with an increase of the heating rate (see Figure 3.18) [70].

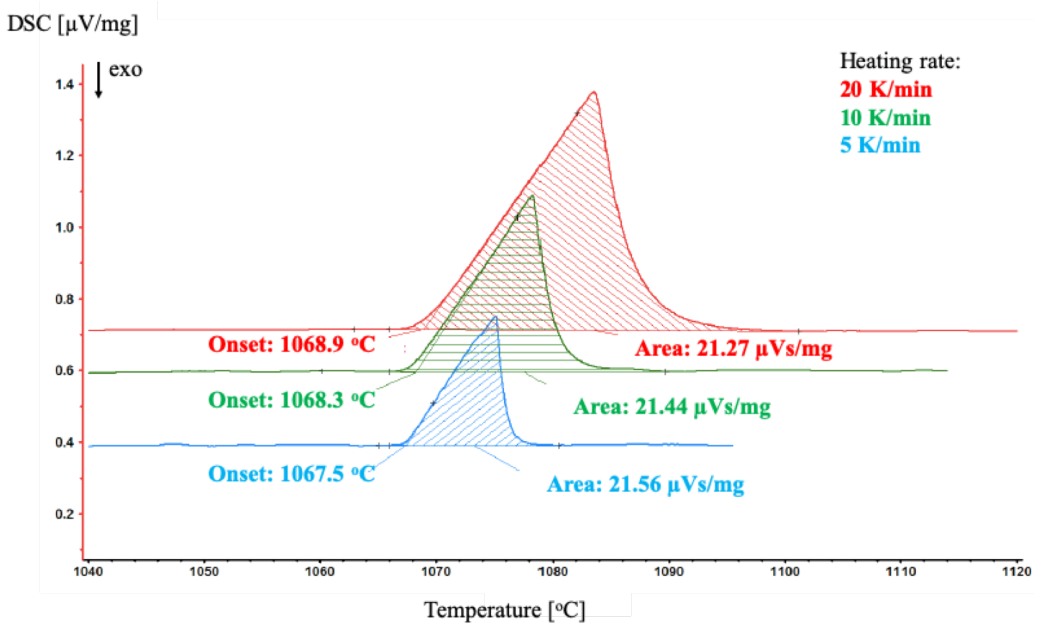

Figure 3.18: *Determination of the onset temperature for the temperature calibration and the peak area for the enthalpy calibration. Modified from the Netzsch Proteus software [69].*

A number of RMs for calorimetry were developed and certified by national standards laboratories (e.g., the National Institute of Science and Technology in the USA, the Association Française de Calorimétrie et d'Analyse Thermique in France, etc.) [67]. Table 3.1 represents a list of RMs recommended by the International Union of Pure and Applied Chemistry (IUPAC) and their defined values for DSC temperature and enthalpy calibration procedures [68].

Table 3.1: *Recommended values of temperatures and enthalpies of fusion of pure metals. Modified from Della Gatta et al. [68].*

Element	$T_{melting}$ [°C]	ΔH_{fus} [J g^{-1}]
Mercury, Hg	-38.8344	-
Gallium, Ga	29.7646	80.07 ±0.13
Indium, In	156.598	28.62 ±0.04
Tin, Sn	231.928	60.38 ±0.15
Bismuth, Bi	271.402	53.18 ±0.12
Cadmium, Cd	321.069	55.25 ±0.68
Lead, Pb	327.462	23.08 ±0.11
Zinc, Zn	419.527	108.09 ±0.43
Antimony, Sb	630.628	162.55 ±4.91
Aluminum, Al	660.323	399.87 ±1.33
Silver, Ag	961.78	104.61 ±2.09
Gold, Au	1064.18	64.58 ±1.54
Copper, Cu	1084.62	203.44 ±4.36

However, when performing DSC, it is necessary to account for possible chemical interactions between a sample and the crucible. Such interactions may result in a change of the reported melting points, leading to invalid calibration measurements [71]. A number of DSC crucibles made of different materials were examined in terms of compatibility with pure metal calibrants. Table 3.2 summarizes the compatibility of various combinations of calibrants and crucible materials [71].

As an alternative to pure metal calibrants, organic and inorganic substances can also be used for calibration purposes [72]. Such substances proposed by the International Confederation for Thermal Analysis and Calorimetry (ICTAC) are high purity compounds mainly presenting solid-solid transition temperatures rather than solid-liquid transitions [72]. A number of calibrants recommended by ICTAC were mainly tested in order to confirm the compatibility with a platinum crucible. Table 3.3 represents inorganic substances for temperature and enthalpy calibration.

Beneš et al. calibrated their DSC instrument with the custom made crucible using a BN liner [73] (see Figure 3.15) with Sn, Pb, Zn, Al, Ag, and Au [38]. This procedure was also employed by Vozárová et al. (Swiss Federal Institute of Technology) [55], Beilmann (Heidelberg University)

[62], Capelli (TU Delft) [63], and Ocádiz-Flores et al. (TU Delft) [64, 65].

Table 3.2: *Compatibilities of calibrants with crucible materials. Modified from Cammenga et al. and Beneš et al.[38, 71].*

Crucible material	Calibrants							
	Ga	In	Sn	Pb	Zn	Al	Ag	Au
Corundum, $A1_2O_3$	√	√	√	√	√	√	√	√
Boron Nitride, BN	√	√	√	√	√	√	√	√
Graphite, C	√	√	√	√	√	√	√	◇
Aluminium, Al	◇	√	◇	√	◇	x	x	x
Silver, Ag	◇	◇	◇	◇	◇	◇	x	x
Gold, Au	*	*	◇	◇	◇	◇	◇	x
Nickel, Ni	*	*	*	*	*	◇	√	◇
Stainless Steel, SS	*	√	*	√	◇	◇	√	◇
Platinum, Pt	*	*	◇	◇	◇	◇	◇	◇
Molybdenum, Mo	*	?	*	?	*	?	?	◇

√ no solubility and no influence on the melting temperature to be expected;
? compatibility unknown;
x crucible melts prior to phase transition;
* partial solution processes are possible with negligible change in the melting temperature;
◇ melt dissolves crucible material, greater change in the melting temperature.

Table 3.3: *Inorganic calibrants (their solid-state transition temperatures and enthalpy of solid-state transitions) compatible with platinum crucible.*

Calibration substance	Phase transition temperature [°C]	Enthalpy of phase transition [$J\,g^{-1}$]	Reference
Potassium Nitrate, KNO_3	129.22±0.02 333.7±0.1*	45.2 99.70±0.08**	[74, 75, 76]
Potassium Perchlorate, $KClO_4$	300.41±0.06	93.8	[74, 76]
Potassium Chromate, K_2CrO_4	669.9±3.0	37.08±0.25	[75]
Barium Carbonate, $BaCO_3$***	808.8±1.4	-	[77]
Caesium Chloride, CsCl	476.9±1.9 643.0±0.1*	18.53±0.05 121.77**	[75]
Potassium Sulfate, K_2SO_4	583.7±0.4 1070.1±0.4*	35.06±0.38 -	[75, 77]

* Solid-liquid phase transition temperature (i.e., melting point) [75];
** Enthalpy of fusion [75];
*** Powder sinters resulting in poor contact with the crucible, but grinding the sample appears to improve stability [72, 77].

3.3.3. Sample Preparation

Sample preparation of fluoride salts is an important aspect that plays a significant role in acquiring accurate results of DSC measurements. Due to the hygroscopic nature of most fluorides,

samples must be handled within an inert atmosphere glovebox to prevent contamination coupled with a dehydration process to remove any impurity oxides [61, 63]. Although as-received salt components are often claimed to meet high purity standards (i.e., ~ 99.999 % trace metals basis), various reports in the open literature demonstrated the value of purifying procured materials [38, 62, 63, 64]. A simple dehydration procedure of fluoride salts proposed by Capelli involved subjecting the fluoride salt samples to a heat treatment of ~ 400 °C for 4 hours in an open vessel allowing any moisture to evaporate [63]. It was observed that the oxidative nature of actinoid salts (e.g., ThF_4, UF_4) requires a more complex purification process. Due to the formation of highly stable oxides (e.g., ThO_2), a purification process using F_2 or hydrogen fluoride (HF) gas must be employed [63]. A fluorination process of ThF_4 samples reported by Capelli consists of multiple steps [63]:

1. A mixture of ammonium bifluoride (NH_4HF_2) and ThF_4 was subjected to a heat treatment of 250 °C for 12 hours in a closed Ni reaction vessel;

2. The sample was cooled to room temperature in order to open the reaction vessel in a glovebox;

3. A second heat treatment of 400 °C for 6 hours was employed in an open Ni boat in an tube furnace with a Ar/H_2 inert atmosphere.

The first step was to generate HF gas by dissociation of NH_4HF_2 to NF_3 and HF (see Eq. 3.1) in order to fluorinate oxide impurities; the second step was to evaporate the residual ammonia, water vapour, and excess HF in an open reaction vessel.

$$\begin{aligned} NH_4HF_2 &\xrightarrow{\Delta} NH_3 + 2\,HF \\ ThO_2 + 4\,HF &\longrightarrow ThF_4 + 2\,H_2O \end{aligned} \tag{3.1}$$

A synthesis process of the actinoid fluorides using HF gas was implemented by Souček et al. to re-determine the melting point of UF_4 [78]. A special facility with an installation of two gloveboxes, a high temperature fluorination reactor, and an HF supply gas line was built at JRC-Karlsruhe, Germany [78].

It should be noted that research laboratories at universities are often limited to certain equipment where experiments are performed. Ontario Tech University does not have the infrastructure to install an HF gas line; hence, alternative methods must be employed. As an example, dehydration/purification procedures developed by Hallatt were derived from the reported procedures from Beilmann [62] and Capelli [63] and established within the safety compliance of Ontario Tech University [66]. Individual routines were developed and tested by performing a measurement of their influence on the compositional purity of the salt materials [66].

As outlined by Hallatt, the dehydration procedure of actinoid fluorides required special consideration since HF gas generated from NH_4HF_2 reaction is undesirable for the glovebox sensors [66]. A setup of stacked Ni reaction vessels shown in Figure 3.19 was designed such that the upper Ni vessel containing solid NaOH would neutralize HF gas, which left the lower Ni vessel through the Ni pipe welded to the floor of the upper vessel [66]. This process was not fully qualified by Hallatt and it was uncertain if it was successful. The foregoing experimental procedures were leveraged in establishing methodologies in this work, which are discussed in the next chapter.

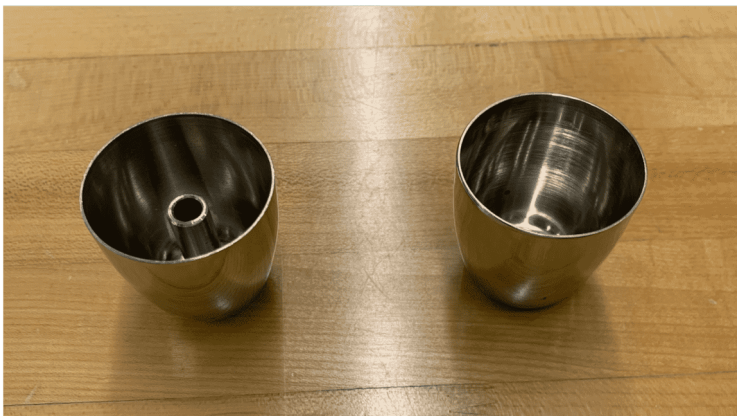

(a) *Ni reaction vessels, from left to right: the upper vessel with the Ni pipe welded to the floor for NaOH, the lower Ni vessel for mixture of ThF_4 and NH_4HF_2.*

(b) *Stacked Ni reaction vessels for purification of actinoid fluorides.*

Figure 3.19: *Stacked Ni reaction vessels for purification of actinoid fluorides designed by Hallatt [66].*

Chapter 4

Methodology

This chapter describes a crucible design and a number of qualification and experimental procedures (i.e., instrument calibration, sample preparation, and DSC measurements of fluoride salts) employed in this thesis. Establishing experimental procedures is an important aspect of this thesis, as it highly correlates with the accuracy and repeatability of the fluoride salts measurements. A crucible design process is presented in §4.1, DSC calibration procedures and their results are given in §4.2, sample preparation and encapsulation techniques are described in §4.3 and §4.4, respectively, and DSC measurement procedures of fluoride salts are explained in §4.5.

4.1 Crucible Design

Thermodynamic investigations of fluoride salts were conducted using the DSC mode of a Netzsch Jupiter 449 F1 STA at Ontario Tech University, which is shown in Figure 4.1. This STA is equipped with two furnaces with individual gas streams a) a SiC furnace with a maximum temperature of 1600 °C for Ar or mixed Ar-O_2, and b) a water vapour furnace with a maximum temperature of 1250 °C. The STA mass balance has a resolution of 25 ng with a maximum sample weight of 5 g, which includes two DSC crucibles [79]. Experience has shown that the balance is subject to a drift of $\sim \pm 0.01$ mg h^{-1} [80], which dominates the uncertainty in the measurements.

A DSC crucible that is capable of meeting the requirements of these measurements was not commercially available from the vendor; therefore, a custom crucible was designed out of necessity [81]. This effort leveraged some design features from Beneš et al., which included a SS body with a Ni liner and a Ni gasket [61]. The design from Beneš et al. [61] could not be used directly as it was developed for a Setaram DSC, which is incompatible with the Netzsch DSC instrument used

in this work. Since SS reacts with fluorides at elevated temperatures (i.e., chromium leaching), an inert liner was needed in the JRC design to contain the sample and to prevent chemical interaction, such as BN or Ni-200/201 alloys [61].

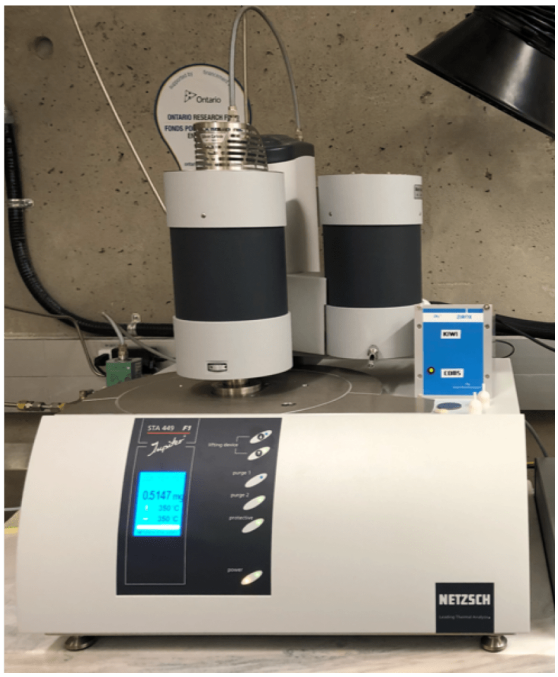

Figure 4.1: *Netzsch Jupiter 449 F1 STA used in this work.*

The crucible design must generally meet the following three requirements: a) maintain a hermetic seal to off-gassing, which may potentially damage the equipment; b) experience minimal wall-salt interactions (preferably none); and c) comply with physical requirements of the DSC sample carrier. The following specific design requirements were identified for a crucible used in a Netzsch Jupiter 449 F1 STA to measure fluoride salts [66, 79]:

- Maintain a hermetic seal at temperatures up to 1200 °C;
- Crucible + sample mass less than 2.5 g;
- Experience minimal wall-salt interaction;
- Less than 18 mm in total height;
- Less than 6.8 mm in outer diameter;
- Constructed with a flat thin floor;

- Constructed with a wall thickness as thin as feasibly possible;
- Axisymmetric.

Ultimately, a design converged on using a commercially available Netzsch SS-316L high-pressure crucible with a screw-on lid (Netzsch product no. 6.239.2-93.41.00), a custom liner made of Ni-201, and a custom gasket also made of Ni-201. Netzsch SS-316L high-pressure crucibles are supplied with gold (Au) gaskets [82]; however, they are rated to a maximum temperature of 500 °C, presumably due to changes of mechanical properties of Au at elevated temperatures. Gold softens at high temperatures, which may compromise the seal of the crucible.

Fabrication of the Ni gaskets to replace the Au gaskets provided by Netzsch was accomplished with a punch set and a manual hydraulic press in the Nuclear Fuels and Materials Laboratory. A 150 mm x 150 mm Ni-201 sheet stock with a thickness of 0.1 mm was inserted in the punch set and then placed on the pressure plates of the hydraulic press (see Figure 4.2). By using a pump handle, pressure was slowly applied to the punch rod (⌀ 6.35 mm) until the rod penetrated through the Ni sheet resulting in a circular-shaped gasket (see Figure 4.2). Safety glasses were used and a polycarbonate transparent clear sheet (ASTM D3935) was placed on the hydraulic press as a shield during this process.

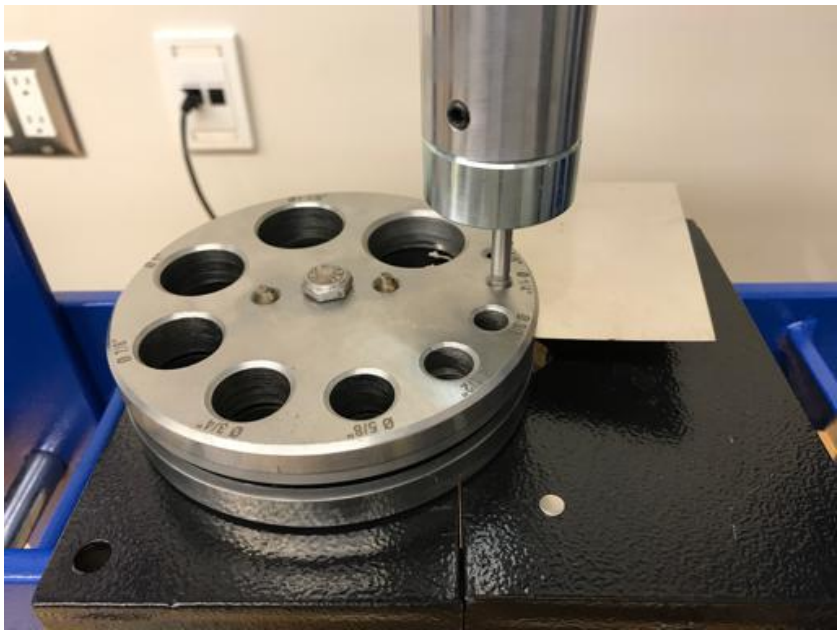

Figure 4.2: *A punch set and a hydraulic press setup to fabricate Ni gaskets.*

An engineering drawing of the Ni liner was developed in this work using the AutoCAD-2019 software and is shown in Figure 4.3. The Ni liners were manufactured by Van Halteren Machine & Tool Ltd (Lindsay, ON). Each Ni liner was visually examined for any obvious defects. Liners were made with a flat bottom and a ~ 0.25 mm wall thickness, and the average mass of a Ni liner was ~ 0.2 g. Figure 4.4 shows the full set of crucible components suitable for DSC measurements of fluoride salts. The total mass of the full DSC crucible set (i.e., Netzsch SS body, Netzsch SS lid, Ni liner, and Ni gasket) was ~ 1.5 g. The centre hole on the SS lid was used to punch used gaskets out to replace with new ones. A commercially available Netzsch sealing press (Netzsch product no. 6.239.2-92.4.00) was used to ensure a hermetic seal with a consistent tightness.

Since a number of modifications were applied to a commercially available Netzsch SS-316L crucible (i.e., a custom made Ni liner and a Ni gasket), qualification of the full DSC crucible set was required prior to obtaining DSC measurements in this work. Quality assurance of the full DSC crucible set was partially achieved through the DSC instrument calibration process.

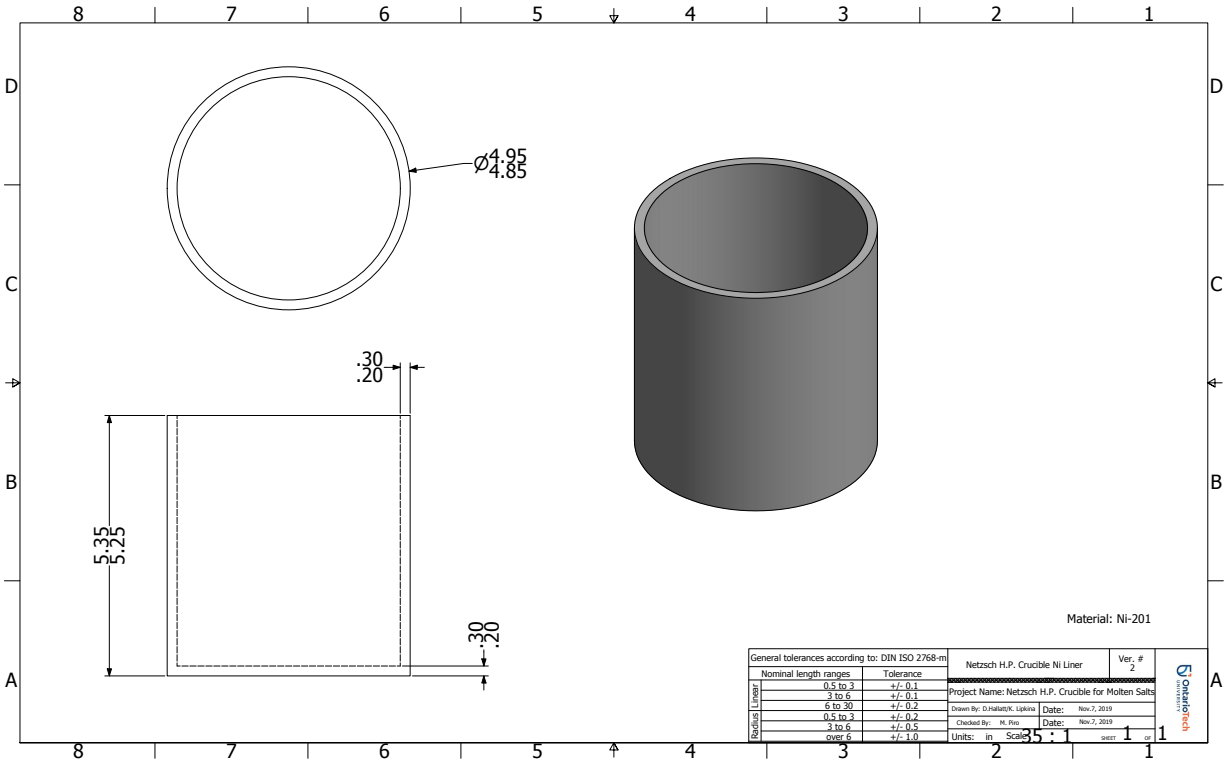

Figure 4.3: *An engineering drawing of a Ni-201 liner developed for DSC measurements of fluoride salts. All units are in mm.*

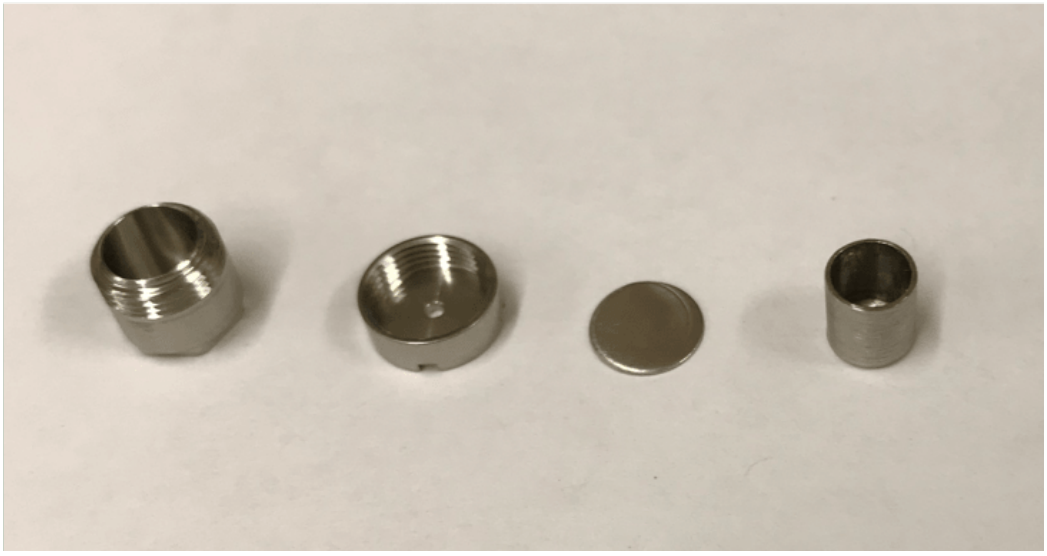

Figure 4.4: *A DSC crucible set for use in a Netzsch Jupiter 449 F1 STA. From left to right: Netzsch SS crucible body, Netzsch SS crucible lid, custom designed Ni-201 gasket, and custom Ni-201 liner.*

4.2 DSC Calibration Procedures

Prior to performing any DSC measurements of fluoride salt systems, the DSC instrument was calibrated, which used the Netzsch software package Proteus and a set of calibrants [69, 79]. Moreover, one must ensure to use a suitable calibration set with the custom crucible design. As part of DSC calibration campaign, the set of suitable calibrants was developed and refined throughout the work.

4.2.1. Suitable Calibrants

A commercially available Netzsch calibration set that is commonly used (Netzsch product no. 6.223.5-91.1.00) consists of pure metal calibrants (i.e., In, Sn, Bi, Zn, Al, Ag, Au, and Ni) [82]. However, the use of some of these pure metals with the Ni liner can result in chemical interactions between the two metals. To prevent undesirable metal-metal interactions, which can introduce a significant uncertainty in calibration, analyses of available phase diagrams of Ni with each pure metal calibrant (e.g., Ni–Au phase diagram) were performed. Furthermore, additional calibrants had to be selected to replace those that were unsuitable with Ni.

A summary of calibrants compatible with crucible materials presented in Table 3.2 was con-

sidered while finalizing a suitable calibrant set for the custom crucible design. Zinc (Zn) can be used as a suitable calibrant with a negligible change in the melting temperature, according to the information available in the open literature (refer to Table 3.2). However, a DSC run with Zn showed that the material reacted with the Ni liner resulting in damaging the crucible and compromised the quality of the measurements. Figure 4.5 shows the appearance of a DSC crucible set after two heating cycles employed for the DSC calibration run with Zn. As one can see in Figure 4.5 (a), the sample crucible containing Zn was heavily affected by the Zn-Ni reaction, whereas the reference crucible appeared normal. Therefore, Zn had to be excluded from the calibration matrix.

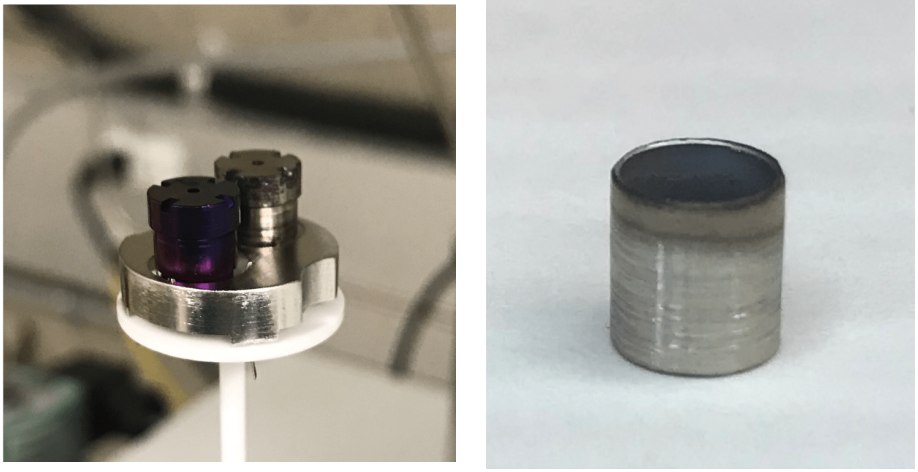

(a) *A DSC crucible set after the Zn calibration run.*

(b) *A Ni liner after the Zn calibration run.*

Figure 4.5: *A full DSC crucible set after the DSC Zn calibration run. The test was stopped after two heating cycles.*

The full temperature range of interest of DSC measurements was taken into account during the selection of calibrants to establish a suitable temperature coverage. Potential metal-metal interactions, especially at elevated temperatures (i.e., >800 °C), prompted the consideration of alternative calibrants, including inorganic compounds. A calibration set of inorganic substances (Netzsch product no. 6.223.5-91.2.05-07) offered by the vendor (i.e., $RbNO_3$, $KClO_4$, Ag_2SO_4, CsCl, K_2CrO_4, and $BaCO_3$) was partially applicable. Some of these substances were not used due to their hazardous nature (i.e., $K_2CrO_4, KClO_4$) and were unnecessary because suitable metals were found with similar phase transition temperatures [82]. Figure 4.6 shows the temperature

range of interest chosen for further DSC measurements of fluoride salts, which demonstrates comprehensive temperature coverage. A derived temperature and sensitivity calibration matrix is presented in Table 4.1.

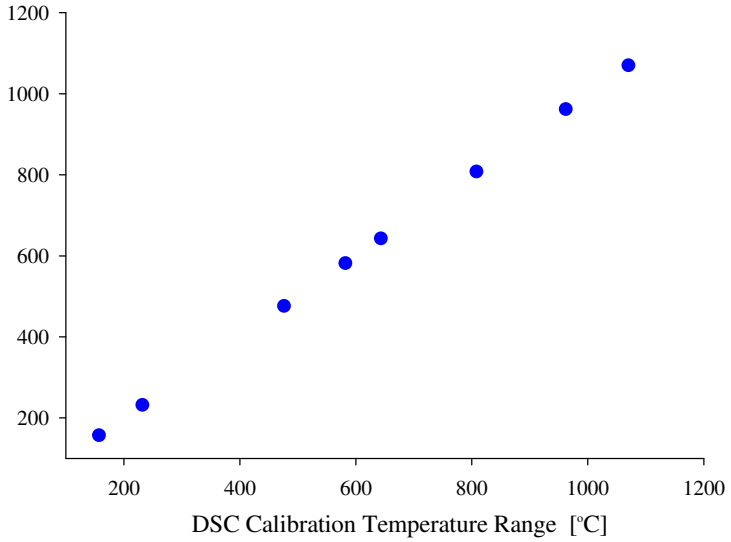

Figure 4.6: *An illustration of the temperature range for DSC calibration.*

Table 4.1: *DSC temperature calibration matrix developed in this work for the custom crucible design.*

Calibrant	Phase transition temperature [°C]		Phase transition enthalpy [J g $^{-1}$]		Reference
	Solid-Solid	Solid-Liquid	Solid-Solid	Solid-Liquid	
In	-	156.6	-	-28.60	[68]
Sn	-	231.9	-	-60.50	[68]
CsCl	476	644.35	-17.2	-121.77	[75, 70]
K_2SO_4	582	1070*	-35.06	-197.36	[74, 77]
$BaCO_3$	808	-	-94.90	-	[77]
Ag	-	961.8	-	-104.60	[68]
Au	-	1064.2**	-	63.7	[68]

* K_2SO_4 solid-liquid transition temperature value was used during the first two calibration campaigns.
** Au calibrant with BN liner was employed in the third calibration campaign.

As noted in the previous chapter, fluoride salt samples must be handled within an inert atmosphere (e.g., Ar glovebox) due to their hygroscopic nature; hence, preparation of the calibrant samples was performed within the Ar glovebox. All calibrants (i.e., pure metals and inorganic compounds) were prepared within the Ar glovebox for sake of consistency.

Pure metal calibrants (i.e., In, Sn,Ag, and Au) did not require any specific preparation, whereas

inorganic compounds (i.e., CsCl, K_2SO_4, and $BaCO_3$) needed to be milled and dehydrated within the glovebox, as per recommendations available in the open literature [75]. The milling and dehydration processes were applied to inorganic compounds in order to reduce an error in measurements and were as follows:

- Decanted substance was milled using an agate mortar and pestle for $\sim$ 5 minutes;
- Milled substance was transferred to a Ni reaction vessel;
- The Ni reaction vessel with the sample was placed on a hotplate and heated to $\sim$ 200 °C for 1 hour.

It should be noted that K_2SO_4 solid-liquid transition temperature values showed inconsistent results during multiple calibration campaigns employed in this work. Therefore, it was replaced with an Au calibrant (T_{ref} = 1064.2 °C) in the final temperature calibration campaign. Detailed information regarding K_2SO_4 is provided in §4.2.2.

DSC crucibles were prepared with the following process: crucibles were initially cleaned with soap and water; second, they were submerged in a small beaker with ethanol in an ultrasonic bath filled with distilled water at 40 °C for 30 minutes; third, crucibles were dried in a furnace at 45 °C in air for 1 hour prior to being ingressed into the glovebox. A set of two crucibles was used per measurement for the calibration procedure: one crucible contained the sample and the other was an empty reference crucible.

4.2.2. Calibration Measurements

A standard temperature calibration procedure with three consecutive heating cycles followed best practices recommended by Netzsch [70], which included: heating 100 °C above the transition temperature at the heating rate of 10 K/min and then cooling down to 100 °C below the transition temperature. The first calibration campaign was performed at 2, 5, and 10 K/min heating rates to gain experience on the sensitivity of the temperature ramp on DSC measurements.

Figure 4.7 shows a programmed DSC sequence of the Sn calibration run with three different heating rates. Following the dynamic step (i.e., heating) of the temperature program, the thermal energy is gradually absorbed by the sample resulting in the appearance of the first upward

(endothermic) peak (see Figure 4.7). When the temperature program was switched to a cooling cycle, the sample started releasing thermal energy, as represented by the second downward peak. This process was repeated three times at each heating rate resulting in multiple peaks, as shown in Figure 4.7.

The first peak at each heating rate is commonly discarded as the machine builds up a thermal history during the first heating cycle, whereas the last two heating cycles typically provide more accurate data detected by the DSC instrument [70]. Each peak is the representation of a phase transition occurring at a specific temperature. The rest of the calibrants had similar DSC patterns with different phase transition temperatures specific to that material. The results of the last two heating cycles at each heating rate were averaged, as recommended by Netzsch [70]. Onset temperatures of the last two melting curves were used for temperature determination, whereas areas of the last two melting curves were applied for sensitivity determination (i.e., enthalpy of fusion).

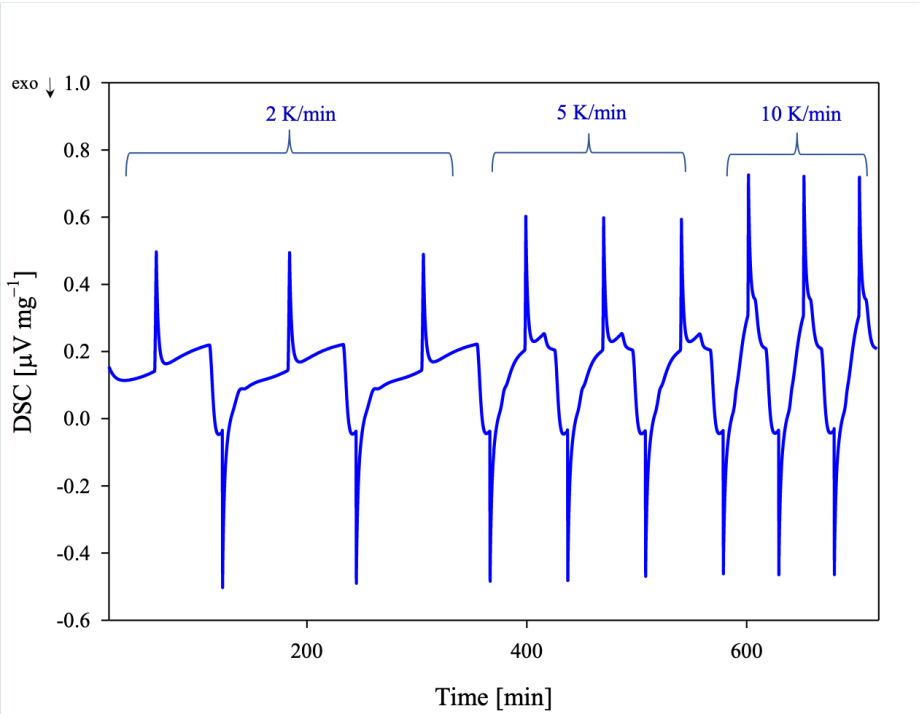

Figure 4.7: *DSC sequences of the Sn calibration run at 2, 5, and 10 K/min heating rates.*

It is worth noting that only one heating cycle was applied to a solid-liquid phase transition temperature (i.e., 1070 °C) of K_2SO_4 due to the possibility of liquid melt creeping up the crucible walls, as mentioned in the open literature [77]. This effect was experimentally confirmed in this

work. Figure 4.8 shows an open crucible with clear evidence of K_2SO_4 being in contact with the Ni gasket and Ni liner walls (i.e., discolouration on the lid and the gasket).

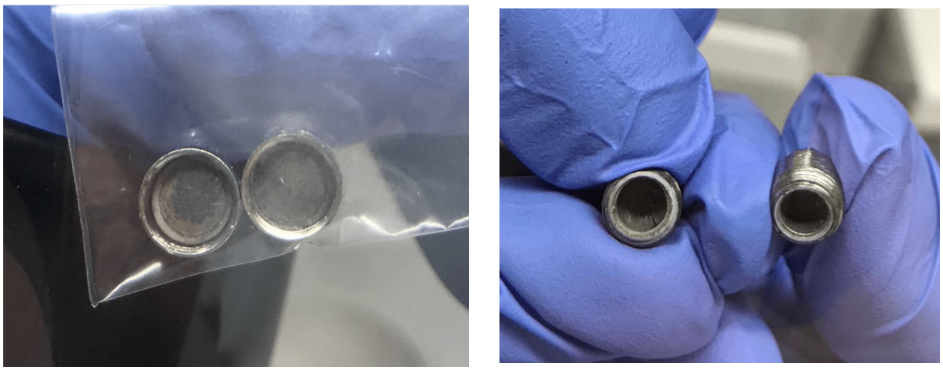

(a) *K_2SO_4 in contact with the SS lid and the inserted Ni gasket.*

(b) *A liquid melt of K_2SO_4 creeped up Ni liner walls.*

Figure 4.8: *Evidence of the chemical interaction between a DSC crucible and K_2SO_4 after a calibration run. The sample crept up the walls.*

In order to establish more appropriate heating rates for further DSC measurements of fluoride salts, a linear regression analysis was performed for every heating rate. A linear fit for all calibrants employed in this work is shown in Figure 4.9. The temperature difference (i.e., T_{ref} - T_{exp}) at 5 and 10 K/min showed similar results for most of the calibrants, whereas 2 K/min had a larger discrepancy with respect to reference values. All three heating rates showed consistently positive temperature differences. To optimize experimental work flow in the laboratory, a heating rate of 10 K/min was selected for DSC measurements of fluoride salts. This heating rate showed accurate and consistent results with the optimized duration of the DSC calibration campaign, while also reducing the time needed to perform a single measurement.

4.2.3. Calibration Profiles

DSC calibrants with their phase transition temperatures were analyzed using the Netzsch Proteus software [69, 83]. The onset temperatures of the last two phase transition curves of each calibrant with exception of K_2SO_4 due to liquid melt creeping up the crucible walls after first heating cycle were averaged to determine the phase transition temperature of the calibrants. The temperature calibration file was created based on a linear regression fit to Eq. 4.1, which is used in the Proteus software [69, 83]. The results of temperature calibration analyses using Proteus

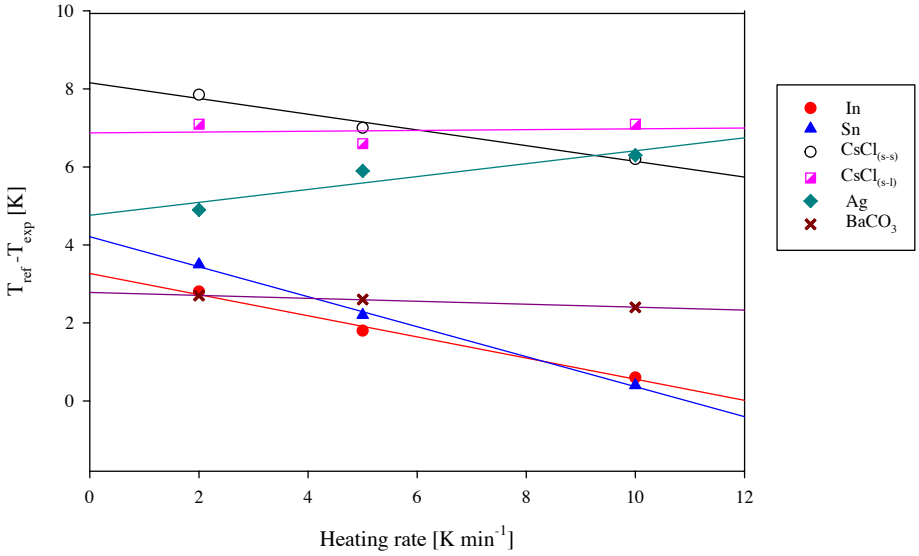

Figure 4.9: *Temperature calibration data at different heating rates.*

are shown in Figure 4.10 and Table 4.2 [83].

$$T_{corr} = 10^{-3}b_0 + 10^{-5}b_1T_{exp} + 10^{-8}b_2{T_{exp}}^2, \tag{4.1}$$

where b_0, b_1, and b_2 represent the temperature calibration coefficients, and T_{exp} represents the measured temperature [69]. The temperature calibration curve represents an adequate trend where only two calibrants (K_2SO_{4s-s} and $BaCO_3$) slightly deviated from the trend.

A weighting factor was selected for each calibrant based on judgements made with each calibrant. For example, the calibrants with measured temperature differences less than 10 °C than the reference values were given a weighting factor of 2.5. After inconsistent results of the K_2SO_4 melting temperature, Au was used as a calibrant with a BN liner instead of K_2SO_4. As confirmed by Beneš et al., BN performed fairly well with all pure metal calibrants and fluoride salts [61]. A lower weighting factor was applied to Au, because it used a different liner material. The standard uncertainty was found to be ± 1.6 °C based on regression analysis (deriving from the residual).

The enthalpy of fusion of each calibrant was determined by averaging peak areas of the last two phase transition curves and calculated by Proteus [69, 83]. The fitting of Eq. 4.2 used in the sensitivity calculation analysis was as follows [69]:

$$y = (P_2 + P_3 z + P_4 z^2 + P_5 z^3) e^{-z^2}$$
$$z = \frac{T - P_0}{P_1} \tag{4.2}$$

where P_0 - P_5 are sensitivity coefficients, and T is the measured temperature. Results of a linear regression analysis using the Proteus software are provided in Figure 4.11 and Table 4.3.

The measured value of Au was -12.145 μV sec /mg; however, a lower weighting factor had to be applied to Au, because BN was used as a liner instead of Ni. The rest of the calibrants with measured sensitivity values followed the general trend, a weighting factor of 1.0 was given as a default value.

During the calibration campaign, the STA had the capability of performing thermogravimetric analysis and DSC simultaneously, where the mass of the sample was actively measured during each DSC measurement. No measurable change in mass was observed in any measurement, which verifies that the crucible was hermetically sealed.

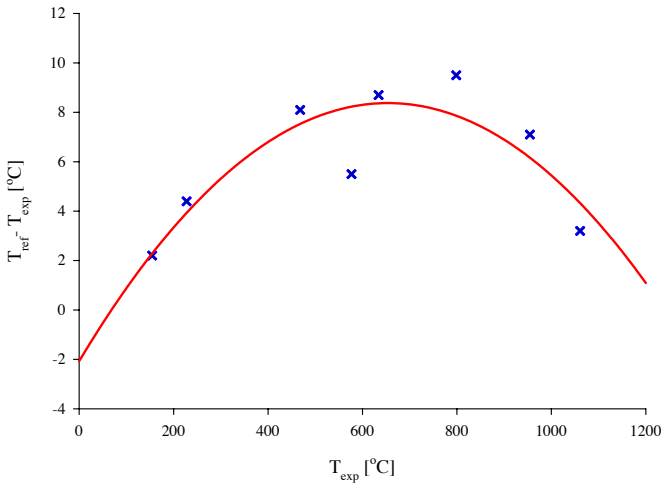

Figure 4.10: *Linear regression analysis of experimentally obtained temperature calibration values.*

Table 4.2: *Temperature calibration matrix.*

Substance	Reference Temperature [°C] [69]	Measured Temperature [°C]	Weighting Factor	Corrected Temperature [°C]
In	156.6	154.4	10.0	156.8
Sn	231.9	227.5	5.0	231.3
$CsCl_{s-s}$	476.0	467.9	2.5	474.8
K_2SO_{4s-s}	582.0	576.5	5.0	584.1
$CsCl_{s-l}$	643.0	634.3	2.5	642.1
$BaCO_3$	808.0	798.5	2.5	806.2
Ag	961.8	954.7	3.0	961.3
Au	1064.2	1061	1.0	1066.4

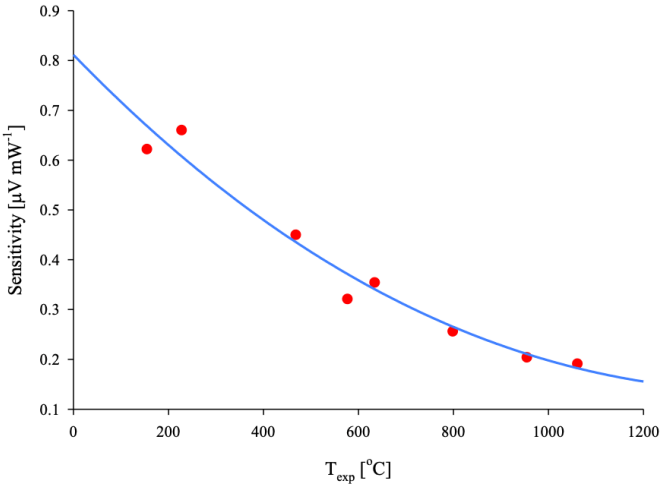

Figure 4.11: *Linear regression analysis of experimentally obtained sensitivity calibration values.*

Table 4.3: *Sensitivity calibration matrix.*

Substance	Reference Enthalpy [J g^{-1}] [69]	Peak Area [μV sec /mg]	Measured Sensitivity [μV/mW]	Weighting Factor	Calculated Sensitivity [μV/mW]
In	-28.6	-17.775	0.622	1	0.642
Sn	-60.5	-39.93	0.66	1	0.629
$CsCl_{s-s}$	-17.2	-7.745	0.45	1	0.457
K_2SO_{4s-s}	-35.06	-11.27	0.321	1	0.363
$CsCl_{s-l}$	-121.77	-43.05	0.354	1	0.322
$BaCO_3$	-94.9	-24.34	0.256	1	0.24
Ag	-104.6	-21.37	0.204	1	0.21
Au	-63.7	-12.145	0.191	0.5	0.202

4.3 Sample Preparation

Fluoride salts are categorized as non-actinoid fluorides or actinoid fluorides. In addition to the hygroscopic nature of most fluoride salts, the relatively high stability of actinoid oxides requires a more rigorous purification process. Dehydration/purification procedures of as-received salt materials play a significant role in the sample preparation process. Moreover, specific laboratory equipment are essential for establishing proper dehydration/purification procedures of fluoride salts.

4.3.1. Laboratory Equipment

To ensure the purity of samples, procured salt components are immediately stored in the glovebox. The MBRAUN glovebox shown in Figure 4.12 provides an inert atmosphere with a constant circulation of ultra-high purity argon gas (Ar). Besides, it serves as a radiation protection barrier when working with radioactive materials (e.g., ThF_4, UF_4). The glovebox is equipped with additional sensors that control levels of H_2O and O_2 (i.e., max <5 ppm, typical $\sim <1$ ppm) inside the glovebox. The two gloveports allow one to manipulate samples and equipment safely, while the two antechambers are used for ingressing/egressing items.

When an antechamber is in use, one must ensure that the atmosphere inside the antechamber and the environment it is open to are identical. This aspect is quite important during the ingressing process as opening the antechamber filled with ambient air may result in compromising the inert atmosphere in the glovebox. The use of antechambers must comply with the following procedure: evacuation of the antechamber atmosphere (i.e., Ar if ingressing or ambient air if egressing) for 30 seconds followed by a re-fill of a desired atmosphere. Prior to opening the antechamber, the cycle must be repeated three times.

A number of instruments and accessories must be available within the glovebox to purify samples. A ThermoScientific Cimarec hotplate with a maximum temperature of 540 °C sitting in the glovebox is shown in Figure 4.13. A beaker with a sand bath is positioned on the hot plate and a thermocouple is placed in the sand adjacent to the beaker to monitor the temperature (see Figure 4.13). The recording of the sand temperature is approximated as the temperature of the sample. Storage and handling of waste is organized such that the radioactive waste is stored in a

Figure 4.12: *The MBRAUN glovebox used for fluoride salts investigations.*

Ziploc bag inside the plastic container on the top shelf, whereas regular waste gets egressed and scanned, as a safety precaution, and disposed of appropriately. As soon as the radioactive waste container is filled, it gets egressed, scanned, and stored in a metallic locked radiation cabinet located in the laboratory for future disposal, which is facilitated by the Radiation Safety Officer.

A number of additional items for sample preparation were used:

- Anti-static plastic trays to avoid spillage of the sample on the surface of the glovebox and the mass balance;
- Agate mortar and pestle to mill samples;
- Thin SS scoopulas ($\sim$ 15 cm long) to minimize spilling when handling small amounts of sample materials;
- Lint-free Kimwipes to maintain a clean working space in the glovebox.

Sample quantity optimization plays a role in DSC measurements. For example, powder samples may experience poor thermal contact with the floor of a crucible [84] resulting in receiving a weak DSC signal [85]. However, it was also observed that a larger sample mass may result in a lower

resolution (i.e., peaks broadening) [85]. The sample mass had to be optimized considering the nature of the fluoride salts (i.e., its form and density) and the free volume of the Ni liner with a maximum height of 5.35 mm.

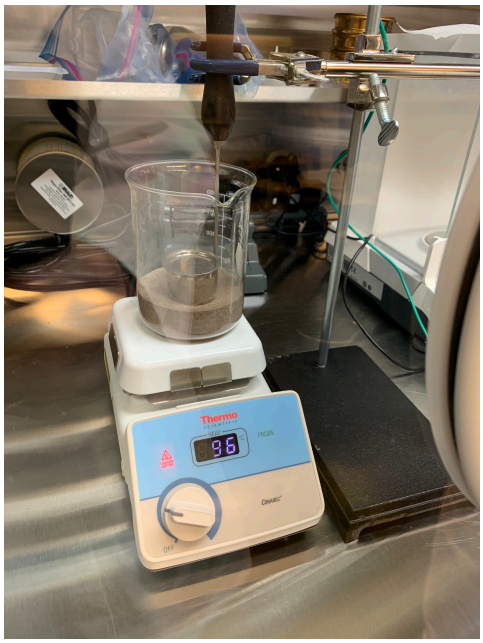

Figure 4.13: *A set-up of the dehydration/purification procedures of the fluoride samples, including a Thermo Scientific Cimarec hotplate with a beaker on top and a retort stand with the thermocouple inserted next to the hotplate.*

While having performed instrument calibration procedures, it was determined that for a powder sample, a mass of $\sim$ 40 - 50 mg was adequate to obtain a sufficient DSC signal without overfilling the crucible. Hence, the sample mass of fluoride salts for DSC measurements was chosen to be in the 40 - 50 mg range with the aforementioned considerations. An amount of as-received materials decanted for dehydration/purification procedures must be more than the targeted mass for DSC measurements, as manipulation of a sample during those processes tend to slightly reduce mass of a sample (e.g., some powder of as-received materials may stick to the mortar and pestle).

4.3.2. Non-Actinoid Fluorides

Non-actinoid fluoride salts that were investigated in this work were the following:

- Lithium Fluoride (LiF) (Alfa Aeser, 99.99 % metals basis);

- Cesium Fluoride (CsF) (Sigma-Aldrich, 99.99 % metals basis);
- A ternary eutectic mixture of the LiF-NaF-KF system (46.5-11.5-42 mol %; a.k.a. "FLiNaK"), which was provided by ORNL [86].

According to safety data sheets provided by the suppliers, LiF and CsF can be safely handled wearing nitrile gloves, a lab coat, and eye protection [87, 88]. During the course of experimental work, there were always at least two barriers between the sample and the researcher (e.g., three sets of gloves).

A simple dehydration process of the samples followed thorough Standard Operation Procedures developed by Hallatt [66], which leveraged some previous experiences published in the open literature. As the first step of the simple dehydration process, an agate mortar and pestle were used to reduce the particle size of as-received salt materials (see Figure 4.14 (a)). This is an important step to ensure uniform contact on the bottom of the crucible for heat transfer, to maximize the surface-to-volume ratio for dehydration, and to facilitate decanting of salt components to precise quantities (this is particularly important for preparing multi-component salts). Secondly, a heat treatment of the sample at 350 °C for 5 hours was implemented in an open Ni reaction vessel on the hotplate within the glovebox[1]. Finally, the sample was milled again at ambient temperature to achieve a fine homogeneous powder before transferring it into a crucible. Figure 4.14 shows (a) a milled sample of CsF after using a mortar and pestle for $\sim$ 5 min and (b) the same sample subjected to a 5 h dehydration process at 350 °C. No significant colour change was observed after the dehydration process; however, the sample was noticeably drier when it was subjected to a second milling.

4.3.3. Actinoid Fluorides

Prior to performing a dehydration procedure, actinoid fluorides were required to undergo a purification stage [63]. A pure component of ThF_4 was studied in this work. Due to the lack of an HF gas line (i.e., a common industrial source of fluorination), an alternative technique was used where NH_4HF_2 powder was added to the ThF_4 sample [62, 63, 89]. This process was intended to fluorinate actinoid oxide impurities, leaving the residual ammonia, water vapour, and excess HF

[1] Fluorides are known to be more chemically aggressive than inorganic compounds. Therefore, the process for dehydrating non-actinoid fluorides was more aggressive by increasing the temperature.

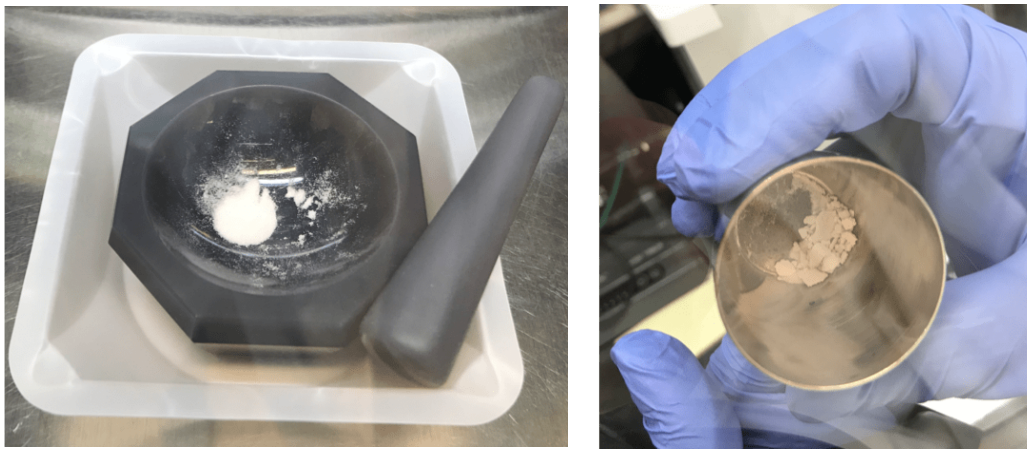

(a) *A CsF sample after a milling process.*

(b) *The same CsF sample after a 5 h dehydration process.*

Figure 4.14: *A CsF sample before and after dehydration.*

to evaporate during the dehydration stage, as discussed §3.3.3. A simplified form of the reaction of ThO_2 fluorination into ThF_4 with NH_4HF_2 is represented by Eq. 4.3.

$$\begin{aligned} NH_4HF_2 &\xrightarrow{\Delta} NH_3 + 2\,HF \\ ThO_2 + 4\,HF &\longrightarrow ThF_4 + 2\,H_2O \end{aligned} \tag{4.3}$$

One of the challenges of the purification process of actinoid fluorides was to determine an appropriate mass ratio of NH_4HF_2 and ThF_4. Unfortunately, this process is not well-established and reported mass ratios of NH_4HF_2 and ThF_4 were found to be rather inconsistent [62, 63, 73, 89]. Moreover, determination of the required mass of NH_4HF_2 for purification varies with respect to the purity of the as-received ThF_4 sample [62, 63, 73, 89, 90].

Based on information available in the open literature, the two methods that were explored in this work with intention to purify as-received ThF_4 samples are:

- Method A was derived from the synthesis of ThF_4 with NH_4HF_2 [90], which was proposed by Hallatt [66] and Che et al. [90]. The mass ratio of NH_4HF_2 to ThF_4 was determined based on a 5.5 : 1 molar ratio of NH_4HF_2 and the impurity of the ThF_4, which was assumed to be entirely ThO_2 [66]. The purification procedure included the upper Ni vessel filled with solid NaOH to neutralize HF gas formed in the lower Ni vessel during the fluorination

process of the mixture of ThF_4 and NH_4HF_2 and evolved through a Ni pipe welded to the floor of the upper vessel (see Figure 3.19 (a)) [66]. The stacked reaction vessels had a loose lid sitting on top of the upper vessel (refer to Figure 3.19 (b)).

- Method B was derived from a fluorination procedure reported by Capelli [63], where the mass of NH_4HF_2 was determined based on mass ratios of NH_4HF_2 and ThF_4. A number of mass ratios explored in this work were as follows: 1 : 3.8 of NH_4HF_2 : ThF_4, 1 : 2.0 of NH_4HF_2 : ThF_4, and 1 : 1.85 of NH_4HF_2 : ThF_4. Fully enclosed DSC crucibles were used as reaction vessels to provide a hermetic seal to prototype the purification procedure.

The approach taken in Method B was derived from a process developed by colleagues at JRC and TU Delft, which used a fully encapsulated reaction vessel shown in Figure 4.15 [89, 91]. The robust reaction vessel consists of a SS body with a screw on SS lid, a Ni liner and a Ni gasket to prevent chemical interaction.

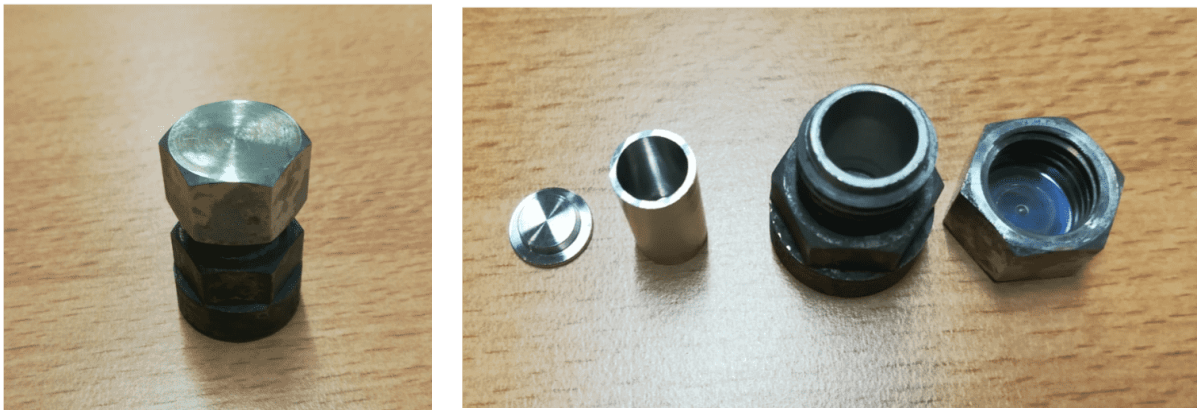

(a) *TU Delft reaction vessel.*

(b) *Four parts of the reaction vessel, from left to right: Ni gasket, Ni liner, SS body, and SS lid.*

Figure 4.15: *Reaction vessel for the ThF_4 purification procedure used at TU Delft. Photographs provided by Ocádiz-Flores [91].*

Each sample of ThF_4 with NH_4HF_2 was subjected to a heat treatment of 250 - 350 °C for 12 hours in a closed Ni reaction vessel within the glovebox following the process established by Hallatt [66]. Unfortunately, the first attempt of purifying ThF_4 by Method A was not successful, as demonstrated by poor DSC results that indicated the presence of impurities within the sample. It resulted in exploring Method B with different equipment, specifically a fully sealed DSC reaction vessel as opposed to the Ni reaction vessel with a loose lid [73].

The pressure that builds up during the NH_4HF_2 dissociation reaction must be considered when designing a reaction vessel. Due to the lack of a dedicated reaction vessel, one of the Netzsch DSC crucible sets was used as a reaction vessel to prototype the ThF_4 purification procedure. Those crucibles are rated to a maximum pressure of $\sim$ 100 bar and 500 °C [82]. Moreover, throughout the calibration procedure, the Netzsch DSC crucible set was qualified to be leak tight up to $\sim$ 1200 °C (refer to §4.2.3). It should be mentioned that DSC crucibles were intended to prototype the purification process, which is undesirable for long term use due to the small volume and high cost ($\sim$ $120 per crucible). To purify a larger amount of ThF_4, two DSC crucibles, donated by JRC [73], were also used as reaction vessels for ThF_4 purification procedures. These crucibles, which were custom designed for a different DSC instrument, are much larger than the Netzsch crucibles. Figure 4.16 shows (a) the preparation setup for decanting ThF_4 into the JRC DSC crucible, and (b) the JRC DSC crucible with ThF_4 placed on the hotplate within the glovebox.

(a) *Decanting ThF_4 into the JRC DSC crucible.*

(b) *Prepared crucible for the 12 hour dehydration process.*

Figure 4.16: *JRC DSC crucibles used as sealed reaction vessels for ThF_4 purification using Method B.*

The gaseous species produced during the purification process (see Eq. 4.3), such as NH_3 and HF, create an internal pressure in the reaction vessel; hence, calculating the number of moles of each gaseous species with respect to the constraints, such as the internal volume of a crucible, maximum operating temperature, and maximum pressure, allows one to determine a maximum mass of ThF_4 and NH_4HF_2. First, one needs to identify those constraints:

1. Internal volume of a crucible: $V_{(\text{JRC DSC crucible})}$ = 1.88 x 10^{-4} L and $V_{(\text{Netzsch DSC crucible})}$ = 0.70 x 10^{-4} L;

2. Maximum operating temperature: $T_{(purification)}$ = 250 °C, 300 °C, and 350 °C (refer to Table 4.4); and

3. Maximum pressure for both crucibles: $P_{(\text{internal})}$ = 100 bar.

Second, gaseous species were determined based on the dissociation reaction of NH_4HF_2 (i.e., $NH_4HF_2 \longrightarrow NH_3{+}2\,HF$); moreover, the glovebox environment (i.e., $Ar_{(g)}$) was also taken into account, as during the preparation of the sample, Ar was inside the reaction vessel. It should be noted that the number of moles of Ar inside the crucible prior to the purification procedure were calculated based on the ambient temperature of 25 °C and the atmospheric pressure of 1 atm. Finally, applying the ideal gas law, the number of moles of each gaseous species were therefore computed via Eq. 4.4:

$$n = \frac{PV}{RT} \tag{4.4}$$

where n $[mol]$ represents the amount of the substance, P $[atm]$ represents the pressure, V $[L]$ represents the volume, R represents the ideal gas constant equals to 0.082057 L atm mol^{-1} K^{-1}, and T $[K]$ is the temperature.

The summation of the amount of gaseous species produced during the purification process, was then used to determine a maximum mass of ThF_4 and NH_4HF_2 for each mass ratio. The purification matrix applied to each ratio of ThF_4 and NH_4HF_2 is summarized in Table 4.4.

After the purification stage, the sample was again milled using the mortar and pestle, and then moved to the open Ni reaction vessel for the dehydration stage. The dehydration procedure of actinoid fluorides included a heat treatment of $\sim$ 400 °C for 6 hours in an open Ni vessel placed on the hotplate allowing residual impurities (i.e., H_2O and NH_3) to evaporate [66].

Table 4.4: *Summarized purification matrix applied to each ratio of ThF_4 and NH_4HF_2.*

Mass ratio of NH_4HF_2 : ThF_4	Mass of components [mg]		Calculated internal pressure [bar]	Approximated Temperature [°C]	Reaction Vessel
	NH_4HF_2	ThF_4			
Method A [66]					
1 : 650	0.81	526	-	250	Stacked Ni reaction vessel
Method B					
1 : 3.8	2.9	11	96	250	Netzsch DSC
1 : 2.0	7.0	13	95	300	JRC DSC
1 : 1.85	6.5	12	96	350	JRC DSC

4.4 Sample Encapsulation in a DSC crucible

When transferring a prepared salt sample into a DSC crucible, a number of steps were executed to minimize spillage of the sample and achieve a desired sample mass.

4.4.1. Single-Component Samples

Once the fluoride samples were prepared within the glovebox, they were placed in a DSC crucible, which was sitting on a Sartorius Quintix high-precision mass balance (0.01 mg resolution) to ensure a desired quantity of the sample was used. The mass of the crucible was tared once the mass balance stabilized. Figure 4.17 shows the process of decanting the sample from the Ni reaction vessel to the crucible within the glovebox.

A Netzsch sealing press (Netzsch product no. 6.239.2-92.4.00) with an adjustable torque wrench was used in order to ensure a consistent leak tight seal of each crucible. A torque specification of 2.0-2.5 Nm was used in accordance with recommendations by the vendor [92]. Figure 4.18 shows (a) the crucible sitting on the sealing press, and (b) the Netzsch sealing press components, including the lid and the torque wrench [82].

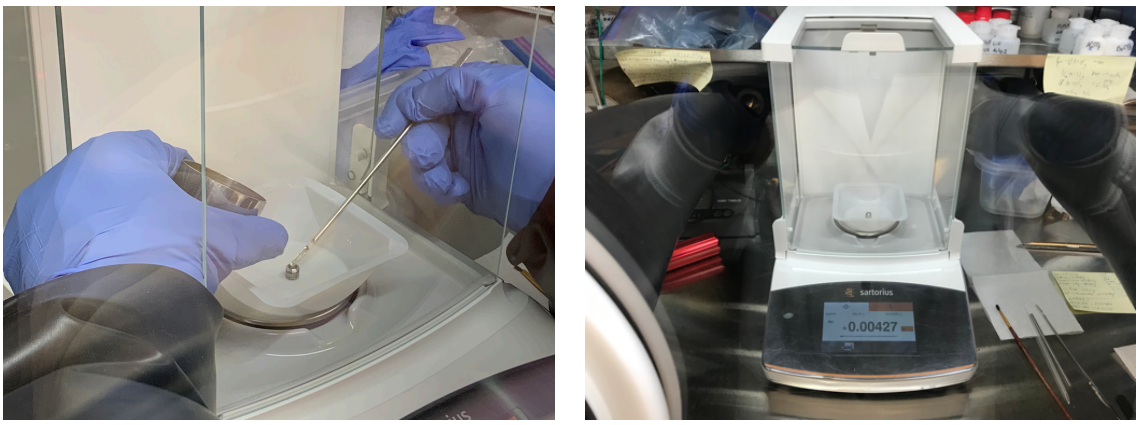

(a) *Decanting a purified sample into a crucible.*

(b) *Measuring the mass of a sample within the crucible with a high-precision mass balance.*

Figure 4.17: *Fluoride salt samples are decanted into the DSC crucible then weighed with a high-precision mass balance within the glovebox.*

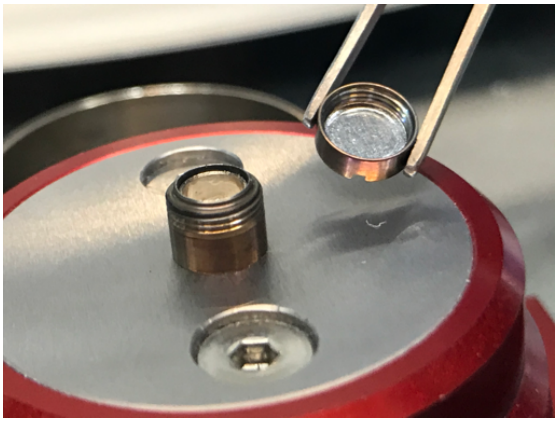

(a) *A DSC crucible positioned on the sealing press.*

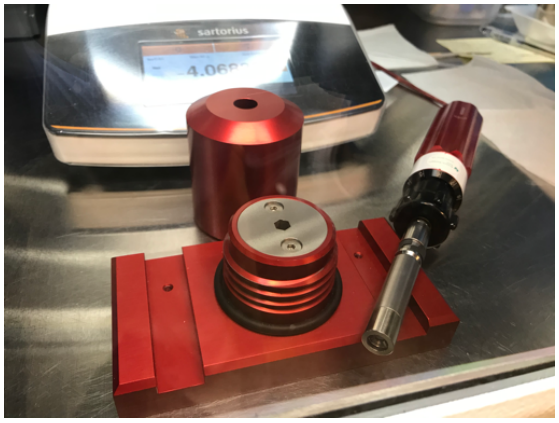

(b) *The Netzsch sealing press components including the base plate, the two-part press, and the adjustable torque wrench.*

Figure 4.18: *The Netzsch sealing press used to tighten the DSC crucibles.*

4.4.2. Multi-Component Samples

In this work, LiF and CsF were the components of the LiF – CsF binary mixture that was investigated. Each component was subjected to the simple dehydration procedure described in §4.3.2. Twelve different compositions of LiF – CsF were intended to be measured, as summarized in Table 4.5. However, only seven compositions were measured due to the university closing in response to the COVID-19 pandemic outbreak. For sake of convenience, the total mass of each binary mixture was fixed to ∼50 mg. The mass of each component presented in Table 4.5 was calculated using Eq. 4.5:

$$n_{(CsF)} = \frac{m}{\left(\frac{1-x_{(CsF)}}{x_{(CsF)}}\right) M_{(LiF)} + M_{(CsF)}} \tag{4.5}$$

where $n_{(CsF)}$ $[mol]$ represents the number of moles of CsF, m $[mg]$ represents the total mass of the LiF – CsF mixture, $x_{(CsF)}$ represents the mole fraction of CsF, $M_{(LiF)}$ and $M_{(CsF)}$ $[g/mol]$ represent the molar mass of LiF and CsF, respectively. Those points were specifically chosen to not be redundant with previously reported measurements in the LiF – CsF system, but to be complimentary and to fill knowledge gaps.

A set of two crucibles per composition was used for all DSC measurements. The component with the lowest melting point (i.e., CsF) was placed first into the crucible followed by the second

component, as recommended by Capelli[63]. This method was implemented by Capelli in order to achieve effective mixing of components while performing phase transition measurements of mixtures. [63]. The preparation of each binary mixture using a direct mixing technique was made in the following order:

1. An empty crucible sitting on an empty plastic tray was placed on the mass balance;
2. After the mass stabilized, the mass balance was tared;
3. Finely milled powder of the CsF sample was placed into the empty crucible;
4. The target mass of the first component was obtained after the stabilization of the mass balance;
5. Prior to decanting the second component, the mass balance was tared again;
6. Finely milled powder of the LiF sample was placed on top of CsF in the crucible;
7. The target mass of the second component was obtained after the stabilization of the mass balance.

Table 4.5: *Planned experimental DSC test matrix of the LiF – CsF system.*

Point #	Mole fraction of each component		Calculated mass of each component [mg]		Total mass [mg]
	CsF	LiF	CsF	LiF	LiF – CsF
1	0	1	0	50	50
2*	0.05	0.95	11.78	38.22	50
3*	0.15	0.85	25.41	24.59	50
4*	0.25	0.75	33.06	16.94	50
5	0.35	0.65	37.96	12.04	50
6	0.45	0.55	41.36	8.64	50
7*	0.55	0.45	43.87	6.13	50
8	0.65	0.35	45.79	4.21	50
9	0.75	0.25	47.31	2.69	50
10	0.85	0.15	48.54	1.46	50
11*	0.95	0.05	49.55	0.45	50
12	1	0	50	0	50

* Unfortunately, points # 2, 3, 4, 7, and 11 could not be completed due to the COVID-19 pandemic outbreak, resulting in the university closure.

It should be noted that the procedure of decanting the second component into the crucible took most of the sample preparation time, as the accuracy of the targeted compositions highly depended on the mass of the second component.

Once the crucibles were fully prepared, they were egressed from the glovebox through the small antechamber (see Figure 4.12) and placed on the DSC sample carrier (see Figure 4.19). Alumina (Al_2O_3) discs were place in between the crucibles and sensor to prevent sticking, as recommended by Netzsch [93]. Despite using ultra-high purity Ar cover gas in the STA, a small – but not insignificant – oxygen partial pressure (e.g., $\sim$ 180 ppm) remained that resulted in the crucible oxidizing at $\sim$ 400 - 1200 °C. To eliminate concerns about crucible oxidation affecting DSC measurements, an Oxygen Trap System (OTS) (Netzsch product no. HTP40000A97.010-00) from Netzsch was used in all DSC measurements (shown in Figure 4.19). This reduced the oxygen partial pressure to about 20 ppm at temperatures above $\sim$ 750 °C, which was measured with a Zirox ZR 5 oxygen probe downstream from the STA. The OTS was found to be ineffective below $\sim$ 750 °C. Crucible oxidation was observed >400 °C; therefore, DSC measurements between about 400 °C and 700 °C should be carefully scrutinized.

Figure 4.19: *A pair of crucibles sits on top of inert Al_2O_3 discs (not visible) within the high sensitivity TGA-DSC-C_p sample holder. The Netzsch OTS is shown on the bottom, which is a Zr metal ring.*

4.5 DSC Measurements

Benchmarking DSC measurements in this work with other known quantities served as a form of verification of the overall experimental procedures established within the Nuclear Fuels and Materials Laboratory. Methods that were used to measure phase transition temperatures, heat

capacity, and enthalpy of fusion are described in this section.

4.5.1. Phase Transition Measurements

Melting point measurements of FLiNaK performed in this work served as a form of verification of experimental procedures. Phase transition measurements are known to be the most accurate method to confirm the purity of the sample. In case of a single-component sample, one must verify the melting point of the investigated material. Hence, a number of ThF_4 samples subjected to the complex purification and dehydration procedures (see §4.3.3) were tested using a DSC melting point determination technique. Furthermore, the purity of components of the LiF – CsF system after dehydration procedures were also verified by employing DSC melting point measurements of the pure components.

To perform DSC measurements, the sample and the crucible sets were prepared following the procedures described in §4.3. A DSC temperature program was similar to the standard temperature calibration described in §4.2.2 with a constant heating rate of 10 K/min. A DSC sequence of the last two heating cycles of FLiNaK analyzed by the Netzsch Proteus software is presented in Figure 4.20. To determine the phase transition temperature, one must find an onset temperature of an individual peak whereas the enthalpy of fusion is determined by calculating the peak area. Both operations were performed by the Netzsch Proteus software. It should be noted that for sake of visual simplicity, Figure 4.20 shows methods of phase transition temperature determination (melting point measurements) (2nd peak) and enthalpy of fusion (3rd peak) on separate curves. However, onset temperatures and peak areas of both heating cycles were required for the interpretation of the results [70].

4.5.2. Specific Heat Capacity

Specific heat capacity measurements require a single dynamic heating phase as opposed to multiple heating cycles. Specific heat capacity obtained by DSC evaluates how much energy is required to heat a substance over a temperature range of interest. It should be noted that in this work, specific heat capacity was measured at constant volume as opposed to constant pressure due to the fact that the FLiNaK sample was fully encapsulated in the DSC crucible in the Ar glovebox prior to DSC measurements. Hence, specific heat capacity is denoted as C_v in this

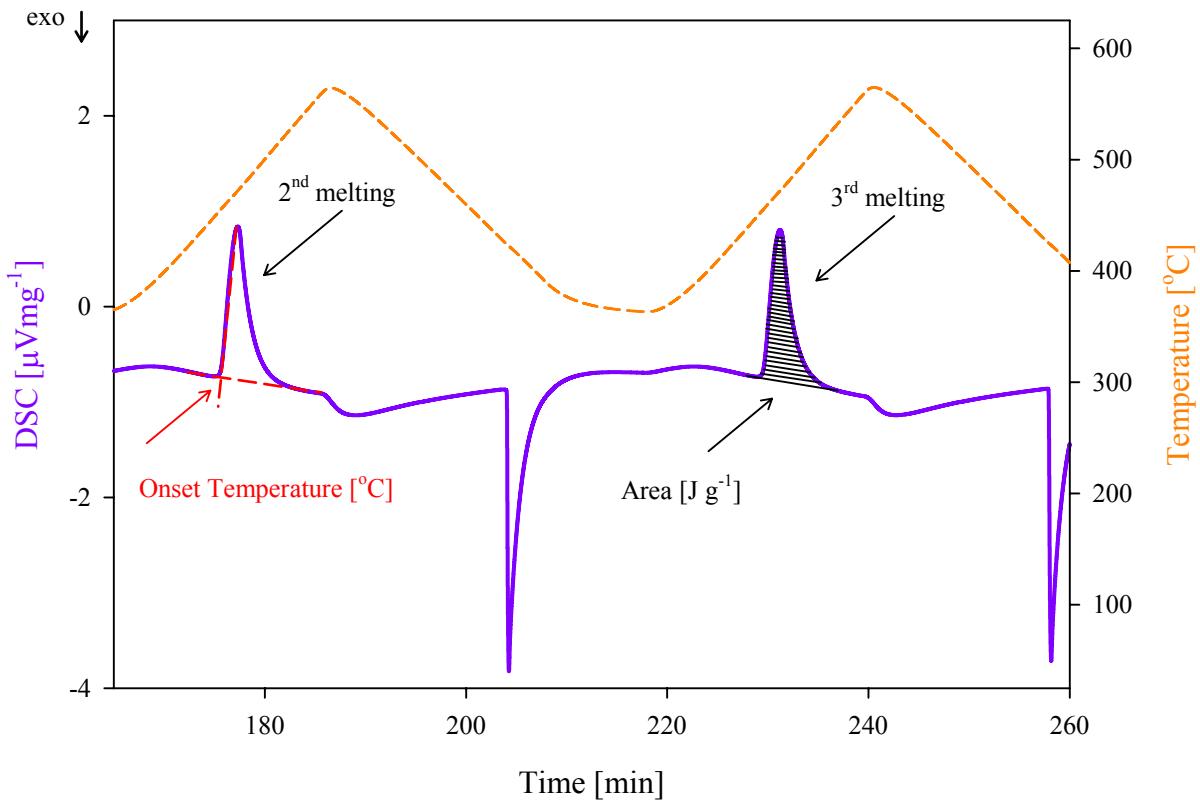

Figure 4.20: *A DSC sequence of FLiNaK for the phase transition measurements: the 2nd melting shows the onset temperature for melting point determination, while the 3rd shows the peak area for the enthalpy determination.*

work. A standard procedure to measure specific heat capacity consists of a baseline run (i.e., both crucibles are empty), a standard sapphire run, and the sample run [69, 94]. It is important to note that all conditions (i.e., crucibles, heating rate, and temperature program) must be identical for all three measurements [93]. Well-defined heat capacity data of sapphire allows one to use the sapphire sample as a standard calibrant under the same conditions as the sample [68, 94]. Subtraction of the sapphire run and the baseline eliminates possible heat flow offset experienced by the DSC instrument. Moreover, it is highly recommended to perform these tests consecutively to ensure the consistency in measurements under the same conditions [69]. The temperature range of interest was selected based on the most available data of heat capacity reported in the open literature [95, 96, 97, 98].

The temperature program for C_v measurements of FLiNaK executed in this work followed

Netzsch recommendations [93]:

1. Ramp up to 40 °C at 10 K/min;
2. Isothermal hold at 40 °C for 15 min to stabilize the start temperature and the DSC signal;
3. Ramp up to 700 °C at 10 K/min;
4. Isothermal hold at 700 °C for 15 min to stabilize the end temperature and the DSC signal;
5. Cool down.

Isothermal holds presented in the temperature program were taken into account in the heat capacity calculations of the behaviour of the DSC curves to correct for any drift, as per Netzsch explanations [93]. The specific heat capacity was plotted and calculated automatically by the Netzsch Proteus software using Eq. 4.6 [69, 93]:

$$C_v = \frac{DSC_{sample} - DSC_{baseline}}{m_{sample} \cdot r \cdot Sensitivity} \tag{4.6}$$

where m_{sample} [mg] represents the mass of the sample, r [K/min] represents the heating rate, DSC_{sample} and $DSC_{baseline}$ [μV/mg] represent the DSC signal of the sample and the baseline, respectively. The *Sensitivity* calculated by Eq. 4.7 is derived from the sapphire run [93]:

$$Sensitivity = \frac{DSC_{sapphire} - DSC_{baseline}}{m_{sapphire} \cdot r \cdot c_{v_{sapphire}}} \tag{4.7}$$

where $m_{sapphire}$ [mg] represents the mass of the sapphire, $c_{p_{sapphire}}$ [J g^{-1} K^{-1}] represents the heat capacity of sapphire (well-known reference [93]), $DSC_{sapphire}$ and $DSC_{baseline}$ [μV/mg] represent the DSC signals of the sapphire and the baseline, respectively.

4.5.3. DSC of Multi-Component Mixtures

A DSC measuring program of mixtures consisted of three consecutive heating cycles and one isothermal hold (10 min) after the first heating cycle with a heating rate of 10 K/min and a cooling rate of 5 K/min for better crystallization of the sample. The maximum temperature of heating cycles was 100 °C above the highest melting point of pure components (in this case, LiF), allowing

both components to melt. While performing DSC measurements of various compositions, it is a common practice to apply a lower heating rate (e.g., 5 K/min) to better separate the DSC curves corresponding to different phase transitions [60]. This method was employed in this work with a number of compositions: 65 mol% LiF-35 mol% CsF, 55 mol% LiF-45 mol% CsF, 35 mol% LiF-65 mol% CsF, and 25 mol% LiF-75 mol% CsF.

DSC signals of multi-component mixtures tend to appear more complex as mixtures are subjected to undergo multiple phase transitions during one heating cycle [27]. As per common practice, the solidus and the eutectic are determined by the first peak, whereas the liquidus is represented by the second and usually broader-looking peak [27]. The last two heating cycles were considered for further analysis, whereas the first heating cycle and the isothermal hold allowed the system to reach a homogeneous state. Transition temperatures of mixtures were derived from the onset temperatures of the melting peaks whereas the offset temperatures were taken for liquidus temperatures [53, 64, 65]. Solidification peaks are not considered in the analyses due to the presence of supercooling effects. This is a common practice as recommended by Beilmann [62] and Ocádiz-Flores et al. [65]. A DSC sequence of the 15 mol% LiF – 85 mol% CsF composition analyzed by the Netzsch Proteus software is shown in Figure 4.21. For sake of visual simplicity, Figure 4.21 represents the interpretation of the DSC signal of the second heating cycle only. The results of experimental investigations of the fluoride salts performed in this work are described in §5.

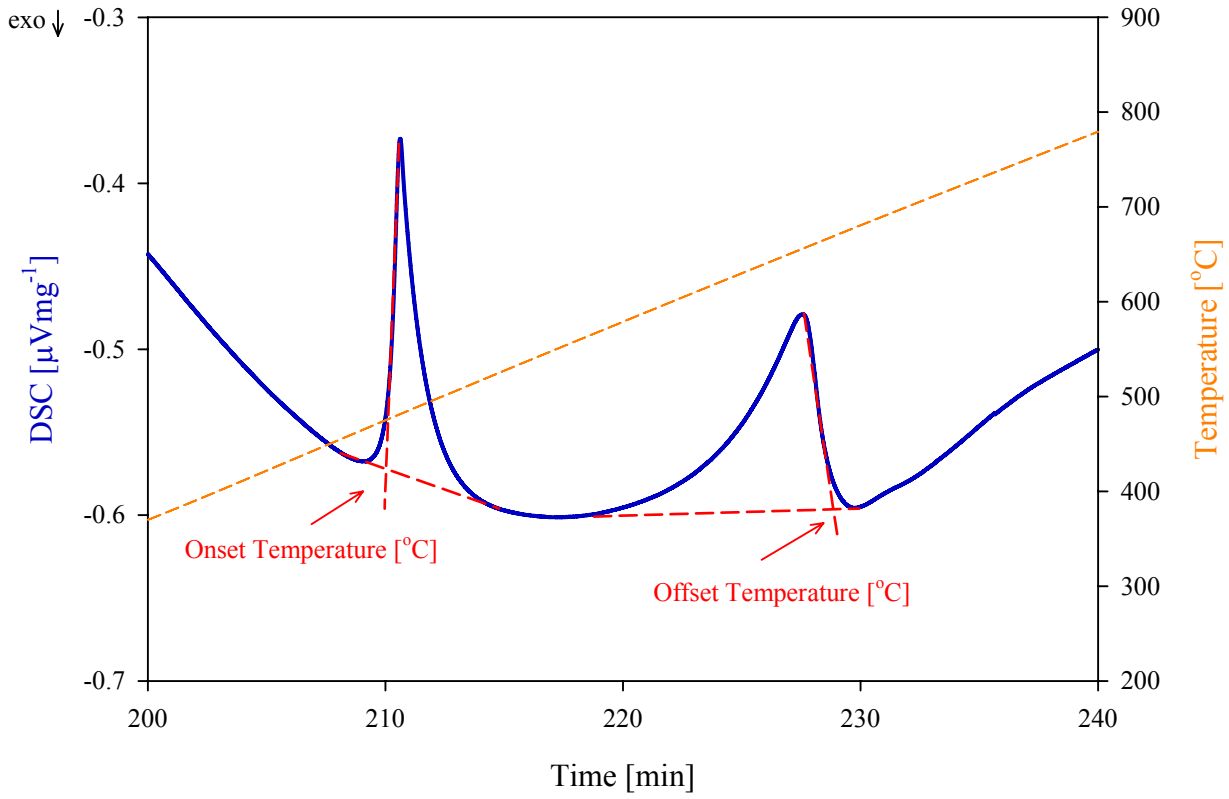

Figure 4.21: *A DSC sequence of the second heating cycle of the 15 mol% LiF – 85 mol% CsF composition for the phase transition measurements: onset temperature - solidus, offset temperature - liquidus.*

Chapter 5

Results

This chapter presents the DSC results of all fluoride salts investigated in this work. Benchmarking results are shown in §5.1, experimentally obtained data of LiF – CsF mixtures are presented in §5.2, and an error analysis is given in §5.3.

5.1 Benchmarking

The essence of a benchmarking campaign in this work was to verify and gain confidence in the experimental approach established for fluoride salt investigations. This provided a better understanding of limitations and capabilities of the custom crucible design, sample preparation procedures, and DSC measurement procedures.

5.1.1. Measurements of FLiNaK

The mass of the FLiNaK sample after the milling and dehydration processes (refer to §4.3) was 42.83 mg. A DSC sequence of the FLiNaK sample was plotted and analyzed by the Netzsch Proteus software, which is shown in Figure 5.1. The experimentally obtained melting temperature of FLiNaK($T_{melting}$) was 455.7 ± 1.6 °C, which is in good agreement with the value of 453.85 °C reported by Serrano-López et al. [99], and the value of 456±0.4 °C experimentally obtained by Johnson [100]. The enthalpy of fusion (ΔH_f) of FLiNaK obtained in this work was 566.6 $J\,g^{-1}$, which has quite a discrepancy with the value of 403.8 $J\,g^{-1}$ reported by Khokhlov et al. [98]. Results of analyses of the DSC measurements of FLiNaK are summarized in Table 5.1. It should be noted that the standard uncertainty ± 1.6 °C calculated based on the temperature calibration profile (refer to §4.2.3) is assigned only to measurements of FLiNaK and pure components LiF

and CsF.

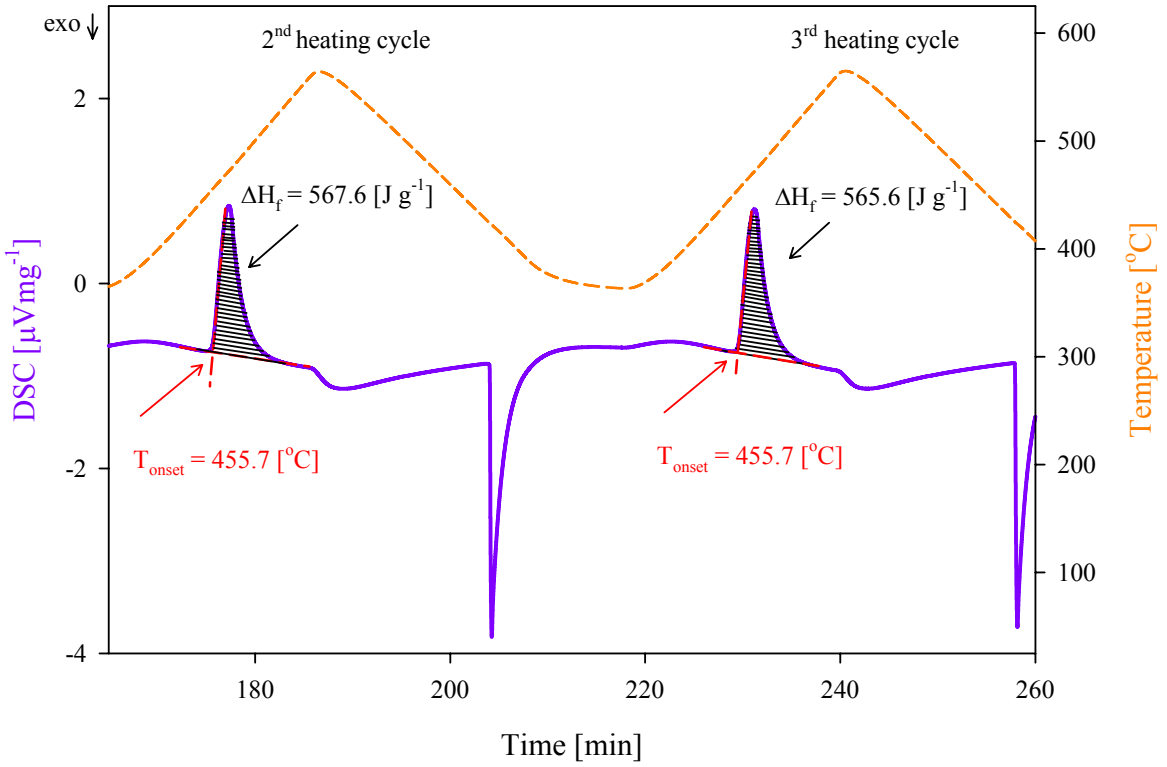

Figure 5.1: *A DSC sequence of the FLiNaK melting point determination and enthalpy measurements.*

Table 5.1: *Results of DSC measurements of FLiNaK, including melting point and enthalpy of fusion.*

Heating cycle #	$T_{melting}$ [°C]	ΔH_f [J g^{-1}]
2nd	455.7	567.6
3rd	455.7	565.6
Averaged	455.7	566.6

DSC measurements of specific heat capacity of FLiNaK obtained in this work were analyzed by Proteus (see Figure 5.2). The specific heat capacity results of FLiNaK were partitioned into the solid state and liquid state, as shown in Figure 5.3 and Figure 5.4, respectively where the phase transition shown in Figure 5.2 is not taken into account.

Despite the thorough temperature and sensitivity calibration campaign described in §4.2.3, the ΔH_f results of FLiNaK were not as successful as the $T_{melting}$ results. The specific heat capacity

results of FLiNaK obtained in this work do not follow the trend reported in the open literature. Some results are questionable and will be discussed further in §6.

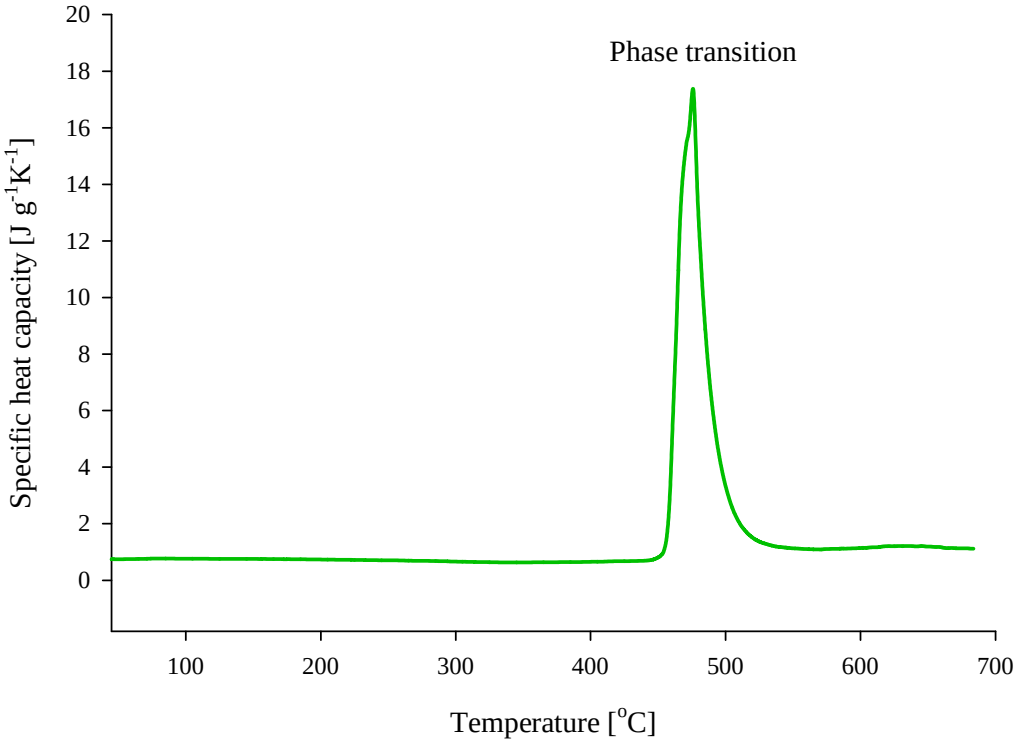

Figure 5.2: *A DSC sequence of FLiNaK specific heat capacity measurements.*

5.1.2. Measurements of ThF_4

As mentioned in §4.3.3, actinoid fluorides require more rigorous purification procedures than non-actinoid fluorides, and the phase transition measurements (in this case, the melting point determination) is the most accurate method to confirm their purity. The melting temperature of ThF_4 determined by DSC as reported by Capelli is 1106.85 °C [63] and Souček et al. is 1111.4 °C [78].

The ThF_4 samples in this work were prepared following both Method A and Method B, which were described in §4.3.3. The DSC temperature program described in §4.5.1 was applied with a maximum temperature of 1200 °C. A DSC sequence of the ∼40 mg ThF_4 sample purified by Method A is shown in Figure 5.5. This first test was stopped after the second heating cycle due to a lack of a first solidification peak and the second melting peak. One would expect

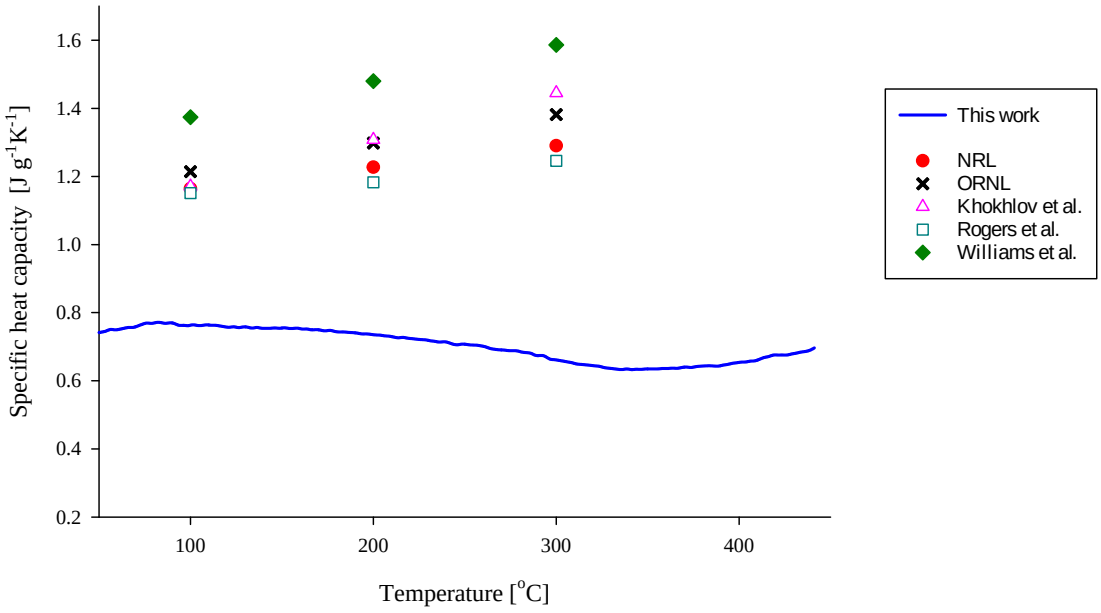

Figure 5.3: *Results of specific heat capacity measurements of solid FLiNaK studied in this work and reported values summarized by Romatoski et al. [95].*

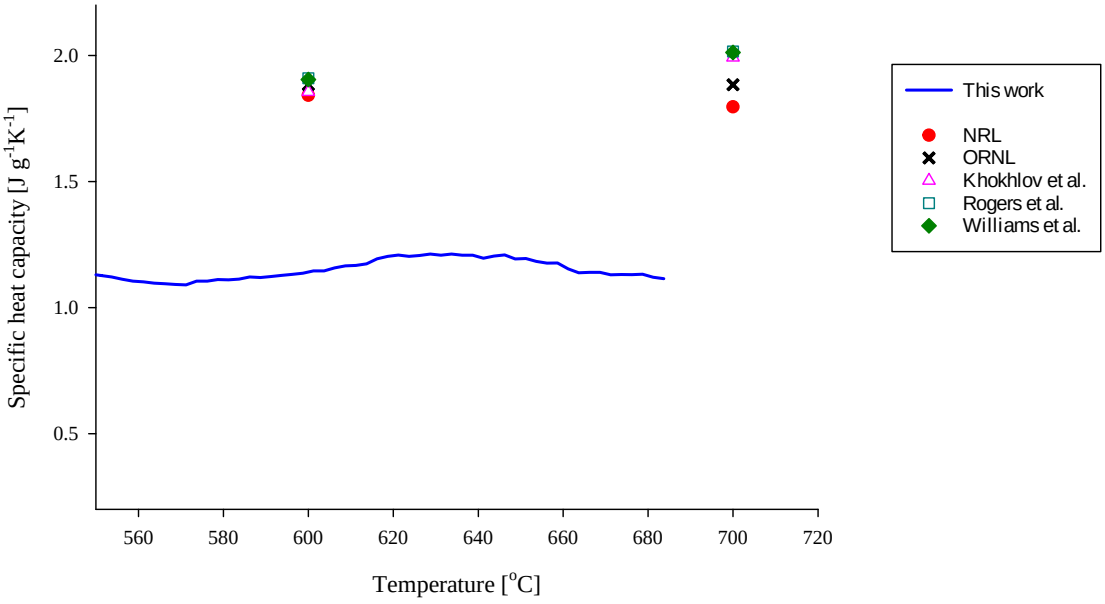

Figure 5.4: *Results of specific heat capacity measurements of liquid FLiNaK studied in this work and reported values summarized by Romatoski et al. [95].*

well-defined peaks starting at least upon the second heating cycle (refer to Figure 5.1). Such abnormal behaviour could potentially indicate chemical interaction (i.e., metal-salt interaction or

an impure sample). Similar behaviour (i.e., broad and not well-defined peaks) of a DSC signal is typically related to DSC measurements of mixtures (i.e., multi-component sample) [60]. First, the crucible was opened with vice grips within the glovebox to perform visual examination. Vise grips were used because the Netzsch sealing press (see Figure 4.18) that is preferred to seal/open DSC crucibles was not available at that time. Also, DSC crucibles appear to be almost welded shut at temperatures above 1000 °C. The ThF_4 sample was in the form of a puck and there was no evidence of interaction with the inner crucible walls, as shown in Figure 5.6. The results of the melting point determination as an indicative method of the purity verification and the visual examination led to revisit purification procedures of Method A.

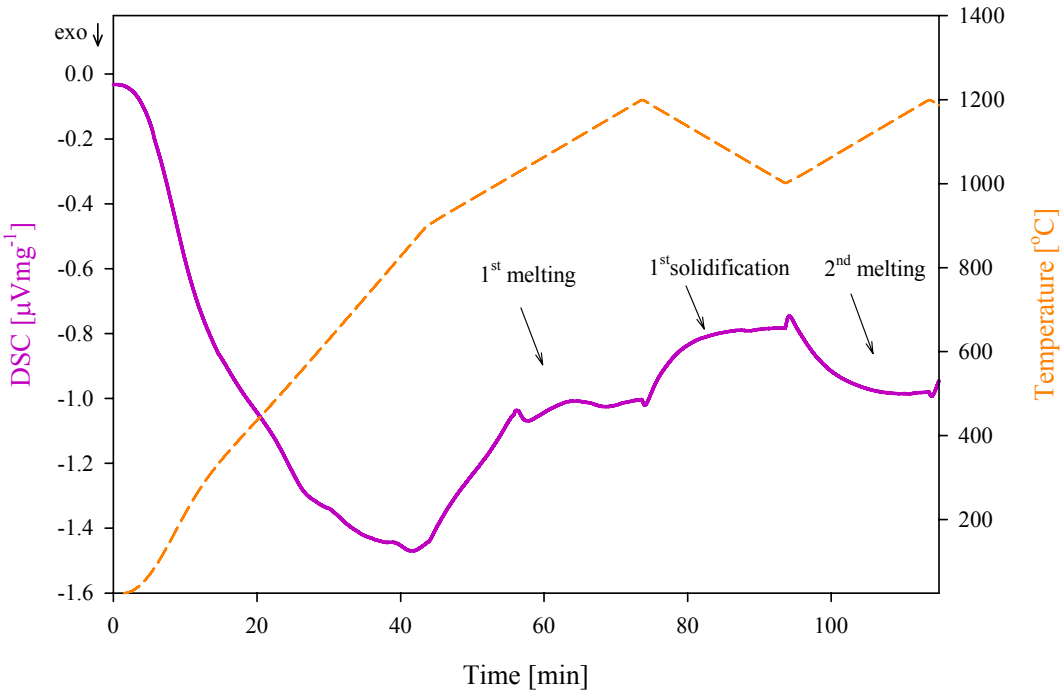

Figure 5.5: *A DSC sequence of ThF_4 purified with Method A.*

DSC measurements of an as-received sample of ThF_4 were performed prior to modifying the purification processes of Method A with the intent of providing a frame of reference. The results shown in Figure 5.7 indicate no evidence of well-defined melting peaks upon heating, whereas solidification peaks around 920 °C were observed. Such a pattern confirmed the impurity of the as-received material as well.

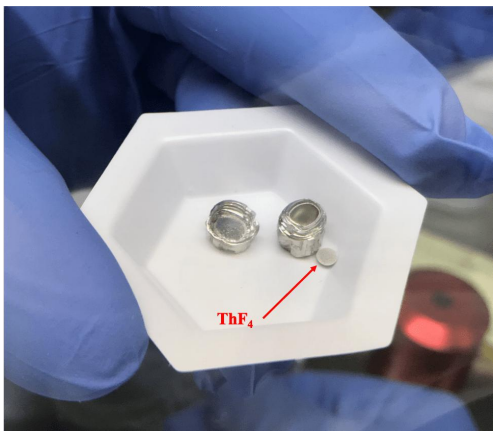

Figure 5.6: *A ThF_4 sample prepared with Method A after a DSC measurement. The sample came out as a puck with no observed wall-salt interaction.*

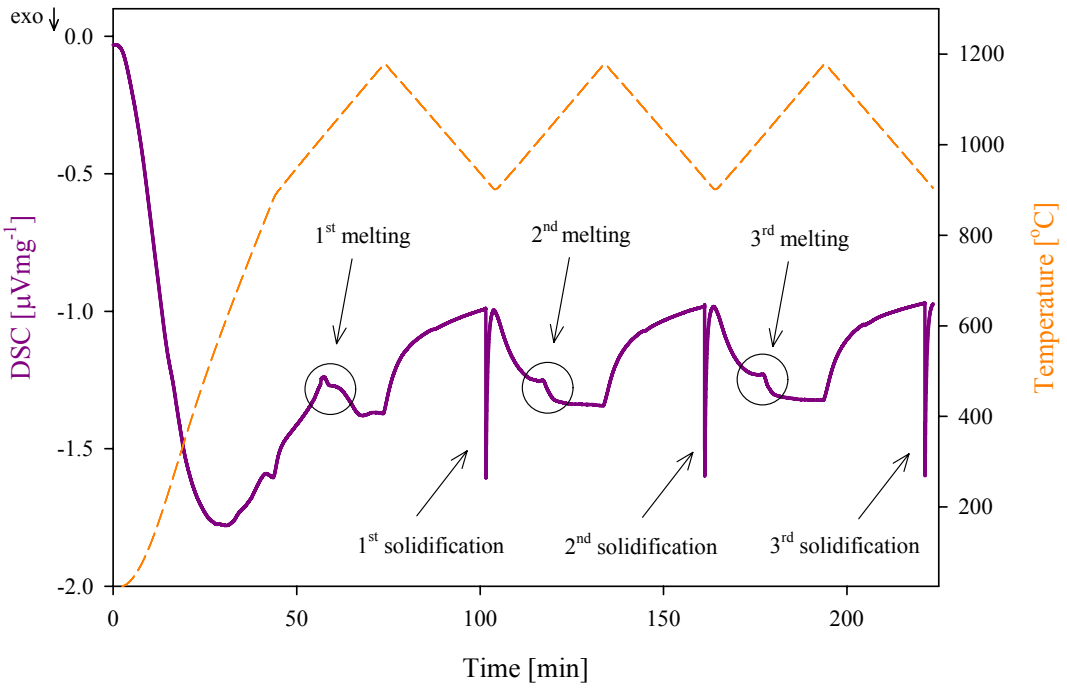

Figure 5.7: *A DSC sequence of an as-received sample of ThF_4.*

An important difference between Method A and Method B was that a fully encapsulated reaction vessel was used in Method B, which did not allow $HF_{(g)}$ to escape during the purification procedure and therefore provides an opportunity for HF to react with oxide impurities. Method B used DSC crucibles as tight sealed reaction vessels and various increased mass ratios of NH_4HF_2 and ThF_4 (see Table 4.4). Three more ThF_4 samples prepared with Method B were tested by

DSC. The results of DSC measurements of the ThF_4 sample (1 : 1.85 mass ratio of NH_4HF_2 : ThF_4) purified in the sealed crucible within the glovebox are shown in Figure 5.8. It was observed that the melting point curves of the second and the third heating cycles were also not well-defined. As a result, the onset temperature values of each curve could not be determined with confidence. A possible leak of the crucible was considered, but continuous mass measurements (i.e., via TGA) throughout the test did not show any evidence of any mass loss (see Figure 5.9).

Despite the unsuccessful DSC measurements of ThF_4, the sample purified by Method B was qualitatively observed to be more dehydrated in comparison to as-received material. Figure 5.10 shows (a) an as-received ThF_4 sample after milling, and (b) the same ThF_4 sample purified by Method B. Photographs shown in Figure 5.10 may not fully describe and justify the difference between the two samples; however, the difference was more noticeable while handling the samples within the glovebox. For example, while decanting, the dehydrated sample was not as sticky compared to an as-received ThF_4. Multiple DSC measurements of ThF_4 purified using different methods verified that the purification procedures of actinoid fluorides require further investigations.

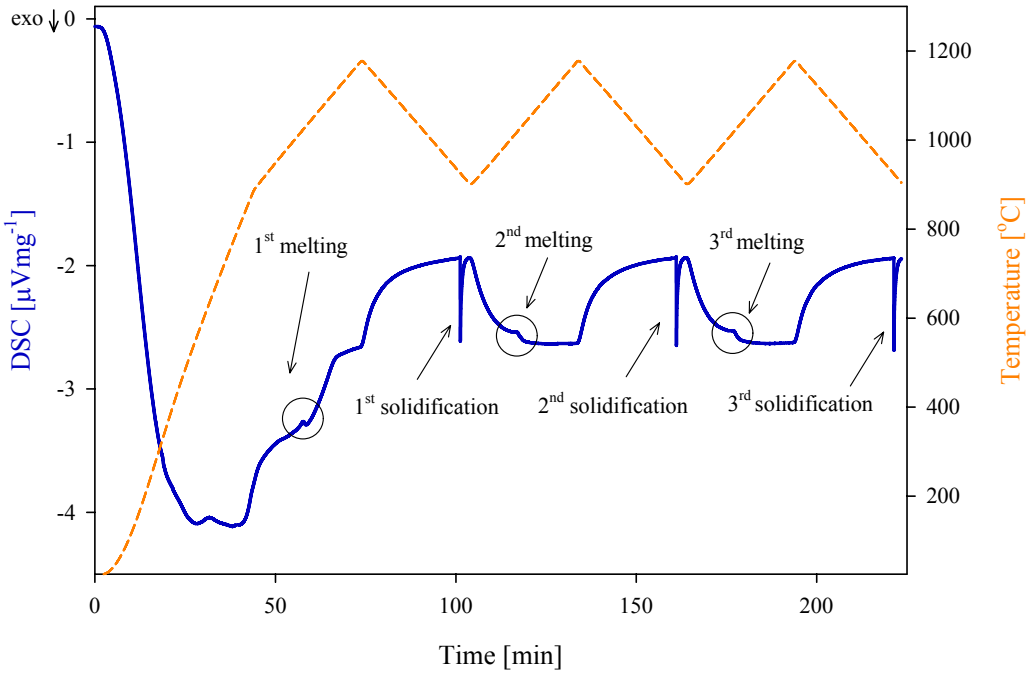

Figure 5.8: *A DSC sequence of the ThF_4 sample purified with Method B.*

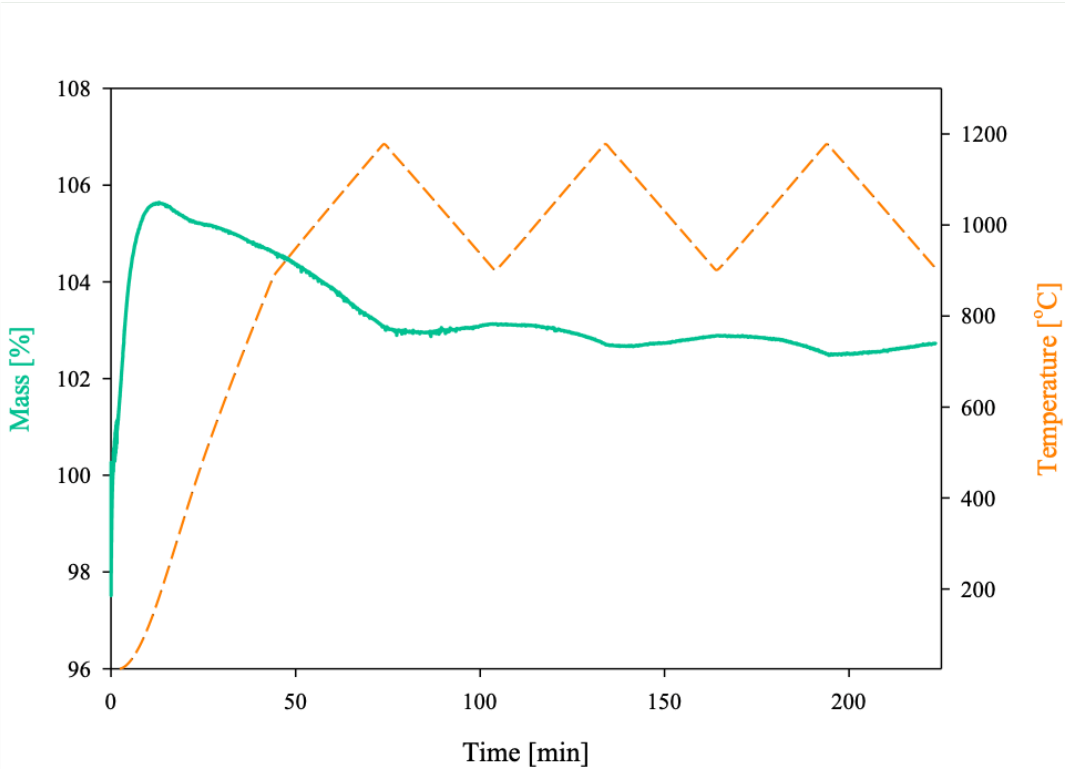

Figure 5.9: *Mass measurements of the ThF_4 sample by TGA signal during the programmed heating cycles.*

(a) *An as-received ThF_4 sample after milling.*

(b) *A ThF_4 sample purified with the 1 : 1.85 mass ratio of NH_4HF_2: ThF_4.*

Figure 5.10: *A comparison of an as-received sample of ThF_4 before and after the purification procedures with Method B.*

5.2 The LiF–CsF system

Prior to DSC measurements of LiF – CsF mixtures, the purity of individual pure components of the system was confirmed by DSC melting point measurements and compared to previously reported values. Samples were prepared following the procedures described in §4.3.2 and §4.4. Results presented in Figure 5.11 and Figure 5.12 verified the purity of pure components LiF and CsF, respectively. The melting temperature of LiF experimentally obtained in this work is 847.7 ±1.6 °C, which is in good agreement with the value of 848.2 ±5 °C reported by Capelli et al. [63]. The melting temperature of CsF experimentally obtained in this work is 703.3 ±1.6 °C, which is also in good agreement with the value of 699.55 ±5 °C determined by Beneš et al. [57].

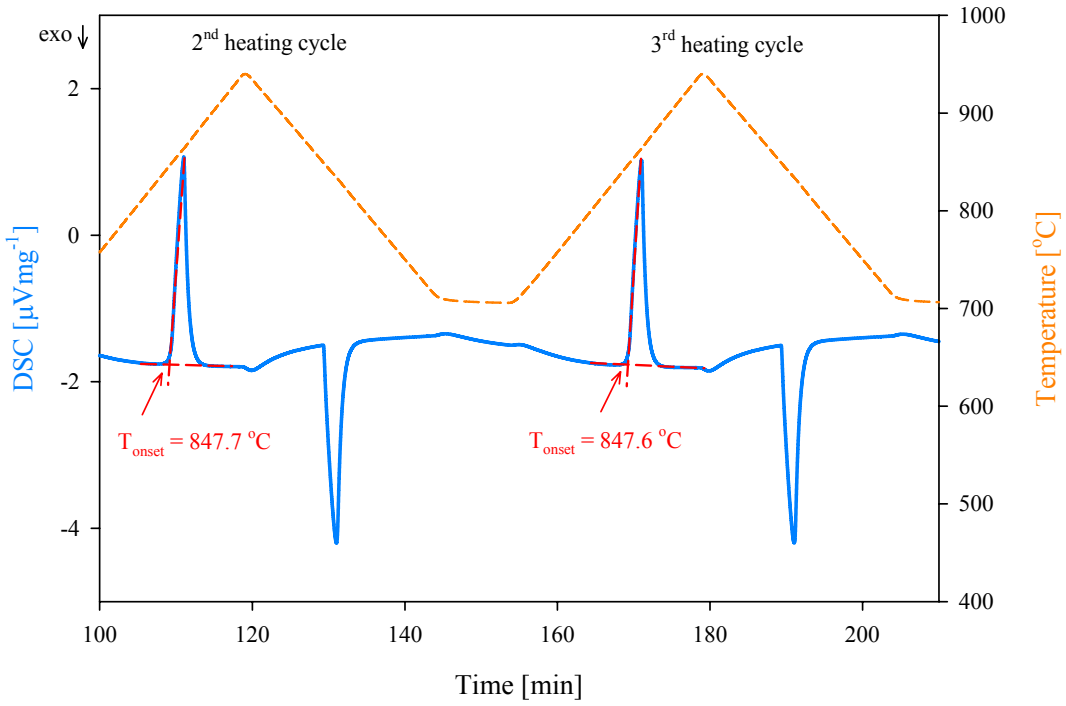

Figure 5.11: *DSC melting point determination of pure LiF.*

Compositions of LiF – CsF compositions presented in Table 4.5 were prepared following the procedures described in §4.4.2. The distribution of composition points was designed to fill knowledge gaps identified in the LiF – CsF phase diagram previously assessed by Capelli et al. [56].

The temperature steps of the DSC measurements of each LiF – CsF mixture were carefully programmed. Unlike single-component sample measurements, the first heating cycle of a multi-

component sample must involve an isothermal hold for at least 5 minutes to achieve a proper mixing of the two components as per recommendations by Ocádiz-Flores et al. [65]. This is illustrated on the left side of Figure 5.13.

The DSC sequence of the 15 mol% LiF – 85 mol% CsF composition was split into segments and the last two heating cycles were analyzed, as per standard best practices [55, 65]. The analysis of the 15 mol% LiF – 85 mol% CsF mixture, which is located on the CsF rich side of the phase diagram, is presented in Figure 5.14. Data obtained from cooling cycles were not considered due to the presence of supercooling effects observed in fluoride salt mixtures [53, 55, 64, 65].

During the DSC measurements of the 55 mol% LiF – 45 mol% CsF mixture, upon the second heating cycle it was observed that a lower heating rate had to be implemented to separate the DSC curves corresponding to different phase transitions that took place in a narrow temperature window. DSC measurements of the compositions located on the LiF rich side of the phase diagram were performed with the heating rate of 5 K/min. During the temperature calibration campaign, DSC measurements performed at 5 K/min and 10 K/min showed similar results (refer to §4.2.2); hence, switching heating rates did not have a significant impact on the DSC measurements.

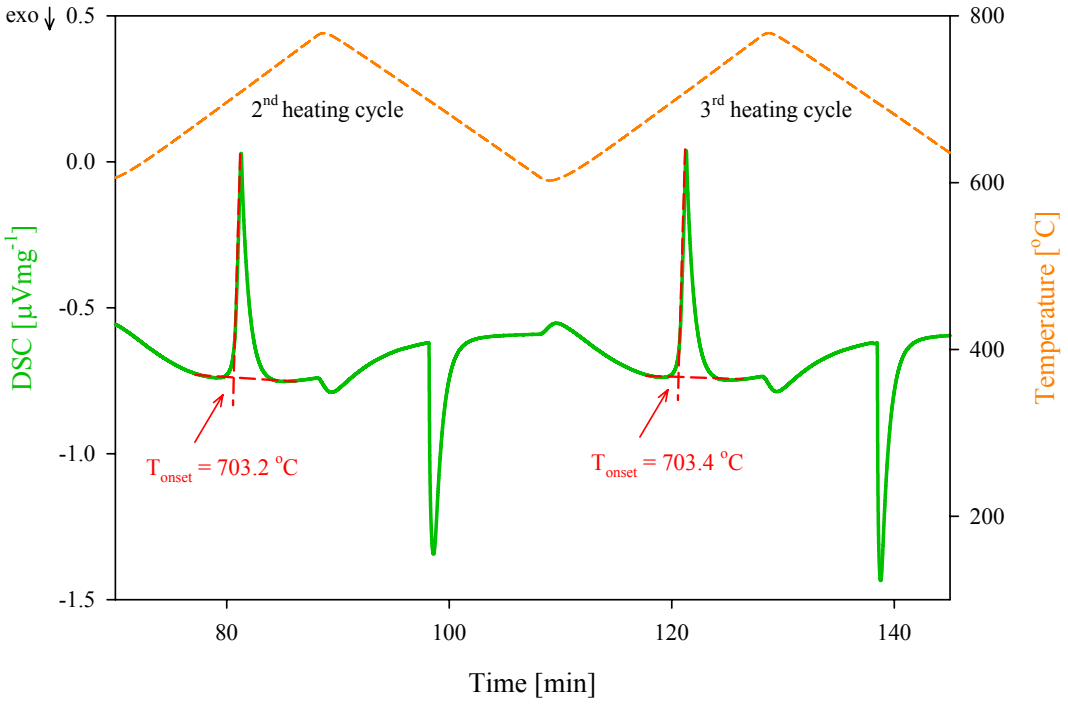

Figure 5.12: *DSC melting point determination of pure CsF.*

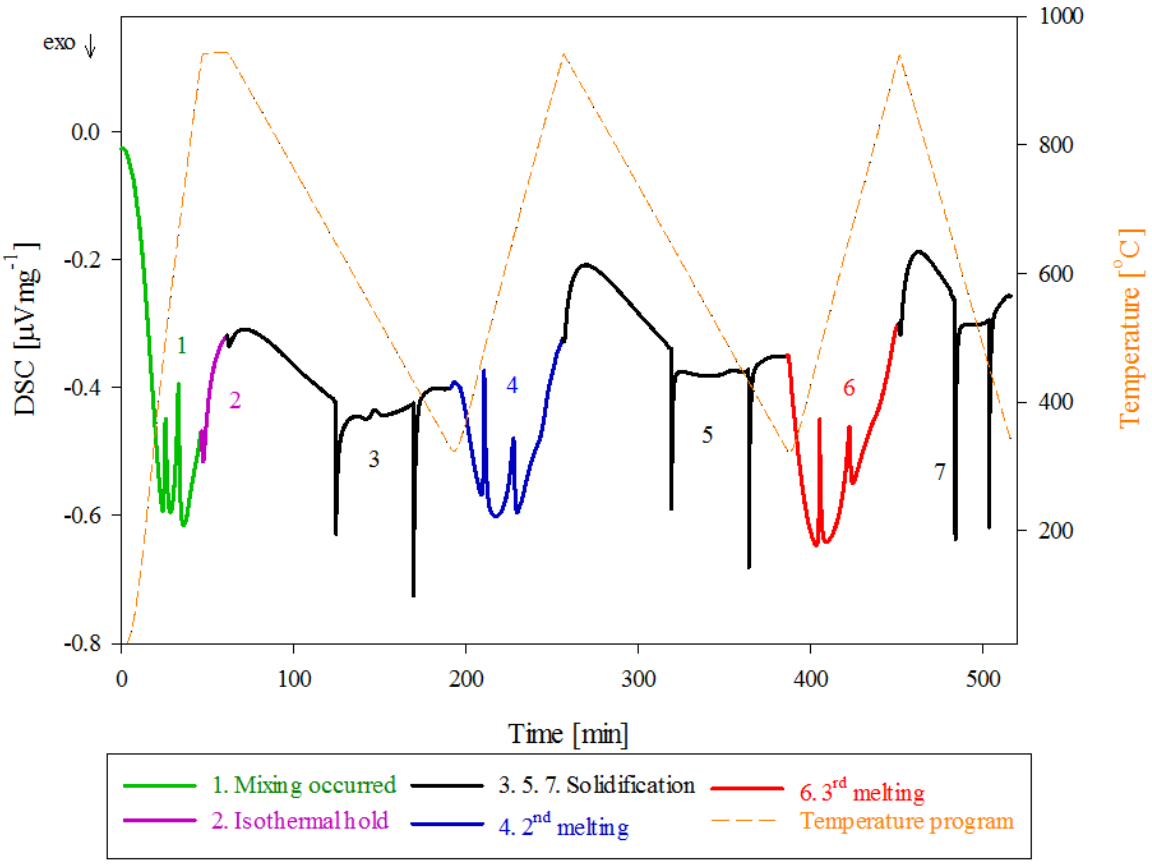

Figure 5.13: *An entire DSC sequence of the 15 mol% LiF–85 mol% CsF composition.*

Figure 5.15 represents DSC signals of the 55 mol% LiF – 45 mol% CsF mixture: (a) analysis of the 2nd melting, and (b) analysis of the 3rd melting. Despite the lower heating rate, the offset temperature corresponds to the liquidus determination of a mixture was generally difficult to identify. However, the Netzsch Proteus software allows one to recognize liquidus peaks with some modest uncertainty. Similar DSC signals were observed for the rest of the compositions; hence the the same analysis was employed to determine the phase transition temperatures.

Severe oxidation of the crucibles used in DSC mixing measurements occurred despite the presence of OTS as crucibles found to be susceptible to oxidation in the temperature range of $\sim$ 400 - 750 °C. This large degree of oxidation rendered the set of two crucibles for DSC mixing measurements as single use. Figure 5.16 gives a comparison of: (a) crucibles before DSC measurements of one mixture, and (b) crucibles after a complete DSC measurement of the same mixture. Fur-

thermore, some crucibles were opened to visually examine the sample after a DSC measurement. Figure 5.17 shows an open crucible with the solidified 15 mol% LiF – 85 mol% CsF sample in the bottom of the Ni liner with no evidence of chemical interactions between the sample and the inner Ni liner walls.

The equilibrium data of the LiF – CsF mixtures obtained in this work are summarized in Table 5.2. DSC measurement results of the LiF – CsF mixtures studied in this work are superimposed on the LiF – CsF phase diagram modelled by Capelli et al. [56] in Figure 5.18 with existing experimental data obtained by Thoma et al. [28]. The targeted compositions of 95 mol% LiF-5 mol% CsF, 85 mol% LiF-15 mol% CsF, 75 mol% LiF-25 mol% CsF, 45 mol% LiF-55 mol% CsF, and 5 mol% LiF-95 mol% CsF could not be measured due to the university closure in response to the COVID-19 pandemic. A discussion of experimental results obtained in this work is provided in §6.

Table 5.2: *Equilibrium data of the LiF – CsF system obtained by DSC measurements.*

Point #	Mole fraction x(CsF)	Measured temperature [K]	Equilibrium type	Reaction
1	0	1120.9	LiF melting point	LiF $\leftrightharpoons$ L
2	0.35	752.4	To be determined	-
3	0.35	763.9	To be determined	-
4	0.35	938.2	Liquidus	LiF+L $\leftrightharpoons$ L
5	0.45	752.2	To be determined	-
6	0.45	762.9	To be determined	-
7	0.45	845.5*	Liquidus	LiF+L $\leftrightharpoons$ L
8	0.65	752.1	Eutectic	CsF+$LiCsF_2$ $\leftrightharpoons$L
9	0.65	794.7*	Liquidus	CsF+L $\leftrightharpoons$ L
10	0.75	751.8	Eutectic	CsF+$LiCsF_2$ $\leftrightharpoons$ L
11	0.75	871.3	Liquidus	CsF+L $\leftrightharpoons$ L
12	0.85	749.1	Eutectic	CsF+$LiCsF_2$$\leftrightharpoons$ L
13	0.85	940.7	Liquidus	CsF+L $\leftrightharpoons$ L
14	1	976.5	CsF melting point	CsF $\leftrightharpoons$ Liquid

* For these compositions, solidus and liquidus signals could not be completely separated at 5 K/min.

5.3 Error Analysis

Each composition of the LiF – CsF system was prepared using a high-precision mass balance with 0.01 mg resolution. The measured mass of each component (i.e., LiF and CsF) slightly deviated from the targeted mass summarized in Table 4.5. The experimental mass error was calculated using a standard experimental error analysis and is presented in Table 5.3.

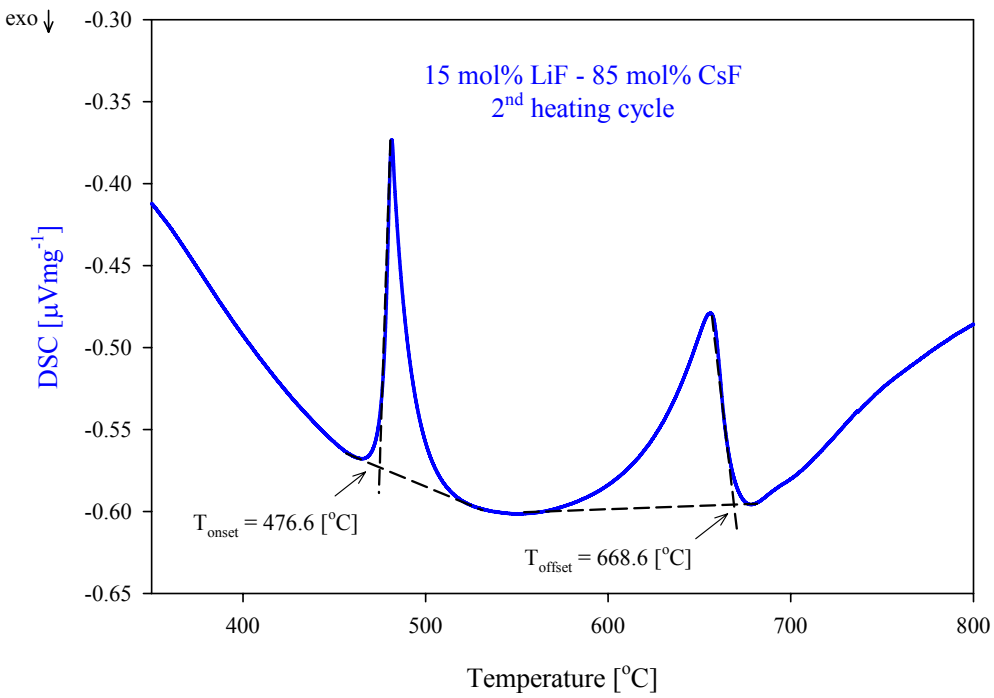

(a) *The 15 mol% LiF – 85 mol% CsF composition: 2nd heating cycle at 10 K/min.*

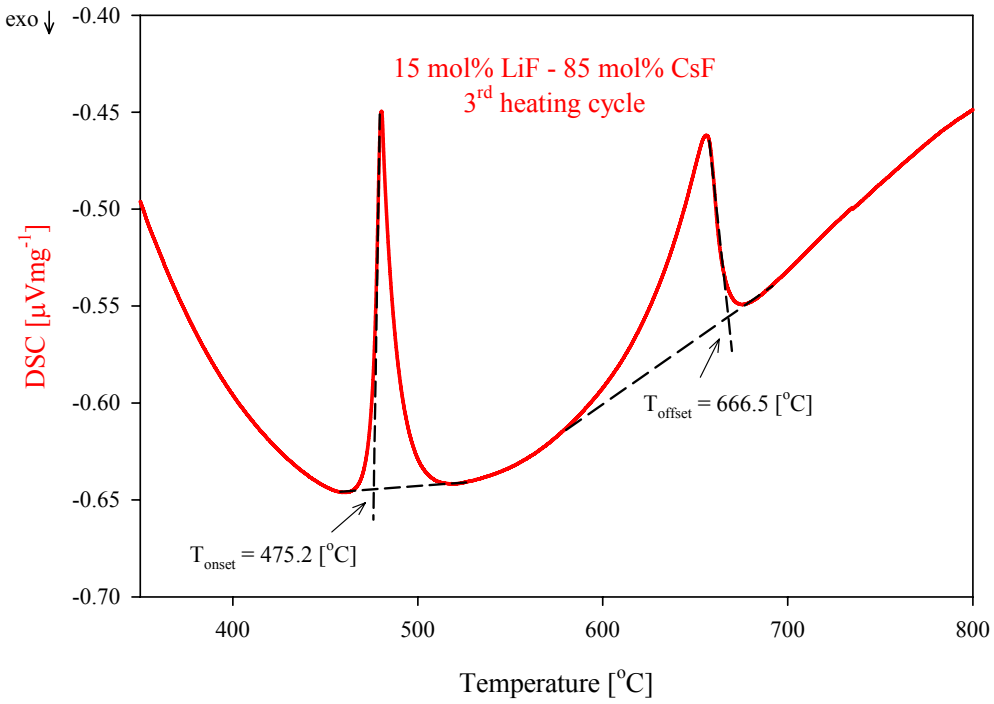

(b) *The 15 mol% LiF – 85 mol% CsF composition: 3rd heating cycle at 10 K/min.*

Figure 5.14: *Analysis of DSC mixing measurements of the 15 mol% LiF – 85 mol% CsF composition.*

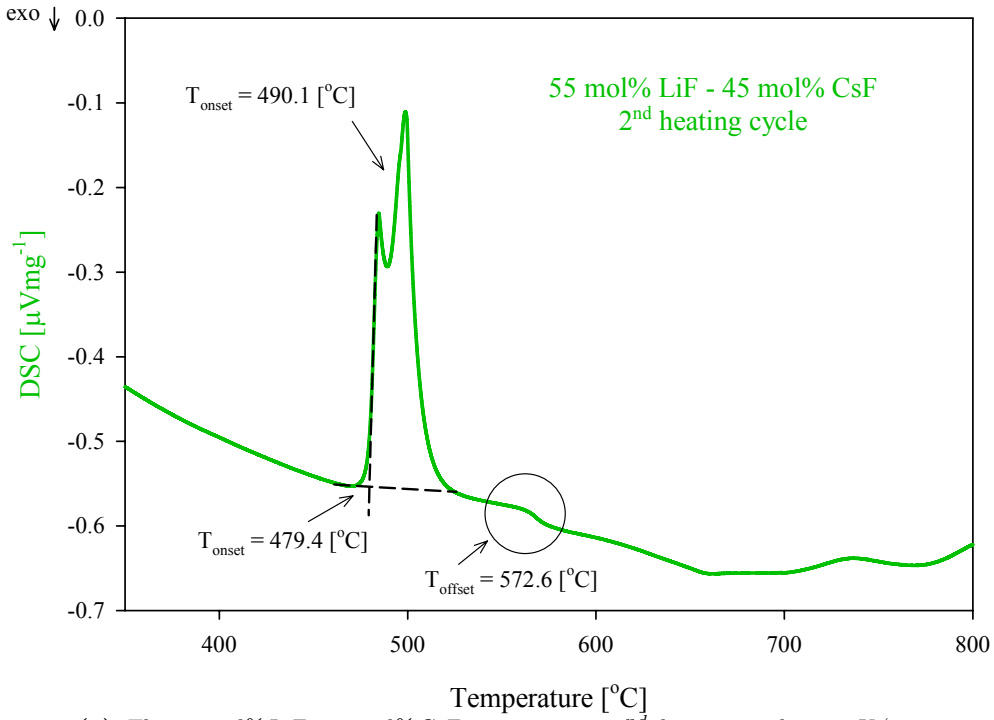

(a) *The 55 mol% LiF–45 mol% CsF composition: 2nd heating cycle at 5 K/min.*

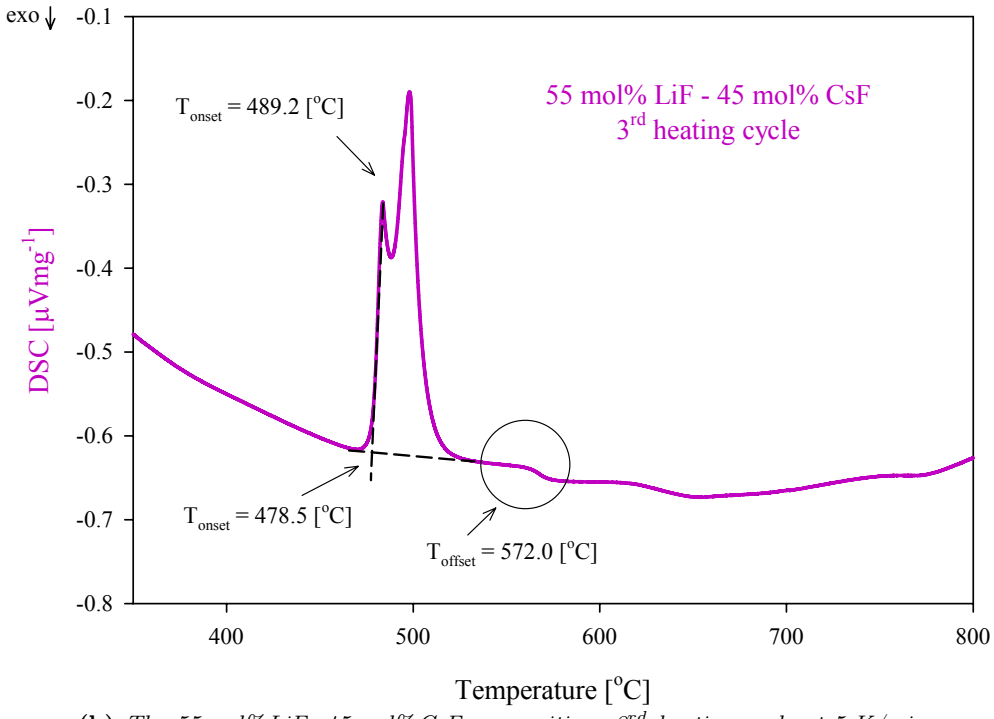

(b) *The 55 mol% LiF–45 mol% CsF composition: 3rd heating cycle at 5 K/min.*

Figure 5.15: *Analysis of DSC mixing measurements of the 55 mol% LiF–45 mol% CsF composition.*

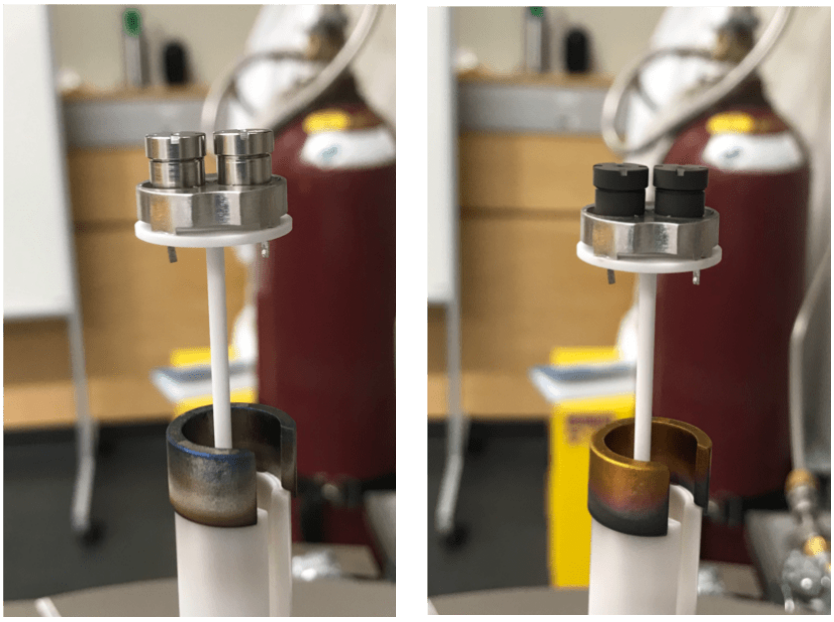

(a) *A set of brand new crucibles before a DSC measurement.*

(b) *A set of heavily oxidized crucibles after a DSC measurement.*

Figure 5.16: *A comparison of crucibles before and after DSC measurements, which shows the degree of oxidation.*

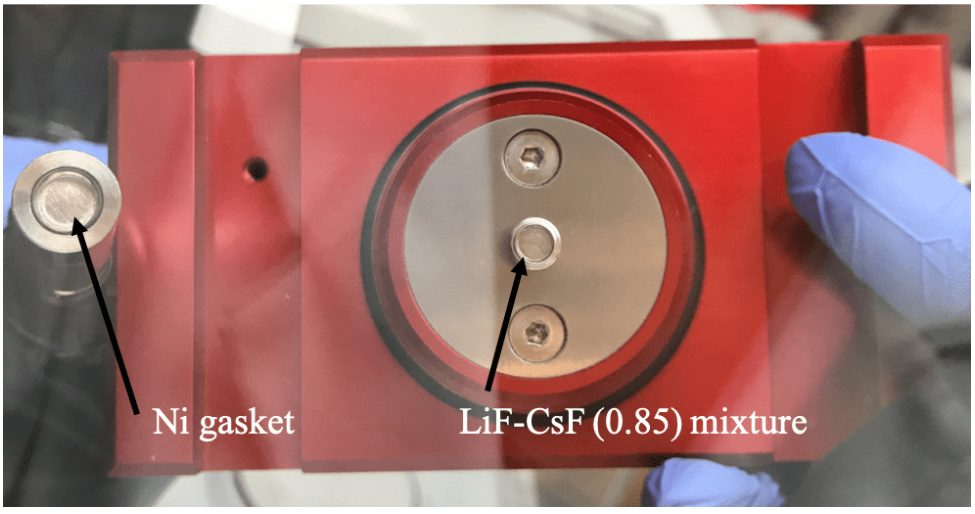

Figure 5.17: *Open crucible with the solidified 15 mol% LiF – 85 mol% CsF sample and Ni gasket after a DSC measurement, which shows no chemical interaction between the salt and the Ni surfaces.*

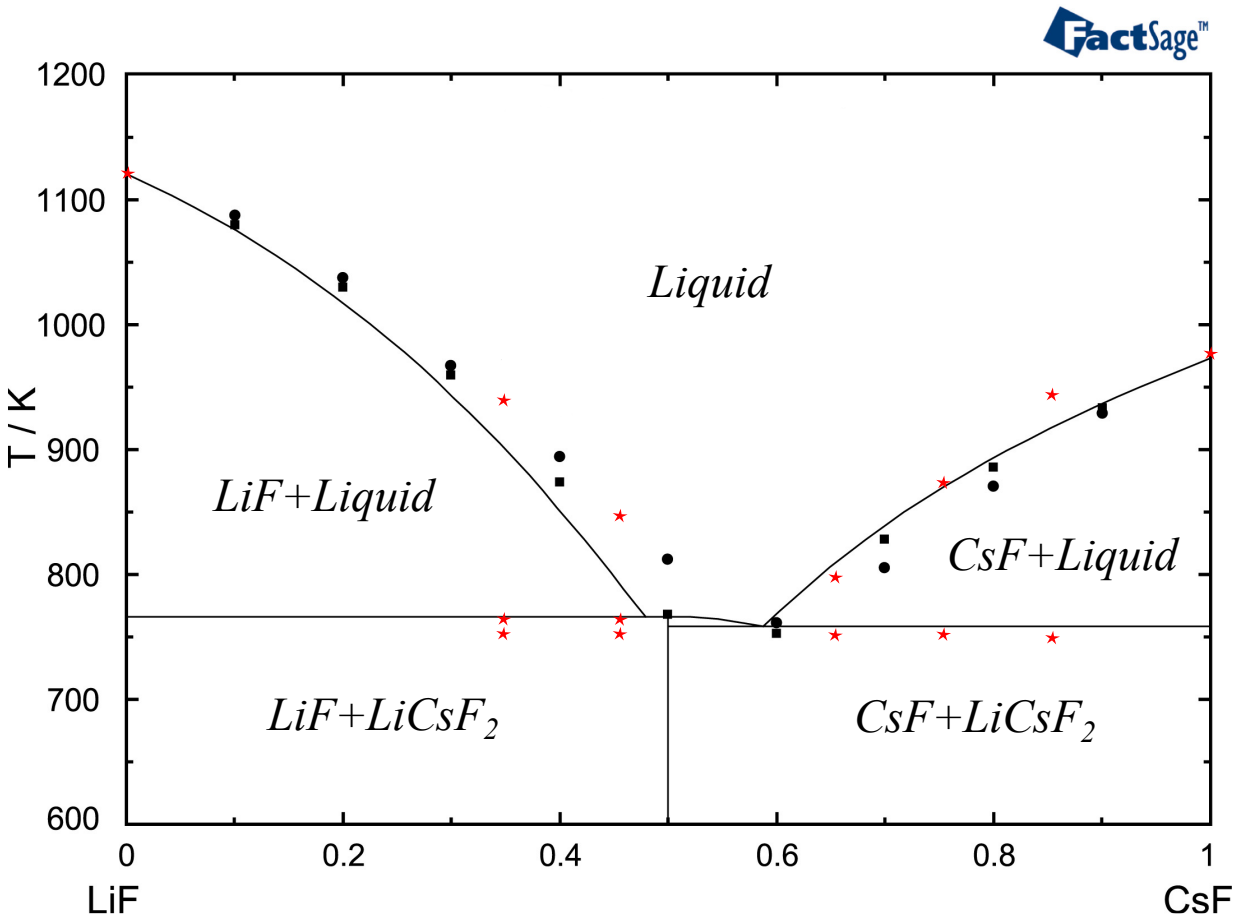

Figure 5.18: *A modelled LiF – CsF phase diagram (black solid lines) from Capelli et al. [56] with superimposed experimental data (●, ■ - previously obtained experimental data [28]; ⋆ - this work).*

Table 5.3: *Measured mass of compositions for DSC measurements of the LiF – CsF system.*

Mole fraction of each component		Measured mass of each component [mg]		% Error*	
CsF	LiF	CsF	LiF	CsF	LiF
0.35	0.65	37.81	12.07	0.39	0.23
0.45	0.55	41.33	8.57	0.08	0.76
0.65	0.35	45.77	4.19	0.04	0.51
0.75	0.25	47.35	2.65	0.09	1.62
0.85	0.15	48.51	1.49	0.06	1.84

* It should be noted that standard uncertainty of measured mass was calculated based on the calculated mass values taken from Table 4.5.
** The results of the error analysis were considered negligible.

Using the combined uncertainty method known as a summation in quadrature, the standard uncertainty $u(T)$ for the temperature values of the LiF – CsF mixtures can be calculated with Eq. 5.1:

$$u(T) = \sqrt{\sum_{i=1}^{n} [c_i u(x_i)^2]} \tag{5.1}$$

where $u(T)$ [°C] represents the temperature combined uncertainty, c_i represents the sensitivity coefficient, and $u(x_i)$ [°C] represents the standard uncertainty. c_i is equal to 1 since the uncertainty contributors are used in the same units of measurements (i.e., °C). The instrumental standard uncertainty in temperature measurements for the Netzsch DSC is ± 0.4 °C [92]. Based on the temperature calibration campaign (refer to Table 4.2) and regression analysis derived from the residual (standard deviation), the standard uncertainty was found to be ± 1.6 °C. The standard uncertainty between the heating rate of 5 K/min and 10 K/min (refer to Figure 4.9) was calculated to be ± 1 °C. By performing regression analysis, the standard uncertainty in the temperature measurements between heating cycles was found to be ± 1.5 °C. Hence, using Eq. 5.1, the combined temperature uncertainty of DSC measurements of LiF – CsF mixtures was determined to be ± 2.5 °C.

Chapter 6

Discussion

An experimental campaign was initiated at Ontario Tech University to fill knowledge gaps in the thermodynamics of fluoride salt systems to support performance and safety assessments of MSRs. In support of this campaign, this thesis was dedicated to qualify a number of procedures and to experimentally measure several fluoride salts. The objectives of this thesis were:

1. Design and qualification of a custom DSC crucible compatible with fluoride salts up to 1200 °C (see §4.1);
2. Development of DSC calibration standards for the custom crucible design (see §4.2);
3. Refinement of fluoride salt sample preparation procedures (see §4.3);
4. Melting point determination of FLiNaK (see §5.1.1);
5. Melting point determination of ThF_4 (see §5.1.2); and
6. Phase transition temperature measurements of several LiF−CsF mixtures (see §5.2).

The results obtained in this work demonstrated the intricate nature of fluoride salts. Despite similar experimental procedures being reported in the open literature, it is important to leverage what is available and develop one's own procedures to study fluoride salts. It should be noted that the following subsections correspond directly to the foregoing enumerated list of thesis objectives.

6.1 Crucible Design & Qualification

An essential task to perform accurate DSC measurements of fluorides salts was to find a crucible design that was not only chemically inert with fluoride salts but also could meet the physical

requirements of the DSC instrument used in this work. As mentioned in §3.3, commercially available DSC crucibles are generally designed for a wide range of materials. Fluoride salts, on the other hand, are complicated by their chemical reactivity and they require rigorous consideration.

A JRC DSC custom crucible design developed by Beneš et al. [61] (see Figure 3.15), a DSC Ni crucible prototype developed by Hallatt (see Figure 3.17), and the identified requirements of the Netzsch DSC used in this work (refer to §4.1) prompted the development of a new custom crucible design that used a Ni liner and a Ni gasket with commercially available Netzsch SS-316L crucibles. It is worth mentioning that an attempt to employ BN liners was initially explored and six BN liners were purchased from CeraQuest Innovative Solutions in Les Clayes-sous-Bois, France. Despite the fact that these liners met all design requirements (see Figure 6.1), visual examination revealed that two out of six liners were already cracked upon arrival due to damage during transit (see Figure 6.2). Extreme embrittlement and a very high cost of BN liners (i.e., $100 US per unit) resulted in abandoning BN as a liner material.

After BN was abandoned, Ni-201 was considered as a liner material. Ni liners were fairly easy to make from a nearby machine shop, reasonably priced, and generally worked well. Ni gaskets were made using a hydraulic press, punch set, and Ni-201 sheet stock in the Nuclear Fuels and Materials Laboratory. Eventually, the task of designing a custom crucible was accomplished and the DSC crucible set was ready for qualification procedure, which was partially achieved through the DSC calibration processes.

Figure 6.1: *Netzsch SS crucibles with inserted BN liners received from the CeraQuest Innovative Solutions, Les Clayes-sous-Bois, France.*

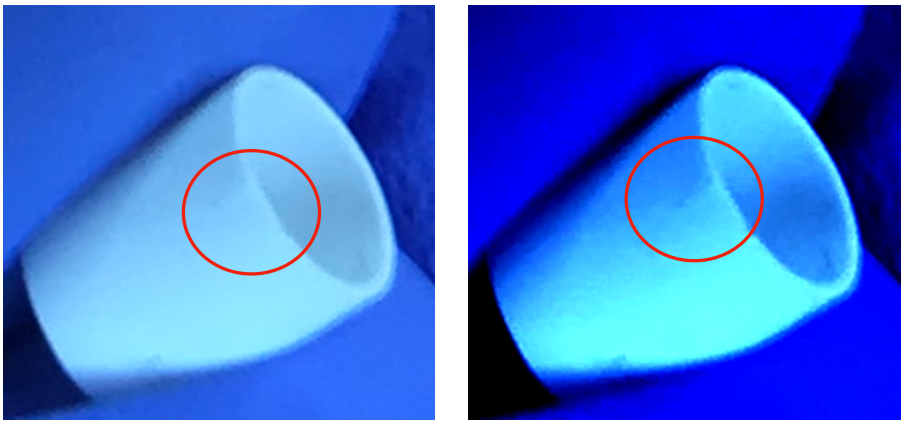

Figure 6.2: *Cracked BN liners received from CeraQuest Innovative Solutions, Les Clayes-sous-Bois, France.*

6.2 DSC Calibration Campaign

The importance of performing comprehensive calibration procedures was recognized at an early stage of this experimental work, as DSC measurements of fluoride salt systems highly depend on the accuracy of the instrument setup. The objective of the calibration campaign was not only to prepare the DSC instrument but also to partially qualify and gain confidence in the custom crucible design.

The execution of standard DSC calibration procedures, which is thoroughly discussed in §4.2, resulted in establishing suitable calibrants for the DSC custom made crucible set. Due to limited information on the compatibility of inorganic calibrants with Ni prior to this work, inorganic materials were chosen based on the compatibility with Pt (refer to Table 3.3). It was experimentally confirmed in this work that Zn could not be used as a calibrant with this particular crucible set. Metal-metal interaction occurred during a DSC run with Zn, resulting in damaging the crucible and compromising the quality of the measurements (refer to Figure 4.5).

The DSC sample carrier was calibrated three times over the experimental work. The inorganic calibrant K_2SO_4 showed inconsistent results between the second and third course of calibration. During the first calibration campaign, it was determined that the second and third heating cycles could not be applied for solid-liquid transition temperature determination of K_2SO_4. The sample crept up the Ni liner walls, as shown in Figure 4.8. Solid-liquid transition temperature measurements with one heating cycle performed during the first two calibration campaigns still showed

consistent results (i.e., 1061.2 °C vs. 1062 °C). However, a DSC run with the K_2SO_4 sample subjected to the dehydration procedure (refer to §4.2.1) revealed that the solid-liquid transition temperature was 1056.9 °C, which is 13.1 °C below the reference melting point of K_2SO_4. Moreover, a comparison between DSC runs of an as-received K_2SO_4 sample and the dehydrated K_2SO_4 sample also showed a big discrepancy (1061.2 °C and 1062 °C vs. 1056.9 °C). This abnormal behaviour requires further investigations, including re-visiting the dehydration process of K_2SO_4 and performing additional DSC measurements with K_2SO_4 (i.e., as-received vs. dehydrated).

As a result of uncertainty with K_2SO_4, Au was used as a calibrant with a BN liner as the highest temperature value ($T_{melting}$ = 1064.2 °C) for the selected temperature range (refer to Table 4.2). It should be noted that the BN liners were used in both crucibles: the sample crucible with Au and the empty reference crucible. As confirmed by Beneš, BN performed fairly well with all pure metal calibrants and fluoride salts with no noticeable difference in melting temperature values when switching liners [73]. The rest of the selected calibrants performed quite well with the DSC custom made crucible sets, which resulted in establishing the temperature calibration matrix suitable for the Netzsch DSC used in this work. Furthermore, the important advantage of performing TGA and DSC simultaneously, where the mass change of a sample is actively measured during each DSC measurement, supported the qualification procedure of the DSC custom made crucible set. No measurable change in mass was observed, which verified that the crucible was hermetically sealed.

Oxidation of the SS crucible was initially observed in the temperature range of 400 - 750 °C during the calibration campaign. The oxide layer was gently removed with 1200 grit sandpaper in order to reuse some crucibles. It is still unclear how many times SS crucibles can be reused. As per Netzsch recommendations, SS crucibles can be reused up to five times [92]. During the temperature calibration campaign, one set of crucibles was reused three times with pure metal calibrants, another set of crucibles was also reused three times with inorganic calibrants; however, a brand new Ni liner had to be used every time for each calibrant.

Discolouration of the DSC sample carrier (see in Figure 6.3 (a)) appeared after a number of DSC calibration runs. To remove this discolouration, which was suspected to affect the accuracy of measurements, the DSC sample carrier was subjected to 1350 °C in air for 30 minutes (a.k.a. "baking procedure"), as per recommendations from Netzsch [92]. Unfortunately, this phenomenon

was not fully understood by Netzsch specialists [92]; however, speculations based on observations made throughout previous oxidation experiments may explain the discolouration appearance. Previous oxidation experiments in synthetic air showed that during severe oxidation of iron-based alloys iron oxides (e.g., FeO, Fe_2O_3) at high temperature interacted with Al_2O_3 resulting in similar discolouration of the Al_2O_3 crucible [80]. It should be noted that in this work, discolouration appeared mainly on the connecting spots of the DSC sample carrier (refer to Figure 6.3 (a)) where the Al_2O_3 adhesive was in place. The presence of O_2 in Ar gas carrier leads to crucible oxidation, whereby during the oxidation process some intermediate iron oxides may get in contact with Al_2O_3 adhesive resulting in discolouration of certain spots of the DSC sample carrier. It is very clear that further tests are required for a better understanding of a possible connection between crucible reuse limitations and the DSC sample carrier discolouration.

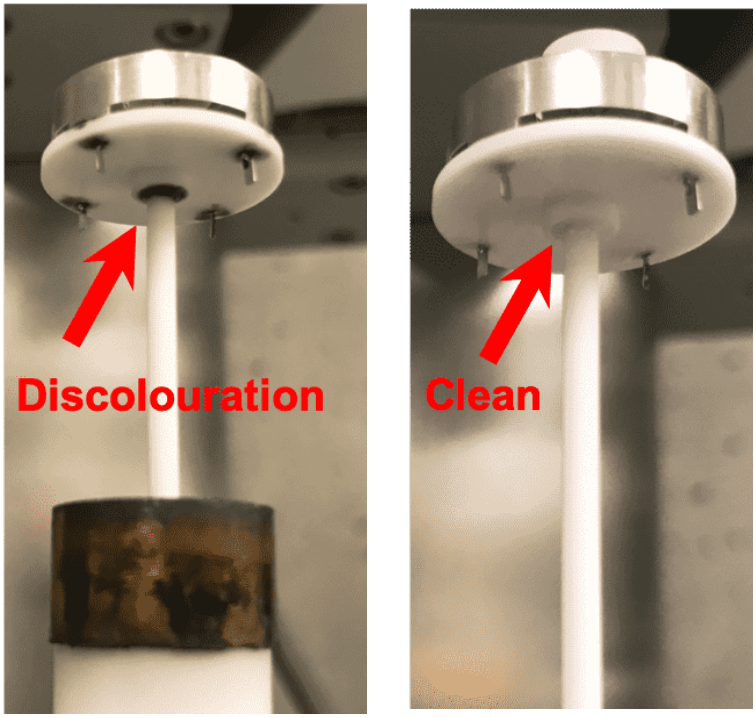

(a) *Discolouration of the DSC sample carrier after continued use with SS crucibles.*

(b) *No evidence of discolouration after baking the DSC sample carrier at 1400 °C for 30 minutes in air.*

Figure 6.3: *The DSC sample carrier behaviour throughout the calibration procedures.*

The baking procedure recommended by Netzsch was applied, the DSC sample carrier came out clean with no evidence of discolouration, as shown in Figure 6.3 (b). An additional DSC run

of the $BaCO_3$ calibrant was performed to verify that the instrument setup was not affected by the aforementioned baking procedure. The phase transition temperature of the additional $BaCO_3$ run showed the melting temperature shifted from 805.5 °C from the first $BaCO_3$ calibration run to 800.6 °C. Given this relatively large change after baking, the DSC was re-calibrated.

Another important aspect recognized from the calibration campaign was the presence of O_2 inside the furnace while purging ultra-high purity Ar. The oxygen probe was used to detect the amount of O_2 downstream from the furnace prior to starting a test. Despite evacuating the system, as soon as Ar was introduced, the O_2 level would spike up to $\sim$ 180 ppm. To initiate each measurement with reduced O_2 content to minimize crucible oxidation, the instrument was purged with pure Ar for $\sim$ 3 hours, which reduced the level of O_2 down to $\sim$ 30 ppm.

In addition to a compatible DSC crucible design and an accurate DSC instrument setup, sample preparation of fluoride salts was another challenge that was addressed in this work.

6.3 Sample Preparation Refinement

Sample preparation of fluoride salts is an important aspect that played a significant role in acquiring accurate results of DSC measurements in this work. Due to the hygroscopic nature of most fluorides, samples must be handled within an inert atmosphere glovebox to prevent contamination and actinoid fluorides need to undergo a dehydration process to remove any impurity oxides [61, 63]. All as-received salt materials, such as FLiNaK, LiF, CsF, and ThF_4 with high purity standards, were subjected to purification/dehydration procedures.

Non-actinoid fluorides (i.e., FLiNaK, LiF, and CsF) studied in this work were prepared following the simple dehydration process developed by Hallatt [66], which leveraged some previous experiences reported in the open literature (see §4.3.2). The phase transition temperature measurements of those fluoride salts showed consistent results with the reported values available in the open literature. The simple dehydration process of non-actinoid fluorides did not require further modifications and proved to be quite effective. The results of DSC measurements of FLiNaK, LiF, and CsF will be discussed in greater detail in §6.4.

Pure samples of ThF_4 were subjected to a more vigorous purification procedure. In fact, the two methods were investigated in this work in an attempt to purify ThF_4 (see §4.3.3). The

lack of well-established procedures involving NH_4HF_2 as a fluorinating agent and the necessity of more suitable equipment led to unsuccessful DSC results; however, the results are still worth discussing, as they were obtained experimentally and might be valuable for future actinoid fluorides investigations.

6.4 Benchmarking

Prior to performing DSC measurements of the targeted LiF – CsF system, a validation process must be established where all procedures, such as crucible design, calibration campaign, and sample preparation could be verified simultaneously. Benchmarking is a common method to verify and gain confidence in any experimental approach while identifying its capabilities and limitations.

6.4.1. Measurements of FLiNaK

Benchmarking FLiNaK melting point measurements gave high confidence in the experimental approach employed in this work. The melting temperature of FLiNaK determined in this work is 455.7 ± 1.6 °C, which is in good agreement with the melting temperature of 456 ± 0.4 °C experimentally obtained by Johnson [100]. It is worth noting that both FLiNaK samples investigated in this work and by Johnson were from the same batch, which was provided by ORNL [86]. The crucible design performed reliably well with the DSC phase transition measurements; the analysis of the obtained DSC sequence of FLiNaK (see Figure 5.1) yielded consistent melting point values of 455.7 ± 1.6 °C within the last two heating cycles (refer to Table 5.1).

It should be noted that the results of the specific heat capacity of FLiNaK obtained in this work technically cannot be compared with the reported values in the open literature, as the DSC measurements of FLiNaK were performed at constant volume as opposed to constant pressure. Oxidation of crucibles observed in the temperature range of 450 - 700 °C could potentially affect the specific heat capacity measurements; however, further investigations are required to justify that fact. Using the same crucibles for three consecutive runs, as per recommendations from Netzsch [93], resulted in the appearance of oxidation after each use, which might slightly change the heat transfer properties of the crucibles.

The effect of thermal lag is also commonly known in DSC measurements when using a crucible with a large integral heat capacity [101]. To get to the encapsulated sample (in this case, FLiNaK), heat must flow through a number of barriers, including an Al_2O_3 disk placed between the crucible and the sensor to prevent sticking, the SS crucible body, and finally the Ni liner. The configuration of DSC is such that the temperature of a sample is measured by the thermocouple, which is located near the sample within the carrier head as opposed to being in direct contact with the sample; hence, heat before being registered by the temperature sensor flows through thermal gap, which may result in an error in specific heat capacity measurements.

The accuracy of specific heat capacity measurements depends on the crucible material. Netzsch recommends crucibles for specific heat capacity measurements made of aluminum, platinum, or graphite [93]. These materials have much higher thermal conductivity compared to SS (e.g., k_{Pt} = 71.60 [$\mathrm{W\,m^{-1}\,K^{-1}}$] compared to k_{SS} = 16.27 [$\mathrm{W\,m^{-1}\,K^{-1}}$]) and much smaller integral heat capacity due to smaller mass [93, 101].

Furthermore, it was observed that the Netzsch SS crucibles were relatively heavy compared to other crucibles, which further degrade heat transfer, to perform specific heat capacity measurements [102]. Considering the discussed limitations of SS crucibles, specific heat capacity measurements require an alternative crucible design.

6.4.2. Measurements of ThF_4

DSC measurements of ThF_4 were performed in an attempt to verify the purification procedure developed for actinoid fluorides. It is worth noting that the purification procedures referred to as Method A (see Table 4.4) was earlier developed by Hallatt [66]. XRD diffraction patterns of both an as-received ThF_4 sample and a purified ThF_4 sample were compared with a reference standard of ThF_4 (database card no. 00-017-0945) represented by the red dots in Figure 6.4 [66]. The two regions around 20° - 28° and 42° - 48° of both XRD patterns were analyzed for potential impurity peaks; however, there was no noticeable difference between both XRD patterns with exception of an unidentified peak at around 29° [66]. As reported by Hallatt, purification did not significantly resolve impurity issues and further investigations were required [66].

The aforementioned hypothesis (i.e., ThF_4 remained impure after purification procedure) based on XRD results proposed by Hallatt [66] was confirmed in this work by performing melting

point measurements of ThF_4 purified with Method A. A DSC signal of the purified ThF_4 sample did not show a single well-defined peak at any heating cycle (e.g., see Figure 5.11), which is indicative that the sample is still impure. A number of DSC runs of ThF_4 samples purified by Method A and Method B executed in this work demonstrated that neither approach was successful.

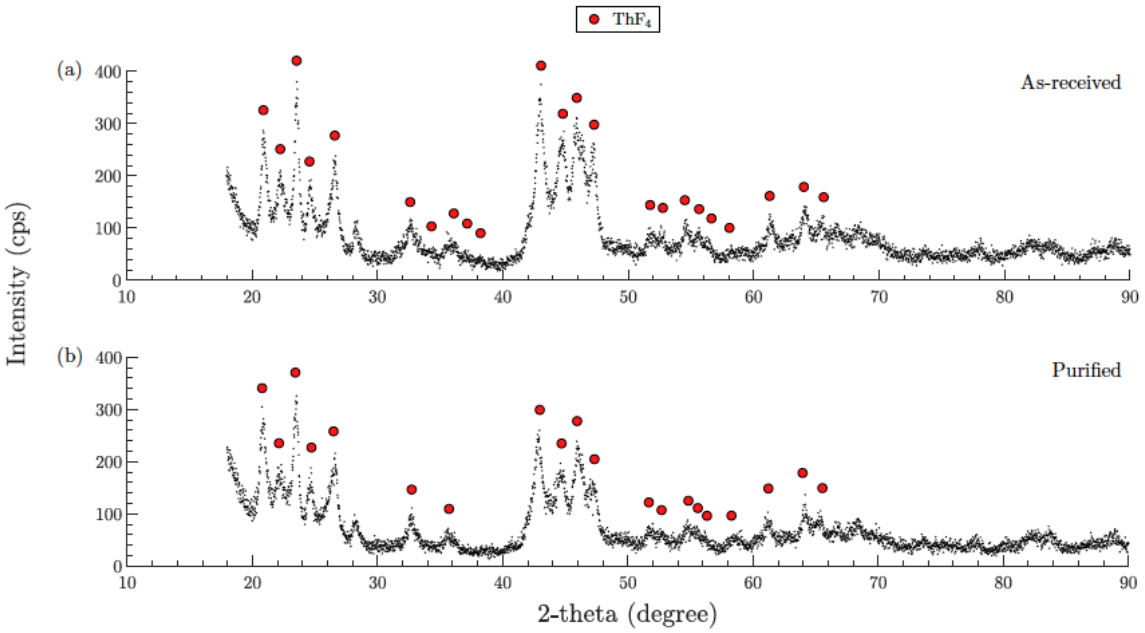

Figure 6.4: *XRD diffraction patterns of (a) an as-received ThF_4 sample, and (b) a purified ThF_4 sample. Copied from Hallatt [66].*

Purification issues were also discussed with colleagues from TU Delft [89, 91] and JRC [73]. Colleagues from TU Delft appeared to have similar purification issues, as evidenced by similar trends in XRD and DSC results of ThF_4. It was suspected that the well-defined solidification peaks shown in Figure 5.8 and an unidentified peak at 29° shown in Figure 6.4 could represent either ThO_2 or the intermediate compound $(NH_4)_7Th_6F_{31}$, which may have formed during the fluorination procedure [91].

Different mass ratios of ThF_4 and NH_4HF_2 explored in this work did not seem to affect the DSC results. All three samples purified with different mass ratios of ThF_4 and NH_4HF_2 using Method B showed similar results with well-observed solidification peaks and poorly-defined melting peaks. The latter was assumed to be a representation of the congruent melt of other compounds, such as $(NH_4)_7Th_6F_{31}$ or ThO_2 [89, 91]. However, this hypothesis is based on observations shared

with colleagues from TU Delft [89, 91] and is not conclusive. A high temperature XRD technique could be used to have a better understanding of the formation of the aforementioned compounds. Nonetheless, it is known for certain that the ThF_4 sample is impure and neither Method A or Method B are effective at purifying ThF_4.

Discussions with colleagues from JRC suggested that Method A was ineffective because a reaction vessel had a loose lid and the vessel should be hermetically sealed (e.g., refer to Figure 4.3) [73]. Method B was then developed involving DSC crucibles to provide a hermetic seal to test the purification process. To purify a larger mass of ThF_4, JRC DSC crucibles had to be used. Unfortunately, none of those crucibles were big enough to increase mass of NH_4HF_2 and ThF_4 without exceeding the 100 bar pressure limitation of both crucible designs. One can argue that residuals (i.e., ammonia, water vapour, and excess HF), which evolve from the 12-hour fluorination process in the sealed reaction vessel cannot be released prior to opening the reaction vessel at room temperature; as a result, they may re-react with ThF_4 upon cooling yielding ThO_2. The process comes full circle and there appears to be no benefit of performing this procedure. At this point, this hypothesis remains speculative.

The difficulties with purification of actinoid fluorides with Method A and Method B prompted the consideration of another approach. This approach incorporates the possibility to release residuals after sufficient heating before the sample reaches room temperature. Since the fluorination process creates high pressure, special equipment has to be used that can withstand high temperature, high pressure, and fluorides.

The Parr Instrument Company was able to design a custom reaction vessel made of primarily of Ni-201 with a needle valve, which allows one to release some of the gasses, including water vapour (see Figure 6.5). The reaction vessel body and the screw-on lid are made of Ni to prevent chemical interaction with a sample. A final design of the purchased Ni reaction vessel for actinoid fluoride salts purification procedures is shown in Figure 6.5 [103, 104]. The delivery time of the reaction vessel did not coincide with the time frame of this work; hence, the equipment is yet to be tested in future research activities.

Multiple DSC measurements performed at temperatures up to ~ 1200 °C resulted in noticeable drift of the DSC signal; moreover, discolouration of the DSC sample carrier started to build up. To avoid introducing uncertainties in the DSC measurements of multi-component mixtures, the

DSC sample carrier was periodically cleaned using the baking procedure recommended by Netzsch; hence, the calibration procedure, which roughly takes a week, had to be employed for a third time prior to the LiF – CsF campaign to ensure high quality and repeatable results.

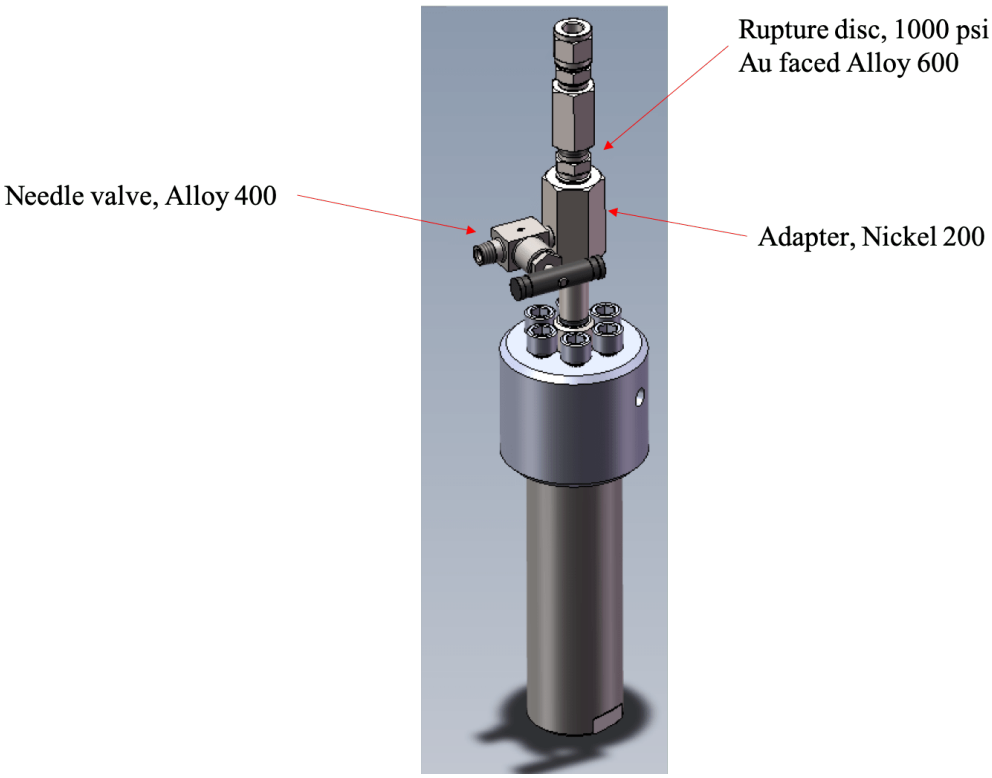

Figure 6.5: *4740 High Pressure/High Temperature Pressure Vessel 75 mL procured for purification procedures of actinoid fluorides. Image provided by Parr Instrument.*

6.5 The LiF–CsF system

DSC measurements of the five compositions of the LiF – CsF system and two pure components were performed in this work with intent to establish a better understanding of the solubility of Cs in LiF bearing salt. Prior to performing DSC measurements of the targeted compositions, the purity of both LiF and CsF components were verified by employing the phase transition temperature measurements (i.e., melting point determination). The results of DSC measurements of both LiF and CsF are consistent with the measurements reported in the open literature. The melting temperature of LiF acquired in this work is 847.7 ± 1.6 °C, which is in good agreement with the reported value of 848.2 ± 5 °C by Capelli [63]. The melting temperature of CsF determined in this work is 703.3 ± 1.6 °C, which can also be comparable with the value of 699.55 ± 5 °C

reported by Beneš et al. [57].

The DSC temperature program for measuring multi-component mixtures has a major contribution in obtaining accurate results. One must ensure that sufficient mixing occurs during the first heating cycle. To accomplish this task, an isothermal hold at 100 °C above the highest melting point of pure components (in this case, LiF) needs to be implemented to guarantee the completion of mixing [63]. Carefully controlled and selected heating rates play a significant role in the interpretation of DSC signals of mixtures. This observation can be explained by the fact that a multi-component mixture can experience various phase transitions at various temperatures resulting in multiple peaks in a DSC pattern. To distinguish one peak from another, a lower heating rate may be employed in DSC measurements of various compositions. For example, the DSC measurements of 65 mol% LiF - 45 mol% CsF and 75 mol% LiF - 35 mol% CsF showed two phase transitions taking place in a narrow temperature range (see Figure 5.15). As a result, a heating rate of 5 K/min was set for both compositions. A number of aspects were considered while choosing a heating rate of 5 K/min:

1. The DSC sample carrier was calibrated for 10 K/min;

2. An earlier temperature calibration campaign revealed similar results between 10 K/min and 5 K/min (see Figure 4.9), which allowed one to minimize the uncertainty in the measured phase transition temperatures;

3. The oxidation of SS crucibles in the temperature range of 400 - 750 °C is inevitable at any heating rate; however, it will be more severe at lower heating rates (e.g., 5 K/min) based on the experience gained in this work (see Figure 5.16).

There is a common practice where DSC measurements are performed at a very low heating rate (e.g., 1 K/min, 0.5 K/min) to obtain a better DSC signal for each of several phase transitions, which may take place in the very narrow temperature range [60]. Despite the presence of crucible oxidation, the overall DSC measurements were not affected; however, the proposed low heating rates of 1 K/min or 0.5 K/min may complicate the interpretation of the DSC sequences. An alternative crucible design that could withstand oxidation effects at lower heating rates is beneficial to explore for future DSC measurements of various mixtures.

The DSC measurements of five different LiF – CsF compositions were consistent with experimental results reported by Thoma et al. [28]. The liquidus points determined in this work slightly deviate from the general trend of the LiF – CsF phase diagram modelled by Capelli et al. [56].

The DSC patterns of two compositions of 65 mol% LiF - 45 mol% CsF and 75 mol% LiF - 35 mol% CsF suggested that there was an additional phase transition on the LiF rich side of the LiF – CsF phase diagram. It was suspected that the additional phase determined by DSC measurements was likely to be an allotropic transformation of $LiCsF_2$ (i.e., $LiCsF_2 – \alpha = LiCsF_2 – \beta$). Given that the existence of $LiCsF_2$ with the different crystal structures at the temperature range of $\sim$ 750 - 765 K was proposed based on the DSC measurements of only two compositions, it would be beneficial to perform more measurements (e.g., 85 mol% LiF - 15 mol% CsF, 75 mol% LiF - 25 mol% CsF) at lower heating rates (e.g., 2 K/min, 1 K/min) to verify this hypothesis. Furthermore, DSC measurements can be supported by the application of high temperature XRD for better interpretation of the DSC measurements of mixtures. It should be noted that the existence of $LiCsF_2$ was assessed by Capelli et al. [105] based on experimental points obtained by Thoma et al. [28]. However, the additional phase was not previously assessed and there is no information available in the open literature.

Due to the COVID-19 outbreak and the university closure, the targeted compositions of 95 mol% LiF - 5 mol% CsF, 85 mol% LiF - 15 mol% CsF, 75 mol% LiF - 25 mol% CsF, 45 mol% LiF - 55 mol% CsF, and 5 mol% LiF - 95 mol% CsF could not be completed.

It is quite clear that the LiF – CsF system requires further investigations. A modified LiF – CsF phase diagram was proposed based on the equilibrium data obtained in this work with experimental data collected by Thoma et al. [28], as shown in Figure 6.6.

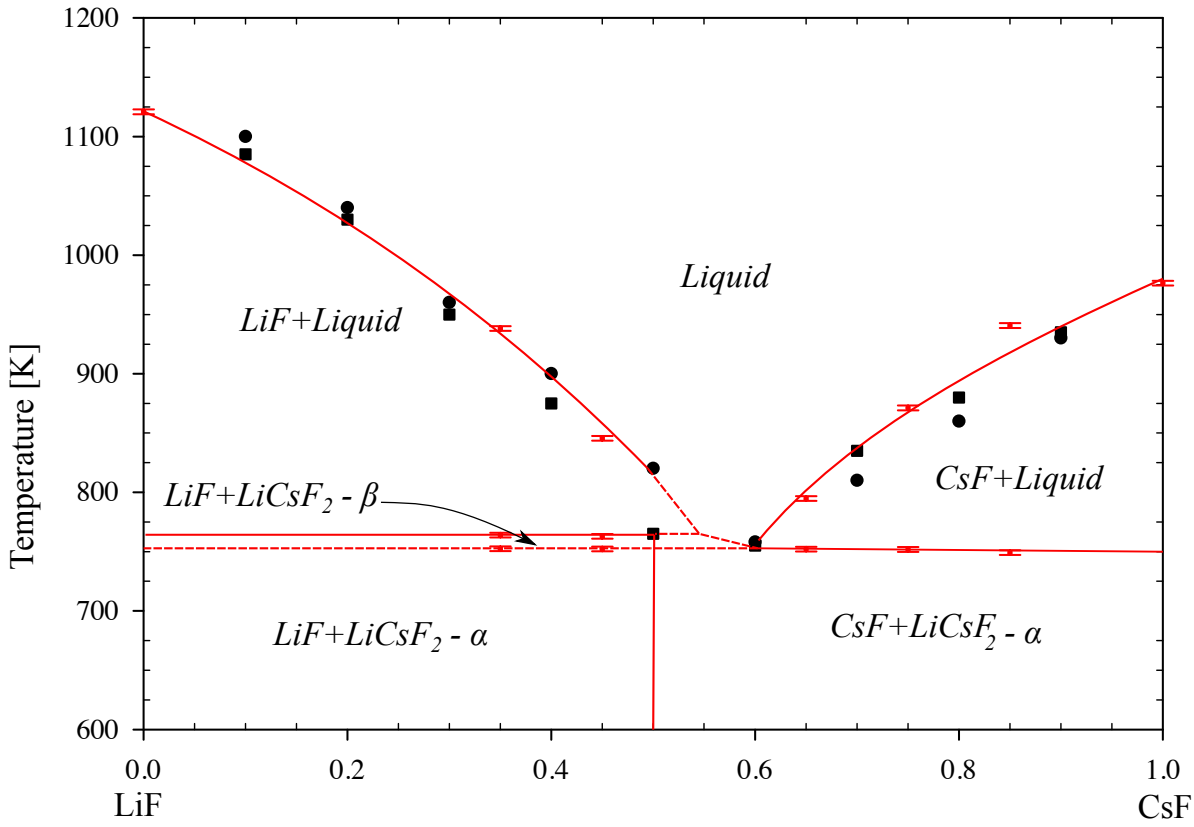

Figure 6.6: *A proposed LiF – CsF diagram based on experimental points obtained by DSC measurements in this work (●) and superimposed experimental data obtained by Thoma et al. (■, ●) [28]. Dashed lines represent phase transitions that require further investigation.*

Chapter 7

Conclusions

The experimental investigations of thermodynamic properties of fluoride salts presented in this work were in support of GEN IV MSR design and safety analyses. The obtained results were intended to develop experimental procedures and to fill knowledge gaps identified in the thermodynamics of fluoride salt systems.

To comply with the objectives of this work, various procedures were implemented:

- A custom crucible design for DSC measurements was developed and qualified;
- A suitable set of calibrants for the custom crucible design was selected;
- Sample preparation processes of fluoride salts were refined;
- The benchmarking of DSC measurements of FLiNaK compared well with reported values in the open literature ($\sim \Delta T = 1$ °C); and
- New DSC measurements of the LiF – CsF system were carried out.

The custom crucible design has performed well thus far, which has demonstrated a hermetic seal, no chemical interaction with fluoride salts, and repeatable measurements of multiple salt components. The melting temperatures of FLiNaK, LiF, and CsF were measured within experimental error of the values reported in the open literature, which gave confidence in the approach implemented in this work. The results of the specific heat capacity and enthalpy of fusion measurements of FLiNaK identified the need for an alternate crucible design.

Purification/dehydration procedures of actinoid fluorides have been refined in this work; however, difficulties remain in purifying ThF_4. The DSC melting point measurements of ThF_4 purified

with Method A and Method B demonstrated the lack of well-established purification procedures of actinoid fluorides and verification of each purification step is required. An alternative reaction vessel has been designed and is to be performed in future research.

Equilibrium data of the LiF – CsF phase diagram obtained in this work are consistent with experimental values reported in the open literature. Slight discrepancies in solidus and liquidus data of the LiF – CsF phase diagram were observed between the LiF – CsF phase diagram modelled by Capelli et al. [56] and experimental measurements obtained in this work. An additional phase was determined by DSC measurements of the two compositions (i.e., 65 mol% LiF - 45 mol% CsF and 75 mol% LiF - 35 mol% CsF) performed in this work. It appears to be a second phase of $LiCsF_2$. This phase has not been reported elsewhere; hence, further investigations of the LiF – CsF system is suggested to come to a more definitive conclusion.

Understanding molten fluoride salt physical and chemical properties are considered a great challenge in the context of developing safe and reliable MSR technologies. Previous MSR studies coupled with various modern and well-designed experiments may give confidence in establishing reliable MSRs.

The experimental work described in this thesis was dedicated to qualify a number of procedures and to measure several fluoride salts, including the system with predominant FP in support of performance and safety assessments of MSRs. The established experimental procedures within the university laboratory and the results obtained in this work may be used in further research to continue contributing to MSRs' future in Canada.

Chapter 8

Recommendations

A number of recommendations have been identified in support of further improvements of experimental activities in the thermodynamics of fluoride salts. This chapter provides some of those recommendations in terms of temperature calibration procedures, DSC measurements, and ThF_4 purification processes.

8.1 Temperature Calibration

To fill the gap in the low temperature region of the newly developed calibration matrix shown in Figure 4.6, a certified calibrant with a well-established melting point and enthalpy of fusion values should be considered. For example, lead (Pb) with a melting point of 327.5 °C is worth considering; however, a DSC run with Pb must be carried out diligently due to possible partial solution processes between a Ni liner and Pb [106]. Also, one should be careful and cognizant of health concerns when working with Pb.

Repeating and analyzing the DSC measurements of the high temperature point (i.e., K_2SO_4) of the same calibration matrix is also advised. During the three calibration campaigns it was observed that inconsistent DSC measurement results might be related to the dehydration process of K_2SO_4 described in §4.2.1 as opposed to the material itself. Hence, re-visiting the dehydration process of K_2SO_4 and performing additional DSC measurements with K_2SO_4 (i.e., as-received vs. dehydrated) are recommended.

It should be noted that the K_2SO_4 solid-liquid transition measurements can be performed with one heating cycle only whereas the rest of the calibrants used three consecutive heating cycles; hence, for sake of consistency, K_2SO_4 is recommended to be replaced with a calibrant that can be

measured with the temperature program of three consecutive heating cycles.

Justification of reusing the Netzsch SS crucibles can be confirmed as part of the temperature calibration campaign. It is still unclear how many times SS crucibles can be reused at modest to elevated temperatures.

8.2 DSC Measurements

Discolouration of the DSC sample carrier during experiments should be closely monitored and studied, as its accumulation may potentially damage the DSC sample carrier. The re-use of SS crucibles susceptible to oxidation without OTS is worth investigating, as it might be related to the DSC sample carrier discolouration.

The current DSC crucible design is suitable for DSC measurements at a maximum temperature of 1200 °C, which limits the range of some fission products that cannot be explored due to their relatively high melting point (e.g., $T_{melting}(NdF_3)$ = 1374 °C); hence, an alternative crucible that can operate at higher temperatures is highly recommended.

Specific heat capacity measurements require a crucible design made of materials with a higher thermal conductivity and thinner walls. Some potential materials may include BN, Ni-201, Mo, or graphite. An alternative design made of one of these materials is recommended.

Performing DSC measurements of multi-component fluoride salts systems at lower heating rates (e.g., 2 K/min, 5 K/min, and 7 K/min) allows one to obtain more accurate DSC sequences of mixtures, as lower heating rates separate DSC curves that correspond to phase transitions within the system. However, the presence of the crucible oxidation effect at low heating rates must be closely monitored. The latter may become less important with a different crucible design.

The compositions of 95 mol% LiF - 5 mol% CsF, 85 mol% LiF - 15 mol% CsF, 75 mol% LiF - 25 mol% CsF are recommended for future studies. DSC measurements of those compositions will allow one to have a better understanding of the phase transitions occurring on the LiF rich side of the LiF – CsF phase diagram. Furthermore, employing a high temperature XRD technique is beneficial to determine the intermediate compound formed on the LiF rich side at the temperature range of $\sim$ 450 - 500 °C.

The central region of the LiF – CsF phase diagram (i.e., between 50 mol% LiF - 50 mol%

CsF and 40 mol% LiF - 60 mol% CsF) requires thorough investigations to accurately identify a composition of a stoichiometric compound. The Tammann method is recommended to be used, where nearest compositions to eutectic or stoichiometric phases are explored in order to accurately determine the eutectic or stoichiometric temperature and composition [60].

It is also advised performing more than three heating cycles (e.g., four or five heating cycles) for DSC measurements of the LiF – CsF mixtures to confirm if the temperature shift occurring with successive heating cycles is related to the CsF volatility, which was observed by Capelli et al. [56].

A possible use of a reducing atmosphere, such as H_2/Ar mixture, for DSC measurements with Netzsch SS crucibles can be considered in order to prevent crucible oxidation at modest temperatures. However, the compatibility of the DSC sample carrier in a reducing atmosphere must be initially verified and confirmed with the vendor.

8.3 ThF_4 Purification

Purification procedures of actinoid fluorides using the reaction vessel shown in Figure 6.5 require comprehensive studies in terms of the following:

- The release of HF(g) within the glovebox is a major concern for H_2O/O_2 sensors and stored salt materials. An HF scrubber (e.g., NaOH) should be explored to avoid potential damage to equipment.
- The determination of an appropriate mass ratio of NH_4HF_2 and ThF_4 must be fully assessed prior to performing the purification procedures in order to not produce a great amount of the radioactive waste.
- The temperature and duration of the purification procedure must be analyzed, as it is uncertain if the heat treatment of 250 °C for 12 hours is appropriate.
- There is still an open question whether residuals (i.e., ammonia, water vapour, and excess HF) formed during the 12-hour fluorination process at 250 °C easily re-react with ThF_4 upon cooling to $\sim$ room temperature. Hence, an option, where the release of these residuals takes place before the sample reaches the room temperature is worth exploring.

References

[1] S.M. Goldberg and R. Rosner. *Nuclear Reactors: Generation to Generation*. American Academy of Arts and Sciences, Cambridge, MA, 2011.

[2] GEN IV International Forum. Technology Roadmap Update for Generation IV Nuclear Energy Systems. Technical report, Organisation for Economic Co-operation and Development (OECD)-Nuclear Energy Agency (NEA), Paris, France, 2014.

[3] GEN IV International Forum. GEN IV Systems. `https://www.gen-4.org/gif/jcms/c_59461/generation-iv-systems`. Accessed: 2019-11-30.

[4] G.D. DelCul and B.B. Spencer. "Reprocessing and Recycling". In M.H.A. Piro, editor, *Advances in Nuclear Fuel Chemistry*. Elsevier, Oxford, 2020.

[5] World Nuclear Association. Small Nuclear Power Reactors. `https://www.world-nuclear.org/information-library/nuclear-fuel-cycle/nuclear-power-reactors/small-nuclear-power-reactors.aspx`. Accessed: 2019-11-30.

[6] Canadian Small Modular Reactor Roadmap Steering Committee. A Call to Action: A Canadian Roadmap for Small Modular Reactors. Technical report, Steering Committee, Ottawa, ON, 2018.

[7] Atomic Energy of Canada Limited. Science & Technology-Small Modular Reactors. `https://www.aecl.ca/science-technology/small-modular-reactors/`. Accessed: 2020-03-24.

[8] World Nuclear Association. Small Nuclear Power Reactors. `https://www.world-nuclear.org/information-library/nuclear-fuel-cycle/nuclear-power-reactors/small-nuclear-power-reactors.` Accessed: 2020-04-06.

[9] Canadian Nuclear Laboratories. SMR Technoloogy. `https://www.cnl.ca/en/home/facilities-and-expertise/smr/default.aspx`. Accessed: 2020-02-04.

[10] Canadian Nuclear Laboratories. Update on CNL's SMR invitation process. https://www.cnl.ca/en/home/facilities-and-expertise/smr/progressupdate/. Accessed: 2020-03-24.

[11] Terrestrial Energy. Integral Molten Salt reactor. https://www.terrestrialenergy.com/technology/how-it-works/. Accessed: 2020-03-24.

[12] Moltex Energy. Stable Salt Reactors. https://www.moltexenergy.com/stablesaltreactors/. Accessed: 2020-04-06.

[13] B.M. Elsheikh. Safety Assessment of Molten Salt Reactors in Comparison with Light Water Reactors. *Journal of Radiation Research and Applied Sciences*, 6(2):63–70, 2013.

[14] J. Serp, M. Allibert, O. Beneš, S. Delpech, O. Feynberg, V. Ghetta, D. Heuer, D. Holcomb, V. Ignatiev, J.L. Kloosterman, L. Luzzi, E. Merle-Lucotte, J. Uhlíř, R. Yoshioka, and D. Zhimin. The Molten Salt Reactor (MSR) in Generation IV: Overview and Perspectives. *Progress in Nuclear Energy*, 77:308–319, 2014.

[15] M.B. Seregin, A.P. Parshin, A.Y. Kuznetsov, L.I. Ponomarev, S.A. Melnikov, A.A. Mikhalichenko, A.A. Rzheutskii, and R.N. Manuilov. Solubility of UF_4, ThF_4, and CeF_3 in a LiF-NaF-KF melt. *Radiochemistry*, 53(5):491–493, 2011.

[16] United States Department of Energy Nuclear Energy Research Advisory Committee and the Generation IV International Forum. A Technology Roadmap for Generation IV Nuclear Energy Systems. Technical Report GIF-002-00, US DOE, Washington D.C., 2002.

[17] H.G. MacPherson. The Molten Salt Reactor Adventure. *Nuclear Science and Engineering*, 90(4):374–380, 1985.

[18] H.G. MacPherson. Fluid Fuels Reactors Task Force. Technical Report TID-8505, Division of Reactor Development, U.S. Atomic Energy Commission, Washington D.C., 1959.

[19] L.C. Olson, J.W. Ambrosek, K. Sridharan, M.H. Anderson, and T.R. Allen. Materials Corrosion in Molten LiF-NaF-KF Salt. *Journal of Fluorine Chemistry*, 130(1):67–73, 2009.

[20] L. Chengliang, Y. Mengjia. The Challenge of Nuclear Reactor Structural Materials for Generation IV Nuclear Energy Systems. In *20th International Conference on Structural Mechanics in Reactor Technology (SMiRT 20)*, Finland, 2009.

[21] O. Beneš and R.J.M. Konings. "Molten Salt Reactor Fuel and Coolant". In : R.J.M. Konings, editor, *Comprehensive Nuclear Materials*. Elsevier, Oxford, 2012.

[22] J.W. McMurray, T.M. Besmann, J. Ard, B. Fitzpatrick, M. Piro, J. Jerden, M. Williamson, B.S. Collins, B.R. Betzler, A.L. Qualls. Multi-physics simulations for molten salt reactor evaluation: Chemistry modeling and database development. Technical Report ORNL/SPR-2018/864, Oak Ridge National Laboratory, Oak Ridge, TN, 2018.

[23] D.F. Williams, P.F. Britt. Molten Salt Chemistry Workshop, "Technology and Applied R&D Needs for Molten Salt Chemistry". In *Molten Salt Chemistry Workshop*, Oak Ridge National Laboratory, Oak Ridge, TN, 2017.

[24] H. Lukas, S. G. Fries, and B. Sundman. *Computational Thermodynamics: The Calphad Method*. Cambridge University Press, 2007.

[25] M.H.A. Piro, S. Simunovic, T.M. Besmann, B.J. Lewis, and W.T. Thompson. The Thermochemistry Library Thermochimica. *Computational Materials Science*, 67:266 – 272, 2013.

[26] O. Beneš and P. Soucek. "Molten Salt Reactor Fuels". In M.H.A. Piro, editor, *Advances in Nuclear Fuel Chemistry*. Elsevier, Oxford, 2020.

[27] D. Manara, A. Seibert, T. Gouder, O. Beneš, L. Martel, J-Y. Colle, J-C. Griveau, O. Walter, A. Cambriani, D. Blanci, D. Staicu, T. Wiss, and J-F. Vigier. "Experimental Methods". In M.H.A. Piro, editor, *Advances in Nuclear Fuel Chemistry*. Elsevier, Oxford, 2020.

[28] R.E. Thoma. Phase Diagrams of Binary and Ternary Fluoride Systems. In J. Braunstein, G. Mamantov, and G.P. Smith, editors, *Advances in Molten Salt Chemistry: Volume 3*. Springer US, Boston, MA, 1975.

[29] M.W. Rosenthal, P.R. Kasten, and R.B. Briggs. Molten Salt Reactors - History, Status, and Potential. *Nuclear Applications and Technology*, 8(2):107–117, 1970.

[30] E.S. Bettis, R. W. Schroeder, G.A. Cristy, H.W. Savage, R.G. Affel, and L.F. Hemphill. The Aircraft Reactor Experiment–Design and Construction. *Nuclear Science and Engineering*, 2(6):804–825, 1957.

[31] C. Wang, H. Qin, D. Zhang, W. Tian, S. Qiu, and G.H. Su. Numerical Study of Tritium Transport Characteristics in Thorium Molten Salt Reactor with Solid Fuel (TMSR-SF). *Nuclear Engineering and Design*, 335:391–399, 2018.

[32] P.N. Haubenreich and J.R. Engel. Experience with the Molten - Salt Reactor Experiment. *Nuclear Applications and Technology*, 8(2):118–136, 1970.

[33] J.R. Engel, H.F. Bauman, J.F. Dearing, W.R. Grimes, and H.E. Jr. McCoy. Development Status and Potential Program for Development of Proliferation - Resistant Molten - Salt Reactors. Technical Report ORNL/TM-6415, Oak Ridge National Laboratory, Oak Ridge, TN, 1979.

[34] E.S. Bettis and R.C. Robertson. The Design and Performance Features of a Single–Fluid Molten–Salt Breeder Reactor. *Nuclear Applications and Technology*, 8(2):190–207, 1970.

[35] D. LeBlanc. Molten Salt Reactors: A New Beginning for an Old Idea. *Nuclear Engineering and Design*, 240(6):1644–1656, 2010.

[36] C.J. Barton, W.R. Grimes, H. Insley, R.E. Moore, and R.E. Thoma. Phase Equilibria in the Systems NaF-ZrF_4, UF_4-ZrF_4, and NaF-ZrF_4-UF_4. *Journal of Physical Chemistry*, 62(6):665–676, 1958.

[37] R.E. Thoma, H. Insley, H.A. Friedman, and G.M. Hebert. Condensed System LiF-NaF-ZrF_4 - Phase Equilibria and Crystallographic Data. *Journal of Chemical & Engineering Data*, 10(3):219–230, 1965.

[38] O. Beneš. *Thermodynamics of Molten Salts for Nuclear Applications - JRC-ITU-TN- 2008/40.* Doctoral Thesis, Institute of Chemical Technology, Faculty of Chemical Technology, Department of Inorganic Chemistry, Prague, Czech Republic, 2008.

[39] W.R. Grimes. Molten - Salt Reactor Chemistry. *Nuclear Applications and Technology*, 8(2):137–155, 1970.

[40] C.J. Barton, H.A. Friedman, W.R. Grimes, H. Insley, R.E. Moore, and R.E. Thoma. Phase Equilibria in the Alkali Fluoride-Uranium Tetrafluoride Fused Salt Systems: I, The Systems LiF-UF_4 and NaF-UF_4. *Journal of the American Ceramic Society*, 41(2):63–69, 1958.

[41] R.E. Thoma, H. Insley, B.S. Landau, H.A. Friedman, and W.R. Grimes. Phase Equilibria in the Fused Salt Systems LiF-ThF_4 and NaF-ThF_4. *Journal of Physical Chemistry*, 63(8):1266–1274, 1959.

[42] C.F. Weaver, R.E. Thoma, H. Insley, and H.A. Friedman. Phase Equilibria in the Systems UF_4-ThF_4 and LiF-UF_4-ThF_4. *Journal of the American Ceramic Society*, 43(4):213–218, 1960.

[43] J.P.M. van der Meer, R.J.M. Konings, M.H.G. Jacobs, and H.A.J. Oonk. A Miscibility Gap in LiF-BeF_2 and LiF-BeF_2-ThF_4. *Journal of Nuclear Materials*, 344(1-3):94–99, 2005.

[44] R.E. Thoma, H. Insley, H.A. Friedman, and C.F. Weaver. Phase Equilibria in the Systems BeF_2-ThF_4 and LiF-BeF_2-ThF_4. *Journal of Physical Chemistry*, 64(7):865–870, 1960.

[45] J.P.M. van der Meer and R.J.M. Konings. Thermal and Physical Properties of Molten Fluorides for Nuclear Applications. *Journal of Nuclear Materials*, 360(1):16–24, 2007.

[46] O. Beneš and R.J.M. Konings. Thermodynamic Properties and Phase Diagrams of Fluoride Salts for Nuclear Applications. *Journal of Fluorine Chemistry*, 130(1):22–29, 2009.

[47] E. Capelli, O. Beneš, M. Beilmann, and R.J.M. Konings. Thermodynamic Investigation of the LiF-ThF_4 System. *Journal of Chemical Thermodynamics*, 58:110–116, 2013.

[48] O. Beneš and R.J.M. Konings. Thermodynamic Assessment of the LiF-CeF_3-ThF_4 System: Prediction of PuF_3 Concentration in a Molten Salt Reactor Fuel. *Journal of Nuclear Materials*, 435(1-3):164–171, 2013.

[49] O. Beneš, M. Beilmann, and R.J.M. Konings. Thermodynamic Assessment of the LiF-NaF-ThF_4-UF_4 System. *Journal of Nuclear Materials*, 405(2):186–198, 2010.

[50] O. Beneš and R.J.M. Konings. Thermodynamic Evaluation of the (LiF+NaF+BeF_2+PuF_3) System: An Actinide Burner Fuel. *Journal of Chemical Thermodynamics*, 41(10):1086–1095, 2009.

[51] E. Capelli, O. Beneš, and R.J.M. Konings. Thermodynamic Assessment of the LiF-NaF-BeF_2-ThF_4-UF_4 System. *Journal of Nuclear Materials*, 449:111–121, 2014.

[52] E. Capelli, O. Beneš, and R.J.M. Konings. Thermodynamic Assessment of the LiF-ThF_4-PuF_3-UF_4 System. *Journal of Nuclear Materials*, 462:43–53, 2015.

[53] M. Beilmann, O. Beneš, R.J.M. Konings, and Th. Fanghänel. Thermodynamic Investigation of the (LiF+NaF+CaF_2+LaF_3) System. *Journal of Chemical Thermodynamics*, 43(10):1515–1524, 2011.

[54] E. Capelli, O. Beneš, P. E. Raison, M. Beilmann, C. Künzel, and R.J.M. Konings. Thermodynamic Investigation of the CaF_2-ThF_4 and the LiF-CaF_2-ThF_4 Systems. *Journal of Chemical & Engineering Data*, 60(11):3166–3174, 2015.

[55] N. Vozárová, A.L. Smith, J-Y. Colle, P.E. Raison, D. Bouëxiére, R.J.M. Konings, and O. Beneš. Thermodynamic Determination and Assessment of the CsF-ThF_4 System. *Journal of Chemical Thermodynamics*, 114:71–82, 2017. Special issue on Thermodynamics of Nuclear Materials.

[56] E. Capelli, O. Beneš, and R.J.M. Konings. Thermodynamics of Soluble Fission Products Cesium and Iodine in the Molten Salt Reactor. *Journal of Nuclear Materials*, 501:238 – 252, 2018.

[57] O. Beneš, R.J.M. Konings, D. Sedmidubský, M. Beilmann, O.S. Valu, E. Capelli, M. Salanne, and S. Nichenko. A Comprehensive Study of the Heat Capacity of CsF from T=5 K to T=1400 K. *Journal of Chemical Thermodynamics*, 57:92–100, 2013.

[58] H.A. Friedman, G.M. Hebert, and R.E. Thoma. Thermal Analysis And Gradient Quenching Apparatus And Techniques For The Investigation Of Fused Salt Phase Equilibria. Technical Report ORNL-3373, Oak Ridge National Laboratory, Oak Ridge, TN, 1962.

[59] E.B. Ferreira, M.L. Lima, and E.D. Zanotto. DSC Method for Determining the Liquidus Temperature of Glass-Forming Systems: DSC Method for Determining the Liquidus Temperature. *Journal of the American Ceramic Society*, 93(11):3757–3763, 2010.

[60] L. Rycerz. Practical Remarks Concerning Phase Diagrams Determination on the Basis of Differential Scanning Calorimetry Measurements. *Journal of Thermal Analysis and Calorimetry*, 113(1):231–238, 2013.

[61] O. Beneš, R.J.M. Konings, S. Wurzer, M. Sierig, and A. Dockendorf. A DSC Study of the $NaNO_3$-KNO_3 System Using an Innovative Encapsulation Technique. *Thermochimica Acta*, 509(1-2):62–66, 2010.

[62] M. Beilmann. *Thermodynamic Investigation of Fluoride Salts for Nuclear Energy Production*. Doctoral Thesis, Heidelberg University, Institute of Physical Chemistry, Heidelberg, Germany, 2013.

[63] E. Capelli. *Thermodynamic Characterization of Salt Components for Molten Salt Reactor Fuel*. Doctoral Thesis, TU Delft, Melkeweg, The Netherlands, 2016.

[64] J.A. Ocádiz-Flores, E. Capelli, P.E. Raison, R.J.M. Konings, and A.L. Smith. Thermodynamic assessment of the LiF-NiF_2, NaF-NiF_2 and KF-NiF_2 systems. *Journal of Chemical Thermodynamics*, 121:17–26, 2018.

[65] J.A. Ocádiz-Flores, E. Carré, J.-C. Griveau, E. Colineau, E. Capelli, P. Souček, O. Beneš, R.J.M. Konings, and A.L. Smith. Thermodynamic Assessment of the KF-ThF_4, LiF-KF-ThF_4 and NaF-KF-ThF_4 Systems. *Journal of Chemical Thermodynamics*, 121:106069, 2020.

[66] D.B. Hallatt. *Developing a Framework for Thermodynamic Measurements of Fluoride Salt Nuclear Fuel*. Master's Thesis, Ontario Tech University, Oshawa, Canada, 2019.

[67] R. Sabbah, An Xu-wu, J.S. Chickos, M.L. Planas Leitão, M.V. Roux, and L.A. Torres. Reference Materials for Calorimetry and Differential Thermal Analysis. *Thermochimica Acta*, 331(2):93–204, 1999.

[68] G. Della Gatta, M.J. Richardson, S.M. Sarge, and S. Stølen. Standards, Calibration, and Guidelines in Microcalorimetry. Part 2. Calibration Standards for Differential Scanning Calorimetry (IUPAC Technical Report). *Pure and Applied Chemistry*, 78(7):1455–1476, 2006.

[69] NETZSCH-Gerätebau GmbH. *NETZSCH Proteus®–Thermal Analysis Software (Version 6.1.0)*. NETZSCH, Germany, 2018.

[70] NETZSCH, Analyzing & Testing Business Unit, TGA–DSC/DTA Training Slides. *Temperature and Sensitivity Calibrations for DSC*. NETZSCH, Instruments North America, LLC, 2016.

[71] H.K. Cammenga, W. Eysel, E. Gmelin, W. Hemminger, G.W.H. Höhne, and S.M. Sarge. The Temperature Calibration of Scanning Calorimeters. *Thermochimica Acta*, 219:333–342, 1993.

[72] M.J. Richardson and E.L. Charsley. Calibration and Standardisation in DSC. In *Handbook of Thermal Analysis and Calorimetry*, volume 1. Elsevier, 1998.

[73] O. Beneš. Personal Communication, JRC, 2020.

[74] K. Kostyrko and M. Skoczylas. Temperature Standard Reference Materials for Thermal Analysis. *Journal of Thermal Analysis*, 38(9):2181–2188, 1992.

[75] G.J. Janz and J.J. Slowick. Investigations of CsCl, K_2SO_4, and K_2CrO_4 as High Temperature Calibrants for Differential Scanning Calorimetry. *Z. Anorg. Allg. Chem.*, 586(1):166–174, 1990.

[76] K. Kostyrko, M. Skoczylas, and A. Klee. Certified Reference Materials for Thermal Analysis. *Journal of thermal analysis*, 33(1):351–357, 1988.

[77] E.L. Charsley, C.M. Earnest, P.K. Gallagher, and M.J. Richardson. Preliminary Round-Robin Studies on the ICTAC Certified Reference Materials for DTA: Barium Carbonate and Strontium Carbonate. *Journal of Thermal Analysis*, 40(3):1415–1422, 1993.

[78] P. Souček, O. Beneš, B. Claux, E. Capelli, M. Ougier, V. Tyrpekl, J-F. Vigier, and R.J.M. Konings. Synthesis of UF_4 and ThF_4 by HF Gas Fluorination and Re-determination of the UF_4 Melting Point. *Journal of Fluorine Chemistry*, 200:33–40, 2017.

[79] NETZSCH. *High Temperature Platform 400 Operating Instructions Simultaneous TG-DTA/DSC Apparatus STA 449 F1 Jupiter®*. NETZSCH, Germany, 2012.

[80] K. Lipkina, D. Hallatt, E. Geiger, B.W.N. Fitzpatrick, K. Sakamoto, H. Shibata, and M.H.A. Piro. A Study of the Oxidation Behaviour of FeCrAl-ODS in Air and Steam Environments up to 1400 °C. *Journal of Nuclear Materials, in-press*, 2020.

[81] D. Hallatt, K. Lipkina, and M.H.A. Piro. Exploring Crucible Designs for Differential Scanning Calorimetry Measurements of Fluoride Salts. in-preparation.

[82] NETZSCH. *Accessories & Spare Parts. STA 449 F1 & F3.* NETZSCH, Germany, 2016.

[83] NETZSCH. *Temperature and Sensitivity Calibration Protocol, Software Manual DSC Instruments.* NETZSCH, Germany, 2012.

[84] NETZSCH, Analyzing & Testing Business Unit, TGA–DSC/DTA Training Slides. *Sample Preparation.* NETZSCH, Instruments North America, LLC, 2016.

[85] NETZSCH, Analyzing & Testing Business Unit, TGA–DSC/DTA Training Slides. *Optimization of Measurement Parameters – Influence on TG and DSC results.* NETZSCH, Instruments North America, LLC, 2016.

[86] S.S. Raiman. Personal Communication, ORNL, 2019.

[87] Lithium Fluoride (LiF); SDS No. 10736; Thermo Fisher Scientific: Ottawa, ON, 2020.

[88] Cesium Fluoride (CsF); SDS No. 255718; Sigma-Aldrich Canada Co.: Oakville, ON, 2019.

[89] A.L. Smith. Personal Communication, TU Delft, 2020.

[90] C.N.A. Che Zainul Bahri, A.F. Ismail, and A.Ab. Majid. Synthesis of Thorium Tetrafluoride (ThF_4) by Ammonium Hydrogen Difluoride (NH_4HF_2). *Nuclear Engineering and Technology*, 51(3):792 – 799, 2019.

[91] J.A. Ocádiz-Flores. Personal Communication, TU Delft, 2020.

[92] M. Hsu. Personal Communication, NETZSCH, 2020.

[93] NETZSCH, Analyzing & Testing Business Unit, TGA–DSC/DTA Training Slides. *DSC Specific Heat (Measuring Principles, Instruments, Optimization) and c-DTA*. NETZSCH, Instruments North America, LLC, 2016.

[94] ASTM E1269. Specific Heat Capacity by Differential Scanning Calorimeter. *Annual Book of ASTM Standards*, 2018.

[95] R.R. Romatoski and L.W. Hu. Fluoride Salt Coolant Properties for Nuclear Reactor Applications: A Review. *Annals of Nuclear Energy*, 109:635–647, 2017.

[96] X-H. An, J-H. Cheng, T. Su, and P. Zhang. Determination of Thermal Physical Properties of Alkali Fluoride/Carbonate Eutectic Molten Salt. In *AIP Conference Proceedings*, page 070001, Abu Dhabi, United Arab Emirates, 2017.

[97] D.J. Rogers, T. Yoko, and G.J. Janz. Fusion Properties and Heat Capacities of the Eutectic Lithium Fluoride - Sodium Fluoride - Potassium Fluoride Melt. *Journal of Chemical & Engineering Data*, 27(3):366–367, 1982.

[98] V. Khokhlov, I. Korzun, V. Dokutovich, and E. Filatov. Heat Capacity and Thermal Conductivity of Molten Ternary Lithium, Sodium, Potassium, and Zirconium Fluorides Mixtures. *Journal of Nuclear Materials*, 410(1-3):32–38, 2011.

[99] R. Serrano-López, J. Fradera, and S. Cuesta-López. Molten Salts Database for Energy Applications. *Chemical Engineering and Processing: Process Intensification*, 73:87–102, 2013.

[100] T.M. Besmann and K. Johnson. Personal Communication, UofSC, 2020.

[101] R. Comesana, M.A. Gómez, M.A. Álvarez, and P. Eguía. Thermal Lag Analysis on a Simulated TGA-DSC Device. *Thermochimica Acta*, 547:13–21, 2012.

[102] M. Saoudi. Personal Communication, CNL, 2020.

[103] C. Collins. Personal Communication, Parr Instrument Company, 2020.

[104] Parr Instrument Company. Series 4740 High Pressure/High Temperature Pressure Vessels, 25-75 mL. https://www.parrinst.com/products/non-stirred-pressure-vessels/series-4740/. Accessed: 2020-03-30.

[105] E. Capelli and R.J.M. Konings. Thermodynamic assessment of the niobium-fluorine system by coupling density functional theory and CALPHAD approach. *Journal of Fluorine Chemistry*, 208:55–64, 2018.

[106] G.W.H. Höhne, H.K. Cammenga, W. Eysel, E. Gmelin, and W. Hemminger. The Temperature Calibration of Scanning Calorimeters. *Thermochimica Acta*, 160(1):1–12, 1990.